약학박사 학위논문

Microenvironmental Regulation of Tumor Resistance to Anti-IGF-1R Monoclonal Antibody

항인슐린유사성장인자수용체 단일클론항체에 대한 미세종양환경매개 내성 발생기작

2017년 2월

서울대학교 대학원

약학과 병태생리학 전공

이 지 선

Microenvironmental Regulation of Tumor Resistance to Anti-IGF-1R Monoclonal Antibody

항인슐린유사성장인자수용체 단일클론항체에 대한
미세종양환경매개 내성 발생기작

지도교수 이 호 영

이 논문을 약학박사학위논문으로 제출함
2016년 11월

서울대학교 대학원
약학과 병태생리학 전공
이 지 선

이지선의 박사학위논문을 인준함
2016년 12월

위 원 장 _____ (인)
부 위 원 장 _____ (인)
위 원 _____ (인)
위 원 _____ (인)
위 원 _____ (인)

Abstract

Microenvironmental Regulation of Tumor Resistance to Anti-IGF-1R Monoclonal Antibody

Ji-Sun Lee
College of Pharmacy
The Graduate School
Seoul National University

Drug resistance is a major impediment to a large repertoire of anticancer therapies. Hence, the rational design of anticancer therapies should include strategies that circumvent treatment-associated drug resistance. Recent studies have demonstrated the importance of the tumor microenvironment (TME) to innate resistance to molecularly targeted therapies.

In this study, I investigated the role of the TME in innate resistance to insulin like growth factor receptor-1 (IGF-1R) targeting therapy based on monoclonal antibody (mAb) that has shown limited clinical efficacy. Anti-IGF-1R mAb treatment stimulated tumor progression with distant cancer metastasis and decreased survival in mouse models harboring orthotopic tumors of human cancer cell lines. In this models, increased tumor angiogenesis and stromal cell infiltration within the TME were concomitantly observed.

Next I performed co-culture experiments with human cancer, vascular endothelial (VE) cells, fibroblasts and monocytes and found that IGF-1R ablated

cancer cells recruited fibroblast and monocytes. Once fibroblasts and monocytes recruited to cancer cells, they were shown to stimulate angiogenic abilities of VE cells.

From the signaling pathway array using protein lysates from IGF-1R blocked cancer cells, we found that anti-IGF-1R mAb treatment stimulated signal transducer and activator of transcription 3 (STAT3)-dependent transcriptional up-regulation of IGF-2 in cancer cells, enabling communication with fibroblast and monocytes through their insulin like growth factor receptor 2 (IGF-2R). Upon the interaction with IGF-1R ablated cancer cells, fibroblasts and monocytes produced potent proangiogenic cytokine, CXCL8.

Silencing IGF-2 or STAT3 expression in cancer cells or IGF-2R or CXCL8 expression in stromal cells markedly inhibited communication between cancer and stromal cells and vascular endothelial cells' angiogenic activities. Moreover, tumor tissue derived STAT3 knocked down cancer cells revealed impairment of anti-IGF-1R mAb's ability to recruit stromal cells.

In conclusion, IGF-1R blockade reprograms cancer cells to produce IGF-2, which alters the TME, thereby stimulating tumor angiogenesis and metastasis. Targeting the STAT3/IGF2/IGF-2R/CXCL8 intercellular signaling loop may overcome the adverse consequences of anti-IGF-1R mAb-based therapies.

***Keywords*: tumor microenvironment (TME) / drug resistance / insulin like growth factor receptor 1 (IGF-1R) / insulin like growth factor-2 (IGF-2) / signal transducer and activator of transcription 3 (STAT3)**

Student number: 2011-31107

Table of contents

List of figures

List of tables

Abbreviations

CAF	Cancer associated fibroblasts
CM	Mouse endothelial cell
CML	Chronic myeloid leukemia
EGFR	Epidermal growth factor receptor
EMT	Epithelial mesenchymal transition
FGF	Fibroblast growth factor
FSP-1	Fibroblast specific protein 1
GIST	Gastrointestinal stromal tumors
HGF	Hepatocyte growth factor
HNSCC	Head and neck squamous cell carcinoma
HUVEC	Human umbilical vein endothelial cell
IGF	Insulin-like growth factor
IGFBP	IGF binding protein
IGF-1R	IGF receptor 1
IGF-2R	IGF receptor 2
IR	Insulin receptor
IRS	Insulin receptor substrate
mAb	Monoclonal antibody
MDA231	MDAMB231D3H2LN
MDSC	Myeloid derived suppressor cells
NOD/SCID	Non-obese diabetic /severe combined immune-deficient
NSCLC	Non-small cell lung carcinoma
PDGF	Platelet derived growth factor

PI3K	Phosphoinositide 3 kinse
STAT3	Signal transducer and activator of transcription 3
TAM	Tumor associated macrophages
TGF-b	Transforming growth factor-β
TKI	Tyrosine kinase inhibitor
TME	Tumor microenvironment
VE	Vascular endothelial
VEGF	Vascular endothelial growth factor
VEGFR	Vascular endothelial growth factor receptor

I. INTRODUCTION

1. Molecular targeted cancer therapy

There are three common therapeutics to treat cancers: classical chemotherapeutics and radiation therapy, molecular targeted therapy, immunotherapy (Figure 1). Chemotherapeutic agents and radiation therapy usually induce DNA damages which result in apoptosis. Those include alkylating agents, antimetabolites and topoisomerase inhibitors. Targeted therapy is to block specific target molecules, which are mainly involved in signaling pathways propagated only in cancer cels, finally inhibit cancer cell proliferation. Immunotherapies focus on enhancement of immune systems against the tumor.

The most serious disadvantage of conventional chemotherapy is systemic side effects throughout the body, as this therapy harms not only rapidly growing cancer cells, but also healthy cells. Most cancer patients who take conventional chemotherapy suffer from systemic side effects, including hair loss, nausea, fatigue, anxiety and depression. Although those symptoms rarely threaten to kill, they exert bad influence on patients' daily lives, producing another psychological problems. To overcome the systemic side effects and enhance the quality of patients' lives, research for therapeutic strategies that kill only vigorously proliferating cancer cells have been pursued. During the cancer progression from benign hyperplasia to invasive and metastatic tumor, cancer cells obtain several genetic and epigenetic abnormalities to maintain the active proliferation and spread to other organs. This suggests that by blocking those molecular defects, proliferation and spread of cancer cells can be repressed while normal cells are not affected by the therapy, and this is the main concept of molecular targeted cancer therapy [1-3].

Because of the genetic complexity of cancer, growth of cancer cells can be inhibited by the inactivation of a single oncogene: this phenomenon is referred to as

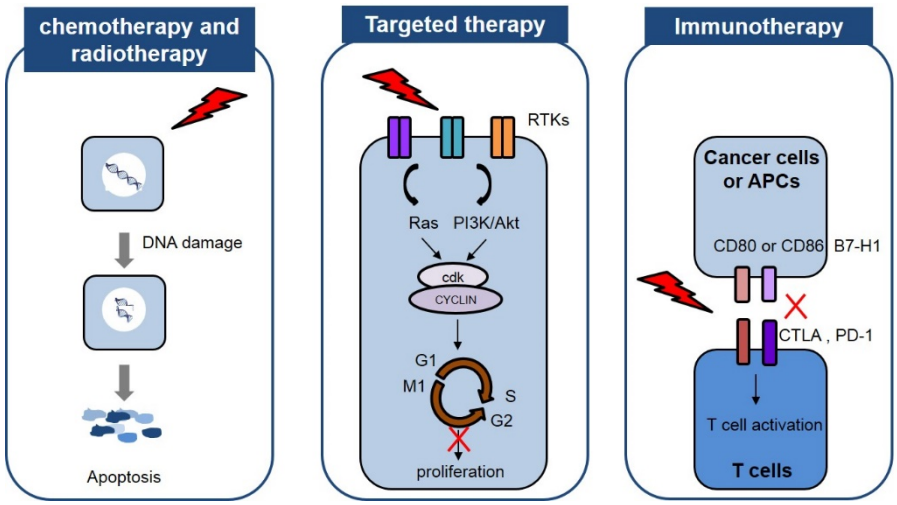

Figure 1. Common treatments for cancer.

Chemotherapy and radiotherapy results in apoptosis by inducing DNA damages. Targeted therapy blocks signaling pathways involved in Ras or PI3K/Akt pathway-regulated cell cycle propagation. Representative immunotherpay invovles checkpoint inhibitors which block interaction between antigen presenting cells or cancer cells and cytotoxic T cells which exerts anti-tumor immunity.

Reference: Sawyers, C., *Targeted cancer therapy.* Nature, 2004. **432**(7015): p. 294-7.

“oncogene addiction”. From genetically engineered mouse models, various oncogene have been reported and therapeutic agents targeting them also have been suggested (Table 1). For example, induction of c-MYC oncogene in hematopoietic lineage promotes T cell leukemia and myeloid leukemia [4, 5]. Among molecular targeted therapies, the most powerful therapeutic agents that shifted paradigm of cancer therapeutics is the small molecule kinase inhibitor, imatinib mesylate (Gleevec). This targeted agent showed neerly perfect clinical success in chronic myeloid leukemia (CML) and gastrointestinal stromal tumors (GIST). Imatinib effectively blocks the activity of mutant kinase fusion protein, Bcr-Abl, constitutive active Abl kinase in CML. Imatinib also has other targets, including KIT and PDGFR which have been known to drive GIST [6].

Molecular targeted cancer therapies can be categorized to small molecule inhibitor or monoclonal antibody. Small molecule inhibitor targets tyrosine kinase domain and block their kinase activity that governs cell proliferation and survival. For example, Gleevec is able to bind the catalytic cleft of the Bcr-Abl tyrosine kinase which activate Ras pathway, the PI3 kinase-Akt/PTB pathway, the JAK-STAT pathway, and transcription factors including Jun, Myc, and NF-Kb. This drug is the first successful molecular targeted drug approved by FDA. On the other hand, monoclonal antibody targets cell surface receptors which signals for proliferation upon ligand binding. By binding to the cell surface receptor, monoclonal antibody interrupt binding of the endogenous ligand and sometimes induces degradation of antibodies. Emergence of those successful targeted therapeutic anticancer drugs encouraged many other attempts at identifying new molecular target for cancer therapy and numerous drugs that target only cancer cells are discovered.

Oncogene	Cancer Type	Approved targeted therapy	Reference
ABL	CML	Imatinib (Gleevec), Nilotinib (Tasigna), Bosutinib (bosulif), Ponatinib (Iclusig)	[7-9]
KIT	GIST	Imatinib (Gleevec), Nilotinib (Tasigna)	[6, 10]
HER2	Breast, ovarian, NSCLC	Trastuzumab (Herceptin), Lapatinib (Tykerb), Pertuzumab (Perjeta)	[11, 12]
EGFR	NSCLC, glioblastoma, colon, pancreas	Gefitinib (Iressa), Erlotinib (Tarceva), Cetuximab (Erbitux), Afatinib (Gilotirf), Necitumumab (Portrazza), Panitumumab (Vectibix)	[13-17]
ALK	ALCL, NSCLC	Crizotinib (Xalkori), Ceritinib (Zykadia), Alectinib (Alecensa)	[18-20]
BRAF	Melanoma, thyroid carcinoma	Vemurafenib (Zelboraf), Dabrafenib (Tafinlar)	[21]
PI3KCA	Colon, breast, lung	Idelalisib (Zydelig), Buparlisib (BKM120)	[22-24]
MEK	Melanoma	Trametinib (Mekinist), Cobimetinib (Cotellic)	[25, 26]
VEGFR	NSCLC, GBM, breast	Bevacizumab (Avastin), Ramucirumab (Cyramza)	[27-29]

ALCL, anaplastic large-cell lymphoma; CML, chronic myeloid leukemia; GIST, gastrointestinal stromal tumor; NSCLC, non-small-cell-lung cancer; GBM,

glioblastoma multiform

Table 1. Preclinically reported oncogenes and their targeted therapy.

Representative targeted therapeutic agents for preclinically identified oncogenes are listed.

2. Insulin-like Growth Factor (IGF) axis in cancer therapeutics

The insulin-like growth factor (IGF) axis is regulated by a complex interplay between ligands, cognate receptors, and binding proteins [30-32]. Unlike insulin whose expression is highly limited to pancreatic beta cells and regulated according to levels of glucose in serum, IGF-1 and IGF-2 are widely expressed in many tissues, playing as growth factors through autocrine and paracrine manners [32]. IGFs also exert activities of insulin, including increase in glucose metabolism in fat, increase in glucose transport, inhibition of lipolysis, and increasing lipid, glycogen, and protein synthesis, but with only 1 to 2% of insulin [33]. Circulating IGFs is regulated in a complex fashion by a family of six IGF binding proteins (IGFBP). By binding to IGFs, these proteins prolong half-lives of circulating IGFs and also limit access to the receptors. IGFBPs are susceptible to degradation by various protease, secreted by malignant cells, suggesting that transformed cells have increased local IGFs bioactivity related to neoplastic characteristics [34]. Another members of IGF axis are receptors, including insulin receptor (IR) and IGF receptor (IGFR) which belong to tyrosine kinase class of membrane receptors [35]. IR exists in two isoforms; the 'B' isoform recognizes only insulin, but the 'A' isoform, which is the isoform that is most commonly expressed by tumors, recognizes both insulin and IGF. Each IR and IGFR gene product is processed and forms alpha- and beta-chains that associate to form a 'half' receptor; two half receptors then associate to form a holoreceptor. Besides, heterodimer also can be formed by association of each different half receptors, and this is called hybrid receptor. Most cancer cells display various hybrid receptors because they own both the IR and IGFR genes, enabling amplified mitogenic effects of IGFs (Figure 2). Upon binding of IGFs to the alpha

subunit of IGFR or hybrid receptors with IR, beta subunit is autophosphoryated and this acts as docking sites for the insulin receptor substrate (IRS)1-4 and other proteins, activating phosphoinositide-3 kinase (PI3K) and mitogen activated protein kinase (MAPK) signaling pathways. PI3K subsequently activates AKT, then inhibits apoptosis by interaction with Bcl2-antagonist of cell death (BAD), mouse double minute 2 (Mdm2) and also stimulates protein synthesis by activating mTOR. As its final tumor promoting result, this signaling axis has been proposed as one of the most promising targets for anticancer therapies. Most clinical reagents that block IGF axis belong to three main classes: monoclonal antibodies (mAbs) against IGF-1R, mAbs against IGF, and IGF-1R tyrosine kinase inhibitors (TKIs). A number of clinical trials with IGF-1R-targeted therapies, mostly using monoclonal antibodies, have sought to abrogate IGF-1R function in various cancers [36-39]. However, the overall response rate to the therapy has been below expectations and enthusiasm for the therapy has declined [40-45]. Accordingly, efforts have focused on understanding mechanisms underlying resistance against anti-IGF-1R mAb-based therapies. Several preclinical studies have proposed mechanisms underlying emergent resistance to the anti-IGF-1R therapies. For application to Ewing's sarcomas, resistant cells switch from IGF-1/IGF-1R to IGF-2/IR-A dependency to maintain sustained activation of Akt and Erk1/2, proliferation, migration and metastasis [46]. In pancreatic neuroendocrine tumors (PNET), IR serves as a second signaling receptor for IGF-2, contributing to resistance to anti-IGF-1R therapy [47]. In IGF-1R TKI-resistant rhabdomyosarcoma cell line, overexpression and constitutive activation of platelet-derived growth factor receptor alpha (PDGFa) contributes signaling bypass upon IGF-1R signaling blockade [48]. Integrin and epidermal growth factor receptor (EGFR) signaling are also reported to have critical role in inherent resistance of cancer cells to cixutumumab, a fully human IgG1 mAb against IGF-1R [49].

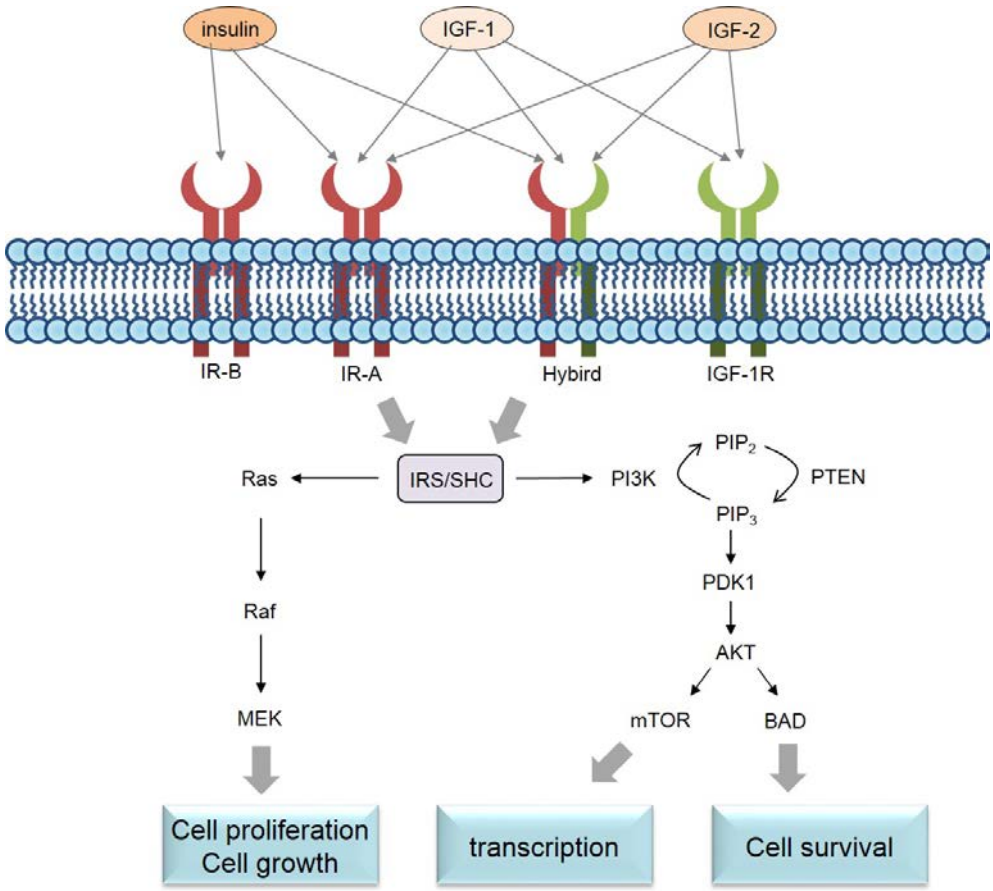

Figure 2. Schematic diagram of IGF axis, their main downstream pathways, and main biological end points.

Binding of ligand to receptors induces autophosphorylation of beta subunit of receptors, signals to adaptor proteins, such as IRS-1 and SHC. This in turn, activates oncogenic pathways, including PI3K/Akt pathway and MAPK pathway, resulting tumor development and progression.

Reference: Pollak, M., *The insulin receptor/insulin-like growth factor receptor family as a therapeutic target in oncology.* Clin Cancer Res, 2012. **18**(1): p. 40-50.

3. Tumor Microenvironment (TME)

Solid tumors exhibit an organ-like structure, consisting of various cell types, including cancer cells, tumor-associated fibroblasts, infiltrating immune cells and endothelial cells [50, 51] (Figure 3). As is important for maintaining normal tissue homeostasis, bidirectional communication between cancer cells and their microenvironment influences on tumor initiation and progression. Cancer was previously viewed as a heterogeneous disease including mutations in tumor cells; however, many evidence suggest that heterogeneity of tumors also arise from their microenvironmental conditions, including cellular and matrix composition [52, 53]. When primary tumor grows, intercellular interactions present in normal tissue are interrupted as tumor is able to circumvent normalizing signals from the microenvironment, and in turn, the microenvironment provide the tumor-promoting environment [54].

As one of the cancer hallmarks, a wide variety of immune cells are infiltrated in tumor region [53], and those cells who have tumor promoting activities are mainly tumor associated macrophages (TAM), myeloid derived suppressor cells (MDSCs), and regulatory T cells (Tregs). TAMs secrete a plethora of pro-tumorigenic proteases, cytokines and growth factors, supporting tumor growth, angiogenesis and invasion [55-58]. Monocytes recruited to tumor region by chemoattractants such as colony stimulating factor-1 (CSF-1) and the chemokine CCL-2 differentiates into macrophages then produces vascular endothelial growth factor (VEGF), activating angiogenic switch. Moreover cancer cells become invasive by paracrine loop of macrophage-expressed epidermal growth factor (EGF) and epithelial cell-expressed CSF-1 loop. TAMs also participates in immunosuppression by enhanced recruitment of Tregs and inhibition of cytotoxic T

cell proliferation. MDSCs are produced as a result of aberrant myelopoiesis under disease state and play an important role in evasion and suppression of the host immune system [59, 60]. MDSCs express high levels of inducible nitric oxide synthase (iNOS) and arginase 1, and subsequently induce shortage of L-arginine which is necessary to T cell proliferation. MDSCs also suppress cytotoxic T cells by producing reactive oxygen species (ROS), nitric oxide (NO), and peroxynitrite. Above this, MDSCs promote tumor vascularization and inhibit M1 macrophage polarization and NK cell cytotoxic activities.

Fibroblasts are present in connective tissue and synthesize extracellular matrix (ECM) and basement membrane components and play multifunctional roles in modulating immune responses and mediating homeostasis [51, 61-63]. Cancer associated fibroblasts (CAF) are highly accumulated in the TME and have distinct role in mediating tumorigenesis from normal fibroblasts. CAFs are activated by growth factors and cytokines in TME, including transforming growth factor-β (TGF-β), monocyte chemotactic protein (MCP1), platelet-derived growth factor (PDGF) and fibroblast growth factor (FGF). CAFs affects cancer progression through ECM remodeling, secretion of soluble factors, regulation of motility and stemness, tumor metabolism remodeling, and preparation of metastatic niche [64].

Endothelial cells which are activated by tumor cell-derived angiogenic factors, including VEGF, FGF, angiopoietin, interleukin-8, and placental-like growth factor (PlGF) are main cellular player of tumor angiogenesis [52, 65]. Once activated, endothelial cells not only proliferate and migrate themselves, but also recruit bone-marrow-derived angiogenic cells (BMC) and pericytes, enhancing tumor vascularization.

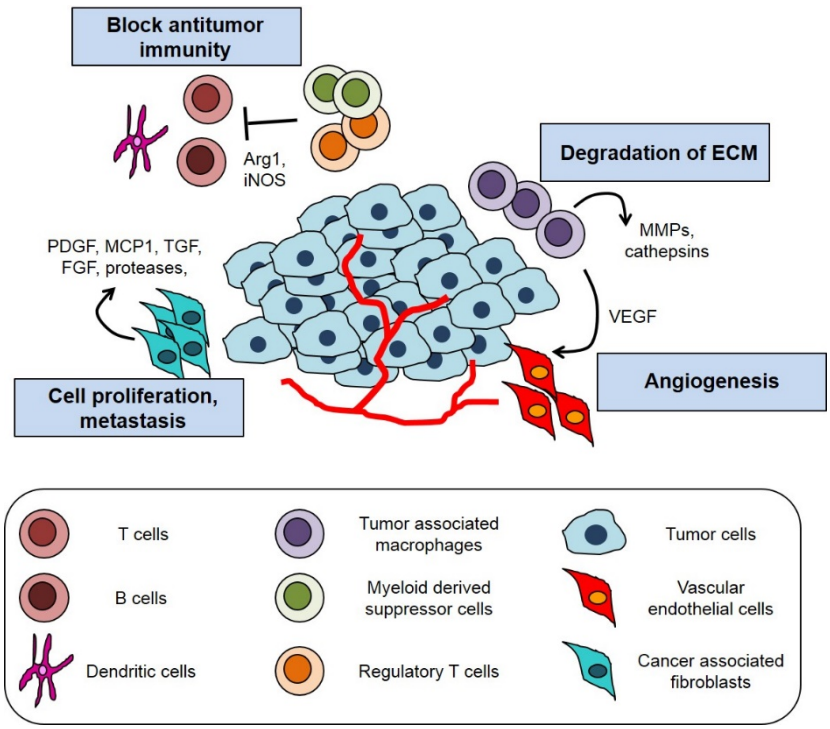

Figure 3. Multiple stromal cell types converge to support a tumorigenic primary niche.

As cancer cells rapidly proliferate, they acquire ability to evade immune response and induce hypoxia, inflammation to the stroma, enabling change of normal stromal cells. Finally, tumor microenvironment consists of various cell types to provide tumor-promoting environment by immune suppression, angiogenesis, providing nutrients and signals to proliferate.

Reference: Quail, D.F. and J.A. Joyce, *Microenvironmental regulation of tumor progression and metastasis.* Nat Med, 2013. **19**(11): p. 1423-37.

4. TME-mediated drug resistance

The emergence of clinical drug resistance has become the major impediment to the successful treatment of cancer, making understanding of mechanism of resistance is necessary to improve the efficacy of anticancer therapy. There are two main categories for drug resistance mechanisms: *de novo* and acquired resistance [66]. While acquired resistance develops over time as genetic changes accumulate, de novo resistance is phenotypic characteristics in place prior to drug treatment. In early days, drug resistance mechanism was studied at a single cell level and revealed that changes affect expression of certain genes encoding proteins that influence uptake, metabolism, and export of drug are important determinants of drug resistance [67]. In addition, substantial evidence suggests that drug resistance develop not only in unicellular event but also in interplay between various types of cellular components of TME [67-69]. Drug resistance which is mediated by TME occurs in two pathways (Figure 4): tumor stroma secretes cytokines, chemokines and growth factors to regulate the response of cancer cells to the drug, which is called soluble factor-mediated drug resistance (SFM-DR); and sometimes tumor cell integrins adhere to stromal fibroblasts or to components of the ECM, receiving signals from the TME, which is called as cell adhesion-mediated drug resistance (CAM-DR) [66].

A variety of stromal cells secrete soluble factors to enhance resistance of cancer cells by paracrine signaling pathway. Hepatocyte growth factor (HGF) secreted from CAFs activates its cognate receptor, MET, then reactivates MAPK and PI3K-AKT signaling pathways, inducing innate resistance to RAF inhibitor in BRAF mutant melanoma [70]. Dual inhibition of RAF and either HGF or MET shows reversal of resistance to the RAF inhibitor, suggesting the importance of

communication between tumor-stroma in development of drug resistance. In mammary tumors, Taxol treatment induced influx of macrophages to tumor region and recruited macrophages produce cathepsin protease. This in turn prevent tumor cells from Taxol-induced cell death. Inhibition of cathepsin in mouse mammary tumor models shows increased response rate to Taxol [71]. CAFs also have been reported to produce PDGF-C and promote angiogenesis in tumor. This leads to the development of resistance to anti-angiogenic therapy [72]. Sometimes, drug resistance needs direct contact between stromal and cancer cells through adhesion molecules. Recruited macrophages bind to cancer cells through receptor vascular cell adhesion molecule-1 (VCAM-1) and protect cancer cells from proapoptotic signals [73].

On the strength of substantial studies of TME-mediated tumorigenesis and drug resistance, several clinical therapies target tumor stroma have been developed. The most well characterized target of stromal cells is vascular endothelial growth factor receptor (VEGFR) which is expressed on mainly vascular endothelial (VE) cells. As VE cells play an important role for angiogenesis, providing oxygen and nutrients to cancer cells, inhibition of this signaling pathway were expected to inhibit cancer progression.

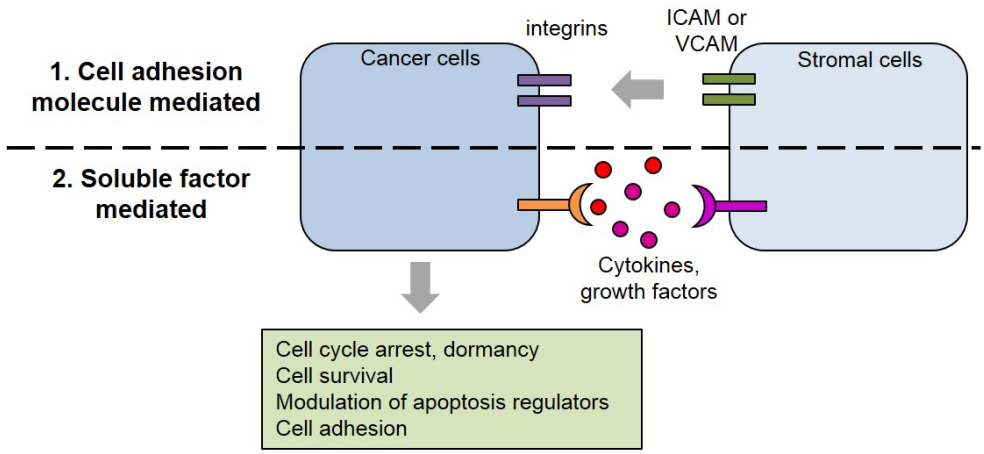

Figure 4. Tumor-stroma communication is the basis of EMDR.

Cancer and stroma interact through soluble factors, such as SDF-1, IL6 or cell adhesion molecules, including VCAM1 or ICAM1. Final results of this interaction is inhibition of apoptosis and stimulation of proliferation, enabling cancer cells acquire resistance to antitumor therapies.

Reference: Meads, M.B., R.A. Gatenby, and W.S. Dalton, *Environment-mediated drug resistance: a major contributor to minimal residual disease.* Nat Rev Cancer, 2009. **9**(9): p. 665-74.

II. PURPOSE OF THIS STUDY

The IGF-1R signaling axis activates a number of oncogenic pathways involved in survival, proliferation and metastasis of cancer cells. Preclinical studies, using mouse models which possess manipulated IGF-1R axis, corroborated malignant potential of this signaling pathways [74-76], thus leading to development of therapeutic agents targeting this pathway. However, clinical efficacies of those therapeutic agents are low and IGF-1R signaling pathway is losing pharmaceutical companies' attention as a therapeutic target. Although mechanisms of resistance to anti-IGF-1R therapies has been reported, it is still lack of understanding of development of resistance in context of interaction between tumor and their microenvironment. As communication between cancer cells and their TME owe big parts in tumorigenesis and development of drug resistance, understanding of resistance mechanism in the view of tumor and their niche is necessary to propose more effective therapeutic strategies to target the IGF-1R pathway.

Based on previously reported studies that illuminated the importance of communication between cancer cells and their microenvironments in the development of drug resistance, I hypothesized that stromal cells may affect cancer cells under the IGF-1R targeting therapy, resulting resistance. In this study, I tried to evaluate the efficacy of anti-IGF-1R mAbs in mouse models of breast, lung, and head and neck cancer to which clinical anti-IGF-1R therapies are applied. Then, I tried to elucidate the changes of the TME under the anti-IGF-1R therapy. Finally, I identified the molecular mechanisms of interaction between cancer and stromal cells which responsible for resistance to anti-IGF-1R therapy. Eventually, the main purpose of this study is to illuminate the role of tumor microenvironment mediate the resistance to anti-IGF-1R therapy.

III. MATERIALS AND METHODS

1. Cell culture and reagents

Human head and neck squamous cell carcinoma (HNSCC) cell line (686LN) was kindly provided by Dr. Jeffrey Myers (MD Anderson Cancer Center, Houston, TX). Human non-small cell lung carcinoma (NSCLC) cell line (H1299) was purchased from the American Type Culture Collection (Manassas, VA, USA). MDAMB231D3H2LN (MDA231)-Luciferase (Luc) cell line was obtained from Caliper Life Science (Alameda, CA, USA). Human fibroblast Wi38 cells were kindly provided by Dr. John V. Heymach (MD Anderson Cancer Center, Houston, TX) and MRC-5 cells were purchased from the Korean Cell Line Bank (Seoul, Republic of Korea). Human monocyte THP-1 cells were kindly provided by Dr. Kyu-Won Kim (Seoul National University, Seoul, Korea). Mouse endothelial cells (SVECs) and mouse breast cancer cell line (4T1) were kindly provided by Dr. Mien-Chie Hung (MD Anderson Cancer Center, Houston, TX). Cells were cultured in DMEM, DMEM/F-12 or RPMI1640 medium supplemented with 10% FBS. Human umbilical vein endothelial cells (HUVECs) were purchased from Invitrogen and grown in vasculife basal medium supplemented with vasculife VEGF life factors (Lifeline cell technology, Frederick, MD, USA). Cells were kept in 37°C with 5% CO2.

Cixutumumab (IMC-A12), a fully human IgG1 mAb, was provided by ImClone Systems (New York, NY, USA). Human recombinant IGF-2, human recombinant CXCL8, and neutralizing antibodies against to the IGF-2 or IGF-2R were obtained from R&D Systems (Minneapolis, MN, USA). Transfection with expression vector, siRNA, or shRNA vectors was performed using Lipofectamine 2000 (Invitrogen, Grand Island, NY, USA) or Fugene 6 (Promega, Madison, WI, USA). Small interfering RNA (siRNA) for negative control #1 and CXCL8 were purchased from GenePharma (Shanghai, China), and negative control #2 were

purchased from Bioneer (South Korea). Sequence for siRNAs was shown in table 2. Matrigel for mouse experiment, migration assay, and tube formation assay was obtained from BD Biosciences (San Jose, CA, USA). Head and neck cancer tissue array HN242a was purchased from US Biomax Inc. (Rockville, MD). All other materials were purchased from Sigma-Aldrich (St. Louis, MO, USA)

2. Mouse studies

All mouse study procedures were performed in accordance with protocols approved by the Institutional Animal Care and Use Committee of Seoul National University. Mice were cared for in accordance with guidelines set by the Association for Assessment and Accreditation of Laboratory Animal Care and the US Public Health Service Policy on Human Care and Use of Laboratory Animals. For orthotopic tumor models, MDA231 (2×10^5 cells per mouse in 40 μl containing Matrigel), H1299 (1×10^6 cells per mouse in 100 μl of phosphate-buffered saline), and 686LN (2×10^5 cells per mouse in 40 μl containing Matrigel) were injected into nude [H1299; 686LN; MDA 231; Fig 4 (1st group)] or non-obese diabetic (NOD)/severe combined immune-deficient (SCID) (MDA231; Fig4 2nd) mice at mammary fat pad, lung, or tongue sites. When the solid tumors of MDA231 reached to a volume of 100 mm3, mice were treated with cixutumumab (10mg/kg, intraperitoneally, once weekly). For orthotopic tumor models of H1299 or 686LN, mice were treated with cixutumumab one week or 3 days after the orthotopic injection, respectively. To establish MDA231 orthotopic tumors in mice, in which the human lymphoid system is reconstituted, the NOD/SCID/JAK3 null mouse model [77] was employed. Human cord blood was obtained from normal full-term deliveries. Informed consents were obtained according to Institute guidelines, and

these works were approved by Seoul Metropolitan Government Seoul National University Boramae Medical Center (IRB No. 16-2014-80) and Seoul National University (IRB No. E1409/002-001) Institutional Review Board. Briefly, NOD/SCID/Jak3 null mice were preconditioned with busulfan (30 mg/kg body weight) and then human $CD34^+$ hematopoietic stem cells purified from human cord blood were transplanted. Peripheral blood from the retroorbital sinus and the spleen samples obtained at 4 weeks after transplantation or at the time of sacrifice, respectively, were analyzed by flow cytometry for the presence of human cells expressing the CD45 human leukocyte antigen. Fluorescent isothiocyanate (FITC)- or allophycocyanin (APC)-conjugated monoclonal antibodies (mAbs) against human or mouse CD45 (eBioscience, San Diego, CA) were added to splenocytes or peripheral blood mononuclear cells, incubated for 30 minutes at 4°C, washed twice, and analyzed using a FACS Calibur flow cytometer (BD Biosciences, San Jose, CA). For orthotopic tumor models from MDA231 cells with reduced expression of STAT3, mixture of cancer cells and Wi38 fibroblast cells (1×10^6 cells: 5×10^5 cells/mouse in 30 μl containing Matrigel) were injected into nude mice at mammary fat pad.

3. Immunofluorescence and immunohistochemistry (IHC) assays

Cells were grown on coverslips and fixed in methanol, blocked with 3% BSA solution, incubated with primary antibodies (IGF-2, Santa Cruz Biotech; 1:200 dilution) and incubated with fluorescence conjugated secondary antibodies (Alexa 488 conjugated goat antibody, Invitrogen; 1:1000 dilution). Samples were counterstained with 10 μg/ml DAPI (4’ ,6-diamidino-2-phenylindole) to detect all nuclei. For immunostaining of tumor tissue, mice were anesthetized by

intraperitoneal injection of Zoletil (Virbac) and Rompun (Bayer) and tumor tissues were dissected and embedded in Optimum Cutting Temperature compound (OCT;Sakura) or fixed with paraformaldehyde and embedded in paraffin. For immunofluorescent staining, 4 μm frozen sections were fixed in 4% paraformaldehyde for 30 min, permeabilized with 0.3% triton X-100 for 15 min, and blocked in protein block solution (Dako) for 30 min. Primary antibodies (CD34 and IGF-2, Santa Cruz Biotech; F4/80, Serotec; 1:100 dilution) were diluted in 3% BSA solution and incubated overnight at 4 °C. Then, samples were washed twice with PBST and incubated with fluorescence conjugated secondary antibodies (Alexa 488 conjugated goat antibody, Alexa 594 conjugated rat antibody, Invitrogen; 1:1000 dilution) for 1 h. Next, samples were counterstained with DAPI. For IHC, 4 μm paraffin sections were rehydrated, blocked, and incubated with antigen retrieval buffer (Vector laboratories) at 95 °C for 20 min. Samples were incubated with primary antibodies (Luciferase, Abcam; CD45, Serotec; F4/80, Serotec; F4/80, Thermo; FSP-1, Abcam; Iba-1, Wako; VEGFR1, Abcam; human mitochondrion; Abcam; 1:100 dilution in 3% BSA solution) overnight at 4 °C, washed twice with PBST, and incubated with appropriate biotinylated secondary antibodies for 1 h at room temperature. Staining were revealed using Diaminobenzidine substrate kit (Vector laboratories). Slides were counterstained with hematoxylin and examined using Nuance fluorescence microscope (Perkin Elmer).

4. Establishment of silenced stable cell line

For stable knockdown cell line establishment, shRNA bacterial glycerol stock complementary to each human gene coding sequences (IGF-2, NM_000612; IGF-1R, NM_000875.2; IGF-2R, NM_000876; STAT3, NM_003150) were

purchased (Mission shRNA, Sigma) and the DNA construct (in PLKO.1 lentiviral vector backbone) was isolated from bacterial culture. Lentiviral production was performed by transfection of HEK293T cells using fugene 6 (promega). Supernatants were collected 24-48 h after transfection, and then filtered through 0.22 μm syringe filter. Cells were infected with lentivirus with 8 μg/ml polybrene for 24 h and then medium was replaced with fresh growth media containing puromycin (1-2 μg/ml) for selection.

5. Isolation of primary monocytes

Primary cells were isolated from 686LN xenografted tumors. After the dissection of tumors, single cells were isolated using tumor tissue dissociation kit (Miltenyi Biotech) then initially positively sorted using CD11b microbeads using a MACS seperator and MS columns (Miltenyi Biotech). CD11b+ population were further sorted using a FACS Aria cells were isolated using magnetic beads (Miltenyi Biotech). Macrophages were sorted using FACS Aria (BD Biosciences). Cells were labeled with fluorochrome-conjugated antibodies, PE/Cy7 anti-mouse Ly-6G, PerCP/Cy5.5 anti-mouse CD11b (Biolegend).

6. In vitro migration and tube formation assay

For transwell (8.0 μm pore size, corning) migration assay, outer membrane was coated with 0.05% gelatin. The indicated cells ($1x10^5$ cells for THP-1 cells; $4x10^4$ cells for other cells) were seeded onto the upper wells and CM from cancer cells or NIH3T3 cells were used as chemoattractant. Cells were incubated for 12-20 h, and the incubation time was dependent on types of the cell lines. After the incubation, membrane was stained with hematoxylin solution and mounted onto the

slide glass. The number of stained cells per field was counted using a microscope at 100x magnification. CM was collected from cells that had been treated with cixutumumab for 6 days, and medium was exchanged with serum-free medium for 24 h. CM was concentrated using the Amicon Ultra-4 centrifugal filter device. For tube formation, 96-well plate was coated with Matrigel (BD Bioscience) then HUVEC ($1x10^4$ cells per well) cells with CM was seeded and incubated. Tube formation was checked after 6-10 h using a microscope.

7. RT-PCR and real-time PCR analysis

Total RNA was isolated from cells or mice using TRIzol® reagent (Invitrogen) and transcribed using a PrimeScript 1st strand cDNA synthesis kit (Takara, Otsu, Shiga, Japan) according to the manufacturers' protocols. For reverse transcriptase polymerase chain reaction, cDNA was amplified using gene-specific primer sets (Table 3) with EconoTaq® 2x Master Mix (Lucigen, Middleton, WI, USA). PCR products were identified using electrophoresis on 1.5 % agarose gels containing RedSafe (Intron, South Korea). Quantitative real-time PCR was performed in triplicate on Light Cycler 480 (Roche Diagnostics, Indianapolis, IN, USA) using Light Cycler® SYBR Green I Master (Roche), and data were analyzed on the basis of threshold cycle values of each sample and normalized with beta-actin. Primer sets used in real-time PCR was shown in Table 4.

8. Western blotting and RTK array

Cells were collected with RIPA lysis buffer (50 mM Tris-HCl pH7.4, 150 mM NaCl, 1% NP-40, 0.25% sodium deoxycholate, 1 mM EDTA), containing 1 mM Na_3VO_4, 100 mM NaF, 10 mM NaPP, and protease inhibitor cocktail (Roche).

Protein lysates were recovered by centrifugation at 13000 rpm at 4 °C, and then protein concentrations were determined by the BCA assay kit (Thermo Scientific, Rockford, IL, USA). Proteins were separated by SDS-PAGE and transferred to PVDF membranes (Bio-Rad, Hercules, CA, USA). The membranes were incubated with primary antibodies against IGF-1, IGF-2, IGF-1R, IGF-2R, actin, IR (Santa Cruz Biotech., Santa Cruz, CA, USA), tubulin, STAT3, phospho-STAT3 (Y705) (Cell signaling technology, Denvers, MA, USA), FAK (BD), and phosphor-FAK (Y397) (Millipore, Billerica, MA, USA). After removing the primary antibody, membranes were incubated with HRP-conjugated secondary antibodies. The signals were visualized using SuperSignal West Femto Chemiluminsecent Substrate (Thermo Scientific). For RTK signaling array, H1299 cells were treated with 25 μg/ml cixutumumab for 6 days followed by assay using PathScan ® RTK signaling antibody array kit (Cell signaling technology) according to the manufacturers' protocols.

9. ELISA

ELISA was performed by coating 96-well plates with 1 mg per well of anti-IL-8 (R&D systems). Before the subsequent steps in the assay, the coated plates were washed twice with 1X PBS containing 0.05% Tween-20 (PBST). All reagents and coated wells used in this assay were incubated for 2 h at room temperature. Following exposure to the medium, the assay plates were exposed sequentially to each of the biotin-conjugated secondary antibodies, as well as AP and ABTS substrate solution containing 30% H_2O_2. The plates were read at an absorbance of 405 nm. Appropriate specificity controls were included, and all samples were run in duplicate.

10. Plasmids and luciferase assay

pGL3-IGF-2 promoter reporter plasmids (P3) were kindly provided by Dr. P. Elly Holthuizen (Utrecht University, Utrecth, The Netherlands). IGF-2 promoter 4 region was inserted into the Xho I-Hind III restriction site of the pGL3 basic reporter vector (Promega). pRL-Tk renilla reporter plasmid was purchased from promega. Cells pretreated with cixutumumab for 6 days were seeded into 24 wells the transfected with each reporter vectors and pRL-Tk vectors. 48 h after transfection, luciferase activity was measured using Dual-Glo Luciferase Assay System (Promega). Transfection efficiency was determined by normalizing the reporter activity with Renilla luciferase activity.

11. Cell proliferation/viability assay

8×10^3 cells were seeded into 24-well dishes, and cell numbers were assessed using a hemocytometer on days 2, 4, and 6. Four replicate wells were used for each analysis. For cell viability assay, cells were seeded into 96-well dish and treated with cixutumumab (25 μg/ml) for various time. Viability of THP-1 cells were measured by 3-(4,5-dimethylthiazol-2-yl)-5-(3-carboxymethoxy phenyl)-2-(4-sulfophenyl)-2H-tetrazolium (MTS) assay. Viability of other cells were measured by 3-(4,5-dimethylthiazol-2-yl)-2,5-diphenyltetrazolium bromide (MTT) assay. The data are presented as the means ± SD compared with the control group.

12. Statistical analysis

Statistical comparisons between two groups were performed with unpaired Student's t-test, and two-sided P-value of less than 0.05 was considered statistically significant. For survival curve analysis, two-tailed p values were calculated using the Mantel-Cox log-rank test.

Target	Sense	Antisense
Negative control #1	UUCUCCGAACGUGUC ACGUTT	ACGUGACACGUUCGG AGAATT
CXCL 8 #1	GAAGAGGGCUGAGA AUUCATT	UGAAUUCUCAGCCCUC UUCTT
CXCL8 #2	GCCAGAUGCAAUACA AGAUTT	AUCUUGUAUUGCAUC UGGCTT

Table 2. Sequence for siRNA.

Target	Sense	Antisense
ABCC1	AGCCGGTGAAGGTTGTGTAC	TGACGAAGCAGATGTGGAAG
ABCG2	GCAGATGCCTTCTTCGTTATG	TCTTCGCCAGTACATGTTGC
Actin	ACTACCTCATGAAGATC	GATCCACATCTGCTGGAA
E-Cadherin	GGCCAGCCATGGGCCCTTGG	CACCTTCAGCCAACCTGTTT
ESA	GCTCGTGTGTGAACACTGCT	ACGCGTTGTGATCTCCTTCT
IGF-1	TGCTCACCTTCACCAGCTCTGCCA	GTGTGGCGCTGGGCAGGGACAGA
IGF-1R	TGGGCCAAGAGTGAGATC	GTATTCAGCCTCCTCCTTC
IGF-2	TCGTGCTGCATTGCTGCTTACCG	GCTCACTTCCGATTGCTGGCCAT
IGF-2R	AGAAGCCTTAATTTGCACAG	TGCTTCTCAGCAATAGAACA
IR	AACCAGAGTGAGTATGAGGAT	CCGTTCCAGAGCGAAGTGCTT
MCP-1	GAGATCTGTGCTGACCCCAA	GACCCTCAAACATCCCAGG
MMP-1	ATTCTACTGATATCGGGGCTTTGA	ATGTCCTTGGGGTATCCGTGTAG
N-Cadherin	GAATCGTGTCTCAGGCTCCAAG	GTAACACTTGAGGGGCATTGTC
Slug	GAGCATACAGCCCCATCACT	GCAGTGAGGGCAAGAAAAAG
Snail	GCGAGCTGCAGGACTCTAAT	TCCAAG GAAGAGGCTGAAGTA
TGF-b1	GGACTATCCACCTGCAAGAC	CGGAGCTCTGATGTGTTGAA
VEGF	CTACCTCCACCATGCCA A T	TCTCTCCTATGTGCTGGCCT A
VEGFR-2	TATAGATGGTGTAACCCGGA	TTTGTCACTGAGACAGCTTGG
Vimentin	CTTCGCCAACTACATCGACA	GCTTCAACGGCAAAGTTCTC

Table 3. Primers for RT-PCR.

Target	sense	antisense
CXCL2	CGCCCAAACCGAAGTCATAG	AGACAAGCTTTCTGCCCATTCT
CXCL8	ACTGAGAGTGATTGAGAGTGGAC	AACCCTCTGCACCCAGTTTTC
IL-10	GAACCAAGACCCAGACATC	CATTCTTCACCTGCTCCAC
IL-11	GGACTGCTGCTGCTGCTGAAG	CACGGAAGGACTGTCTCTAAC
IL-12	TCGGCAGGTGGAGGTCAGC	CGCAGAATGTCAGGGGAAGTAGG
IL-13	AACATCACCCAGAACCAGAAG	CAGAATCCGCTCAGCATCC
IL-18	CCTCCTGGCTGCCAACTCT	GAAGCGATCTGGAAGGTCTGAG
IL-1b	TGATGGCTTATTACAGTGGCAATG	GTAGTGGTGGTGGGAGATTCG
IL-2	CAAGAATCCCAAACTCACCAG	CGTTGATATTGCTGATTAAGTCC
IL-6	GTGTTGCCTGCTGCCTTC	AGTGCCTCTTTGCTGCTTTC
MCSF	TTGGGAGTGGACACCTGCAGTCT	CCTTGGTGAAGCAGCTCTTCAGCC
SDF-1	CCGCGCTCTGCCTCAGCGACGGGAAG	CCTGTTTAAAGCTTTCTCCAGGTACT
VEGF	CCTGGTGGACATCTTCCAGGAGTACC	GAAGCTCATCTCTCCTATGTGCTGGC
Actin	GCGAGAAGATGACCCAGATC	GGATAGCACAGCCTGGATAG

Table 4. Primers for real-time PCR.

IV. RESULTS

1. Increased cancer metastasis after blockade of IGF-1R.

Therapeutic efficacy of anti IGF-1R mAbs has been evaluated in various types of cancers including breast cancer, NSCLC, and HNSCC [44, 45, 78-80]. To estimate the response of tumor to an IGF-1R blockade, I treated a fully human IgG1 mAb (cixutumumab) to immune-deficient mice bearing orthotopic tumors of representative human cell lines with luciferase (Luc) expression for breast cancer, NSCLC, and HNSCC.

1.1. Increased metastasis after anti IGF-1R mAb treatment in orthotopic breast cancer model

Cixutumumab treatment significantly inhibited tumor growth of MDA231-Luc tumor bearing nude mice in the first group over the 4 weeks when compared with vehicle-treated control group (Figure 5). At time of sacrifice, no detectable metastatic tumor nodules were observed. Next, I evaluated the persistence of the anti-proliferative effect of the cixutumumab treatment in the second group of NOD/SCID mice bearing MDA231-Luc tumor. 7 weeks after the cixutumumab treatment, bioluminescence imaging analysis surprisingly revealed metastatic tumors (Figure 6). When the primary tumors were surgically removed, more clear bioluminescence signal in the lung was observed (Figure 6). IHC analysis of the lungs using anti-luciferase and anti-human mitochondria protein antibodies further confirmed that tumors in this tissue were metastatic tumors originated from the orthotopically injected MDA231-Luc cells (Figure 7). Microscopic analysis of hematoxylin and eosin (H&E) stained lung tissue revealed that cixutumumab-treated group showed a 100% metastatic lung tumor incidence with greater level of

multiplicity and volume (Table 5). There were no detectable metastatic tumor nodules in other organs.

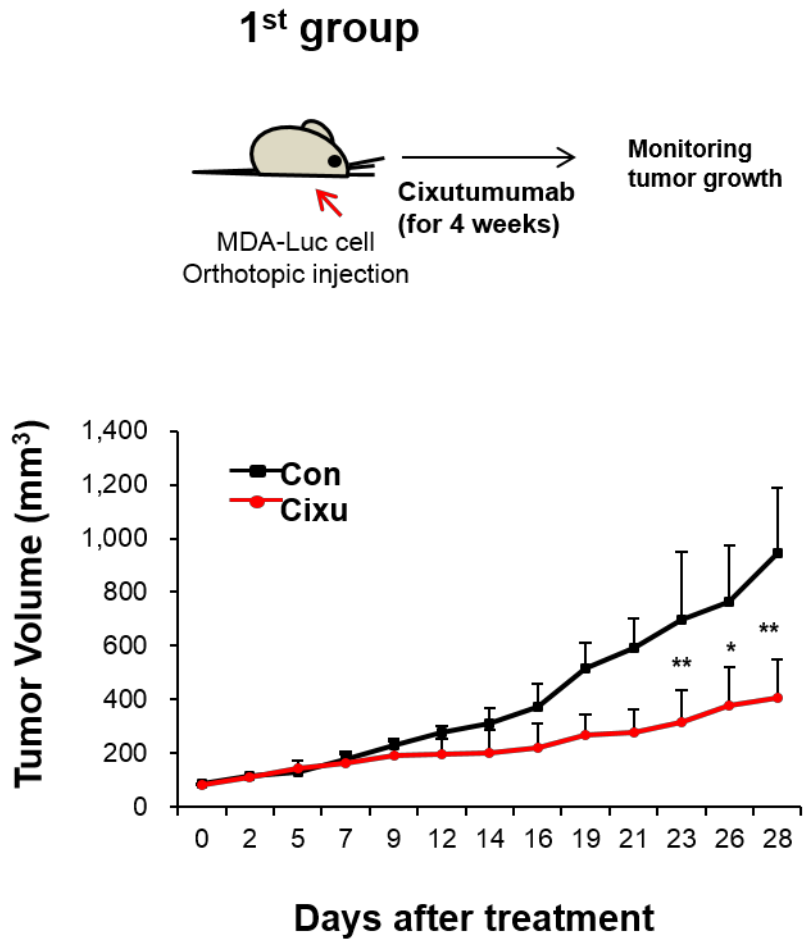

Figure 5. Effects of cixutumumab on primary tumor growth in orthotopic breast tumor models.

MDA231-Luc cells were injected into mammary fat pad of Balb/c nude mice (n=9 per group) and the mice were treated with cixutumumab (10 mg/kg, intraperitoneally, once weekly). Tumor volumes were measured over 4 weeks of drug treatment. Data are presented as the mean tumor volume ± S.D. *P<0.05 and **P<0.01 by two-sided Student's t-test. Cixu, cixutumumab; Con, control.

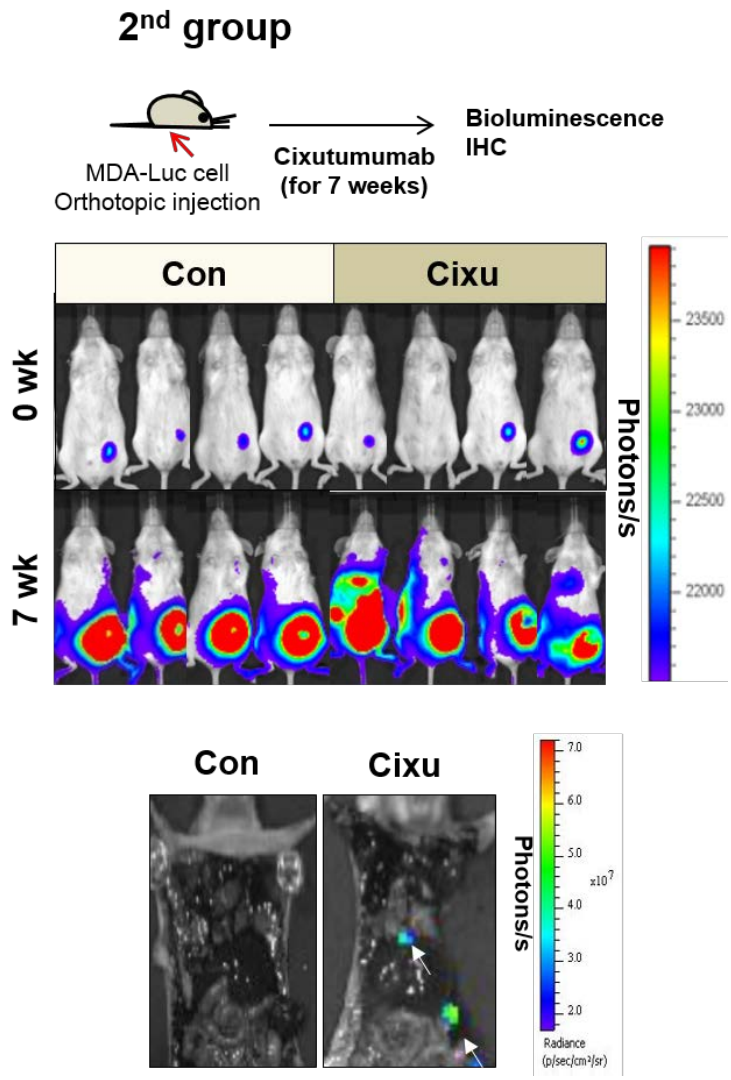

Figure 6. Effects of cixutumumab on tumor metastasis in orthotopic breast tumor models.

MDA231-Luc cells were injected into mammary fat pad of NOD/SCID mice (n=5 per group) and the mice were treated with cixutumumab (10 mg/kg, intraperitoneally, once weekly) for 7 weeks. Top: experimental schedule. Middle: representative bioluminescence images visualizing the tumor cells on week 0 and week 7. Bottom:

bioluminescence images of a representative mouse in each group after killing. White arrows indicate luciferase signal of metastatic tumors. Cixu, cixutumumab; Con, control.

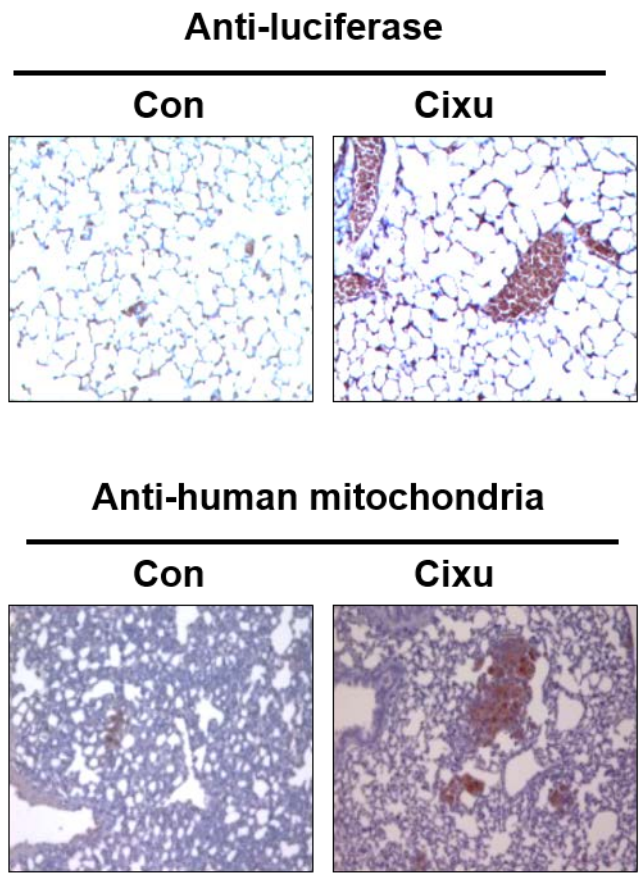

Figure 7. IHC analysis of metastatic lung tumors in orthotopic breast tumor models.

Representative images of excised lungs are presented to confirm the presence of metastasis by anti-luciferase and anti-human mitochondria protein immunostaining. White arrows indicate luciferase signal of metastatic tumors. Cixu, cixutumumab; Con, control.

	Mouse	Lung nodules	Volume (mm^3)
Con	1	0	0
	2	1	92.71
	3	0	0
	4	0	0
	5	0	0
Cixu	1	2	34.79
	2	10	30.64
	3	1	15.57
	4	1	36.4
	5	8	4.69

Table 5. Microscopic analysis of metastatic tumors in MDA tumor bearing mice.

The number and volume of metastatic lung nodules of group 2 mice were scored. Cixu, cixutumumab; Con, control.

1.2. Response to anti IGF-1R mAb in lung cancer models

Next, I evaluated the response to cixutumumab in lung cancer model using human NSCLC cell line, H1299 cells. In mouse model with H1299-xenografted tumors, treatment of cixutumumab significantly reduced survival rate when compared to vehicle-treated mice (Figure 8). As increased metastatic tumor was observed in breast cancer model, I performed bioluminescence imaging analysis in vehicle or drug-treated mice for 4 weeks to monitor tumor metastasis in this model. While bioluminescence images clearly showed primary lung tumor, metastatic tumor could not be seen in other organ. *Ex vivo* bioluminescence image revealed spleen metastasis in cixutumumab-treated group. IHC using anti-human mitochondria protein antibody also confirmed that this metastatic tumors were derived from inoculated cancer cells (Figure. 9). Therefore, anti-IGF-1R mAb treatment induced metastatic tumors and decreased survival of tumor-bearing mice.

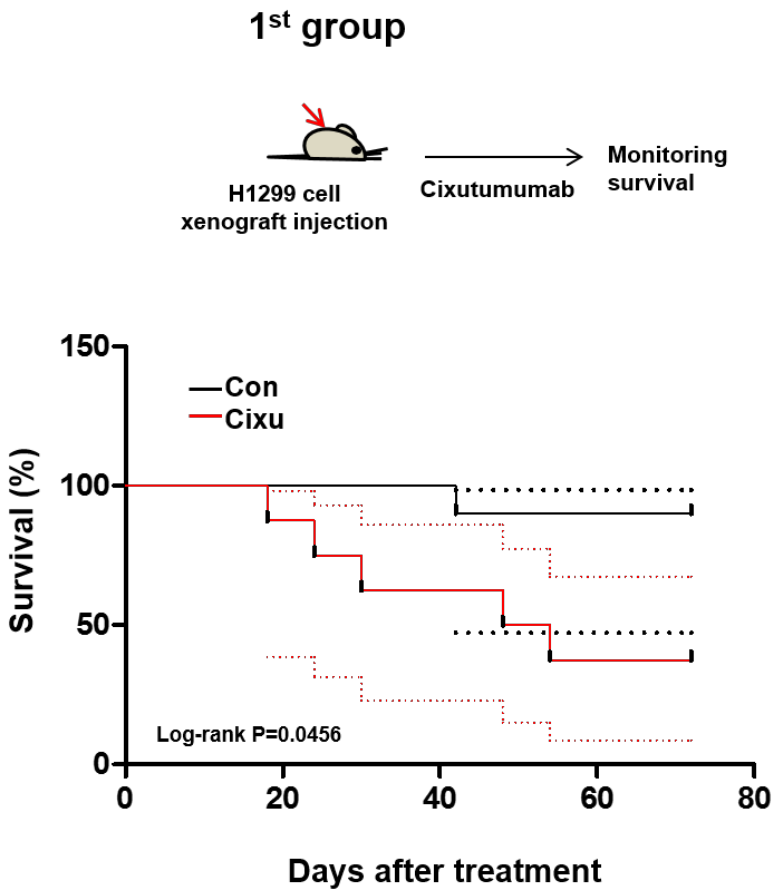

Figure 8. Survival of cixutumumab-treated mouse bearing xenografted tumors. H1299-Luc tumor-bearing mice were treated with cixutumumab (10 mg/kg, intraperitoneally, once weekly) and monitored for survival analyses. Survival graph showed decreased survival of mice with cixutumumab treatment. P=0.045 by two-sided Mantel-Cox log-rank test. Solid line indicates percent survival; dashed line indicates 95 % confidence intervals. Cixu, cixutumumab; Con, control.

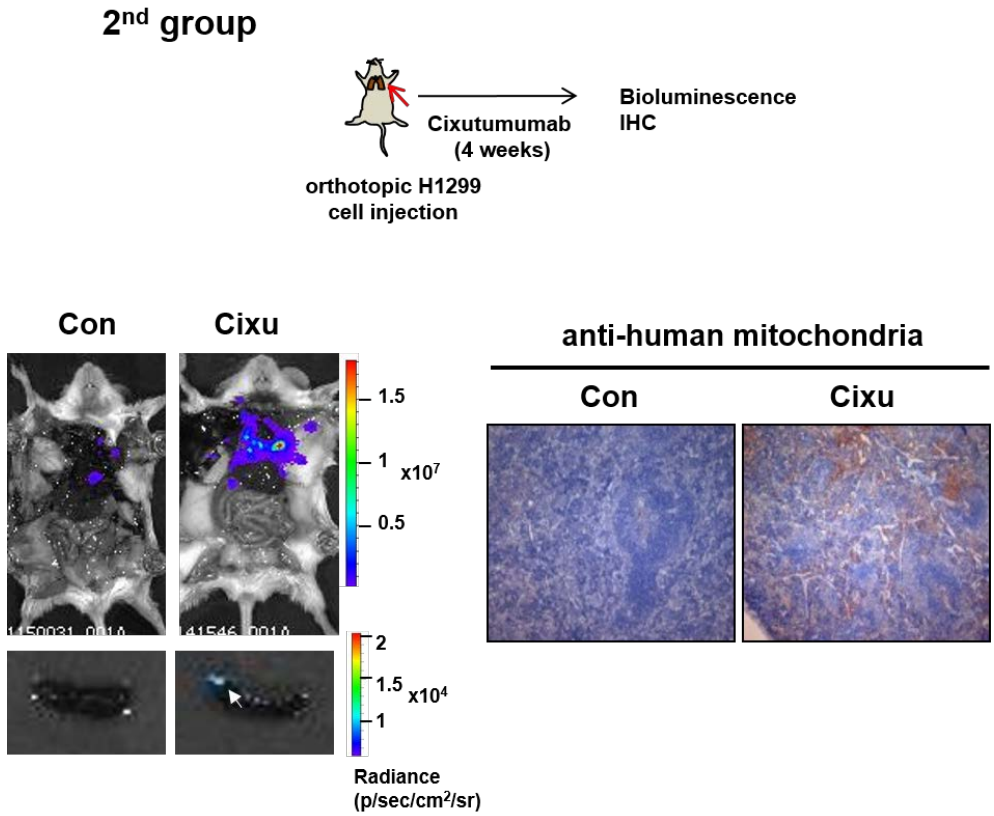

Figure 9. Response to cixutumumab in orthotopic lung tumor models.

(Left) Representative bioluminescence images 28 days after the treatment visualizing the metastatic tumor burden in the spleen. (Right) Representative images of excised spleen are presented to confirm metastatic tumors using anti-human mitochondria immunostaining. Cixu, cixutumumab; Con, control.

1.3. Increased metastasis after cixutumumab treatment in orthotopic HNSCC tumor models

Next, I evaluated the response to anti-IGF-1R mAb in HNSCC tumor models. Cixutumumab treatment also decreased survival of mice bearing 686LN orthotopic tumors (Figure 10), but other mice bearing the same tumor in a different group showed a significant decrease in tumor growth rate after the cixutumumab treatment (Figure 11a, b). It was consistent that cixutumumab decreased primary tumor growth shown in orthotopic breast tumor models. Then, metastatic phenotype was evaluated in a second group in which the primary orthotopic tumors were surgically removed after 2 weeks treatment of cixutumumab (Figure 12a). Consistently with previous findings, bioluminescence images (Figure 12b) and IHC (Figure 12c) analyses revealed spleen metastasis in these mice at 5 weeks after the tumor resection. Unlike drug-treated group, control mice showed no metastases in any organs. Collectively, anti-IGF-1R mAb accelerated tumor progression in immune deficient mice bearing tumors and this was not limited to specific cancer types.

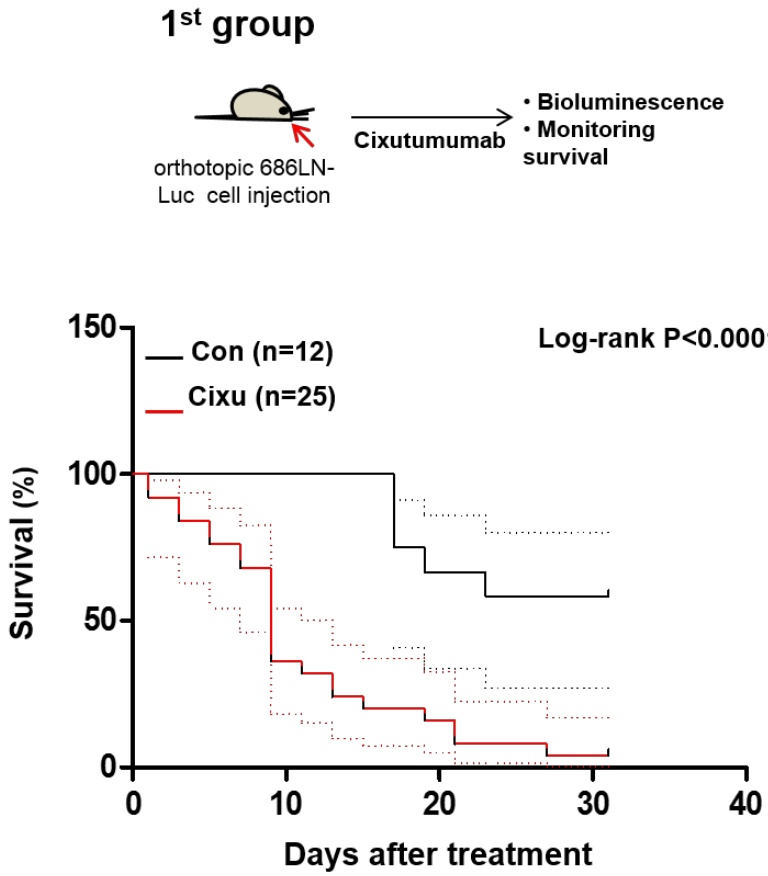

Figure 10. Survival of cixutumumab-treated mouse bearing tongue tumors.

686LN-Luc cells were orthotopically injected into NOD/SCID (for monitring survival analysis) or Balb/c nude mice (for bioluminescence imaging, n=8 per group) and the mice were treated with cixutumumab (10 mg/kg, intraperitoneally, once weekly). Left: experimental schedule. Right: survival graph with decreased survival of mice with cixutumumab treatment. P<0.0001 by two-sided Mantel-Cox log-rank test. Solid line indicates percent survival; dashed line indicates 95% confidence intervals.

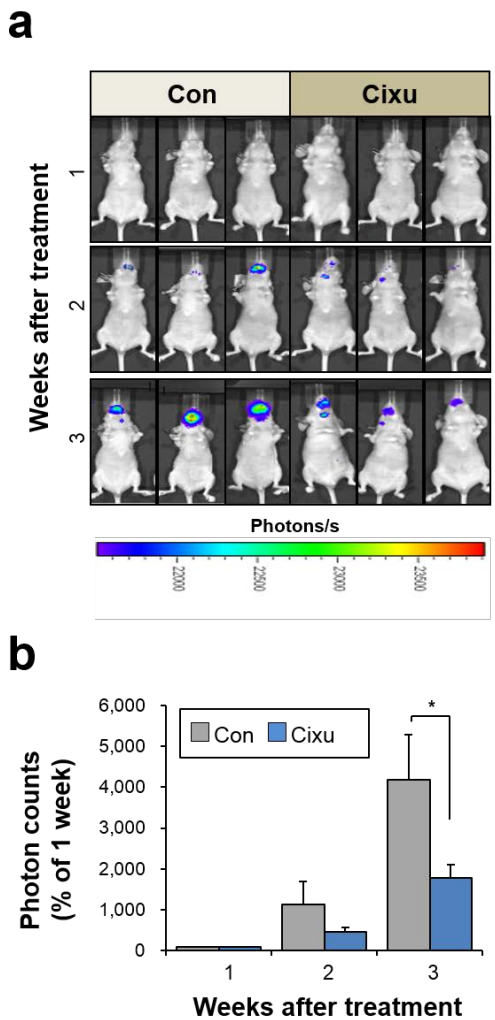

Figure 11. Effects of IGF-1R blockade to survival and tumor growth in HNSCC mouse models.

(a) Representative bioluminescence images visualizing the tumors. (b) Total photon flux of primary tumor region was quantified. Data are presented as mean relative unit of photons per second ± S.D. *P<0.05 by two-sided Stuent's t-test. Cixu, cixutumumab; Con, control.

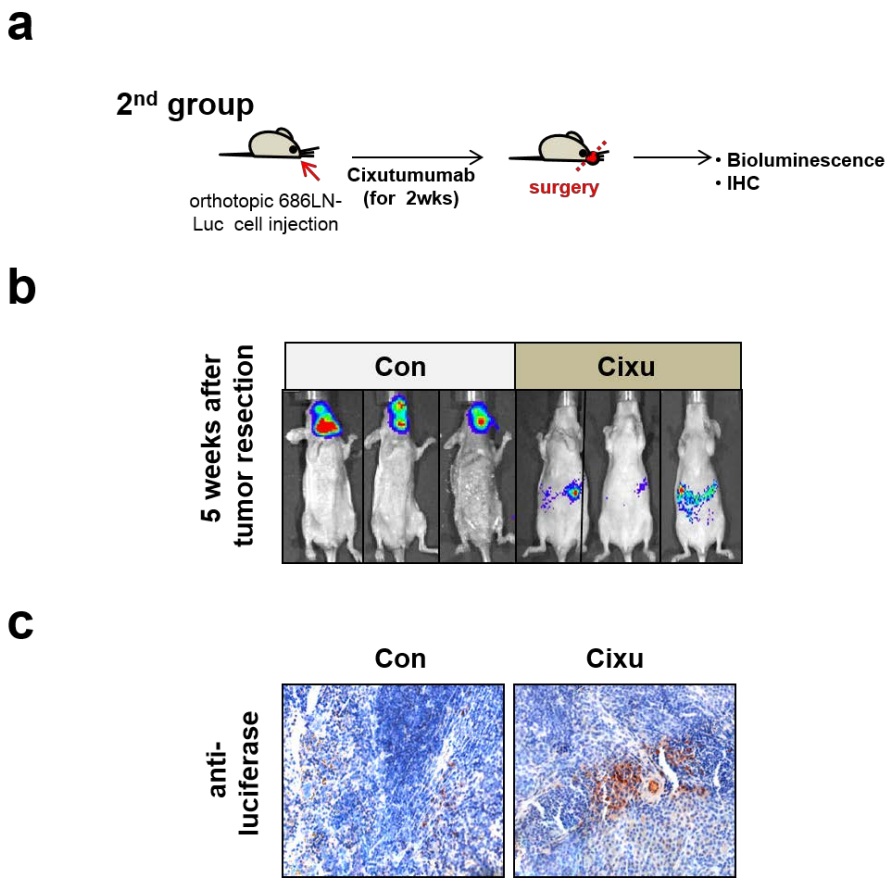

Figure 12. Effects of IGF-1R blockade to metastasis in HNSCC mouse models. (a) Two weeks after cixutumumab treatment (10 mg/kg, intraperitoneally, once weekly) of 686LN-Luc tumor-bearing Balb/c nude mice (n=10 per group), the primary tumors were surgically removed. (b) Representative bioluminescence images visualizing the tumors are shown. (c) Excised spleen was immunostained with anti-luciferase antibody to confirm the metastatic tumors derived from 686LN-Luc cells. Cixu, cixutumumab; Con, control.

1.4. Increased metastasis by cixutumumab treatment in humanized mice with orthotopic breast tumors models

Nude or NOD/SCID mice are immune-compromised and do not represent clinical patients' condition, thus immune-competent hosts may not show the same results which are observed from previous animal experiments (Figures 5-12). To mimic clinical patients' condition, I evaluated the efficacy of cixutumumab in NOD/SCID/JAK3 null mice reconstituted with human-acquired lymphoid system. The reconstitution of human lymphoid system was accomplished by transplantation of human CD34 positive hematopoietic stem cells purified from human cord blood as described previously [77]. Flow cytometry analysis in the peripheral blood cells collected at 4 weeks after transplantation and in the splenocytes collected at the time of killing confirmed the presence of human CD45+ leukocytes (Figure 13). For the orthotopic breast tumor models, MDA231-Luc cells were injected into mammary fat pad of humanized mice and treated with cixutumumab. As with the findings in the immune-compromised mice, bioluminescence imaging and IHC analyses showed lung and lymph node metastasis in cixutumumab-treated group (Figure 14). Therefore, increased metastasis upon cixutumumab treatment was also reproduced in lung tumor models with human lymphoid system. This implies that progression of tumors in anti-IGF-1R mAb-treated mice has no relevance to anti-tumor immunity from interaction between antigen presenting cells and cytotoxic T cells. These results also mirror the low clinical efficacies of anti-IGF-1R drugs [41]. As cixutumumab showed inhibitory effects of tumor growth in NSCLC and HNSCC models, decreased survival seems to come from the increased metastasis.

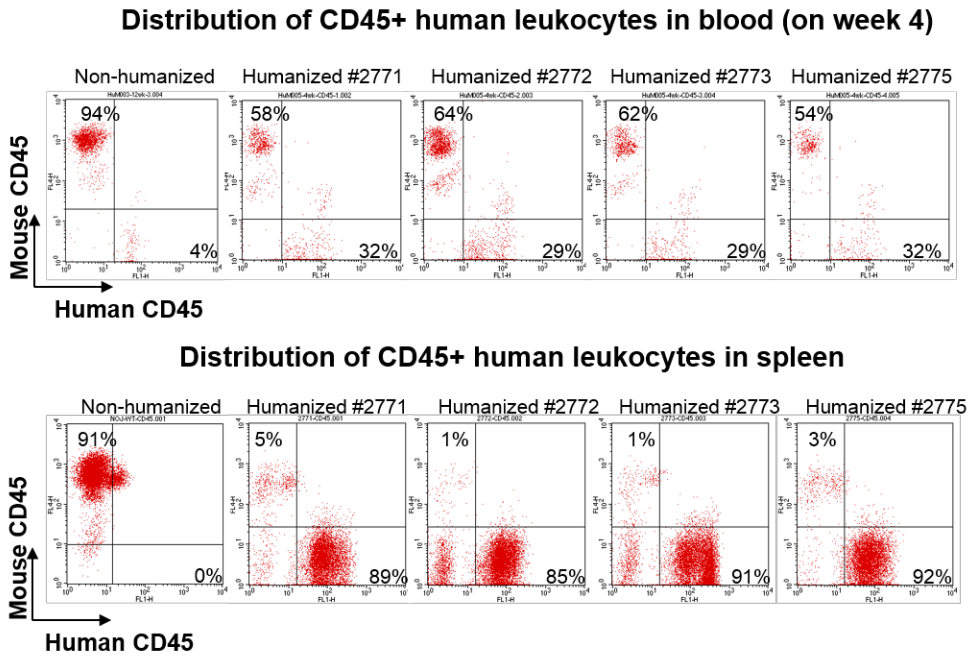

Figure 13. Reconstitution of human lymphoid system in humanized mice.

(Top) 4 weeks after the transplantation with human CD34 positive hematopoietic stem cells, peripheral blood was collected and the presence of human CD45 positive leukocytes was analyzed by flow cytometry. (a, Bottom) At the time of sacrifice, single cells were isolated from the spleen of each mouse and analyzed by flow cytometry.

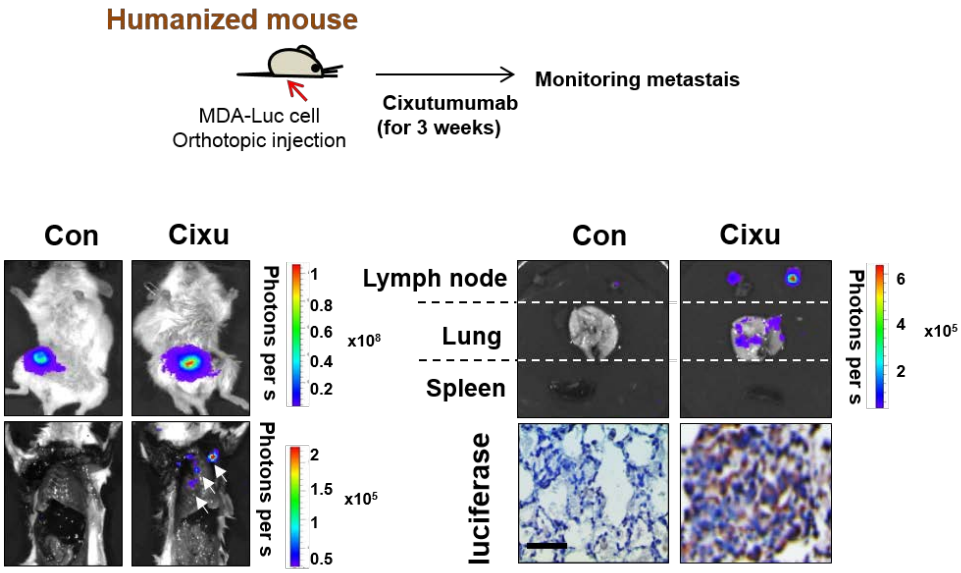

Figure 14. Increased cancer metastasis by cixutumumab in mice with human leukocytes.

MDA231-Luc cells were orthotopically injected into NOD/SCID/JAK3null mice with acquired human immune system (n=2 per group) and the mice tissues and anti-luciferase immunostaining images of excised lung. Scale bar, 50 μm; x 400 magnification. White arrows indicate luciferase signal of metastatic tumors. Cixu, cixutumumab; Con, control.

2. Alteration of TME under the IGF-1R blockade.

2.1. IGF-1R blockade does not induce aggressive phenotype of cancer cells *in vitro*.

To find out the mechanisms of increased tumor metastasis upon cixutumumab treatment, I first hypothesized that this effect was mediated by the induction of aggressive phenotype of cancer cells itself upon IGF-1R blockade. To prove this hypothesis, I treated cancer cells which were used in previous mouse models with cixutumumab and evaluate its effect on cell proliferation and migration abilities. Cixutumumab treatment of cancer cells in vitro completely abolished the IGF-1R expression (Figure 15, top) without any effects on cell proliferation (Figure 15, bottom). Treatment of cixutumumab for short term (6 days) or long term (24 days) did not induce significant changes on migration (Figure 16a) and expression of MMP genes which were known to be involved in the metastasis (MMP-2 and MMP-9; Fig. 16b) of cancer cells. It is well reported that the epithelial-mesenchymal transition (EMT) contributes to cancer cell metastasis and the emergence of drug resistance [81-85]. However, 6 and 24 days cixutumumab treatment failed to induce consistent changes in various EMT and stemness markers (E-cadherin, N-cadherin, vimentin, snail, slug, TGF-β, ABCC1, ABCG2 and ESA) in H1299 and MDA231 cells (Figure 17). Therefore, enhanced cancer metastasis by cixutumumab may not arise from change of cancer cells' aggressiveness upon IGF-1R blockade.

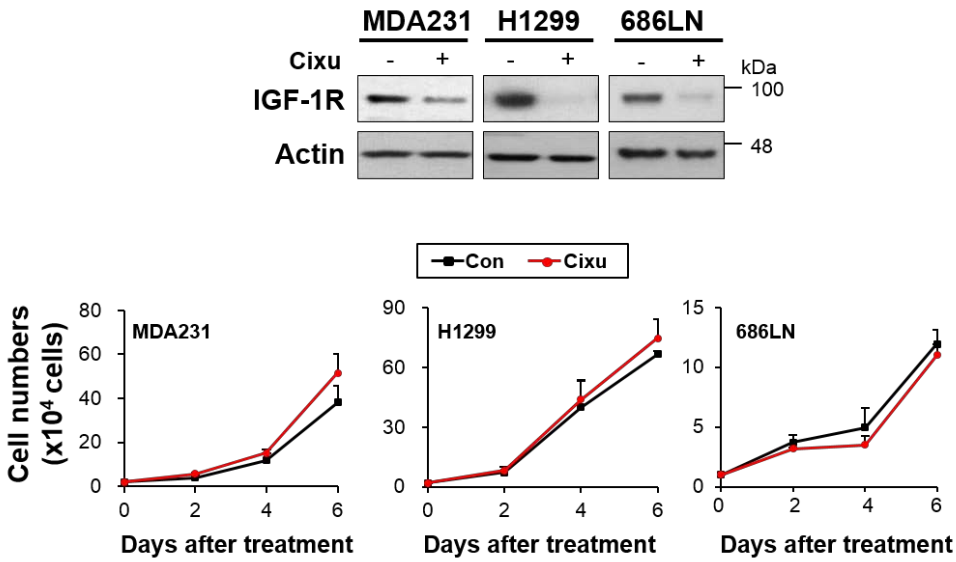

Figure 15. Proliferation of cancer cells under the cixutumumab treatment.

(a, Top) Each cancer cells were treated with cixutumumab for six days, and protein expression of IGF-1R was examined by Western blotting. (a, Bottom) Cell numbers were counted on 2, 4, 6 days treatment of cixutumumab. Value indicate the mean ± S.D.

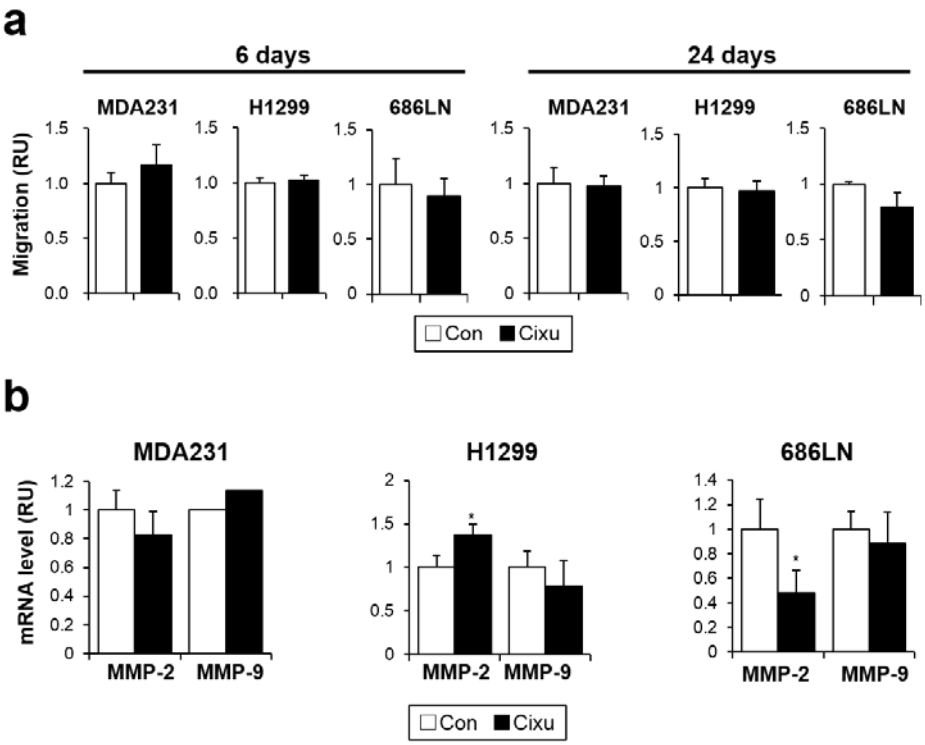

Figure 16. Migration of cancer cells under the cixutumumab treatment.

(a) Migration assay using transwell. Cancer cells were treated with cixutumumab for 6 or 24 days and seeded in the upper well and incubated in conditioned media from NIH3T3 cells for 16-20 h. Each bar represents the mean relative unit (RU) ± S.D of three identical wells of a single representative experiment. (b) mRNA levels of MMP-2 and MMP-9 in cixutumumab treated cancer cells were analyzed by real-time PCR. Cixu, cixutumumab (25 μg/ml); Con, control.

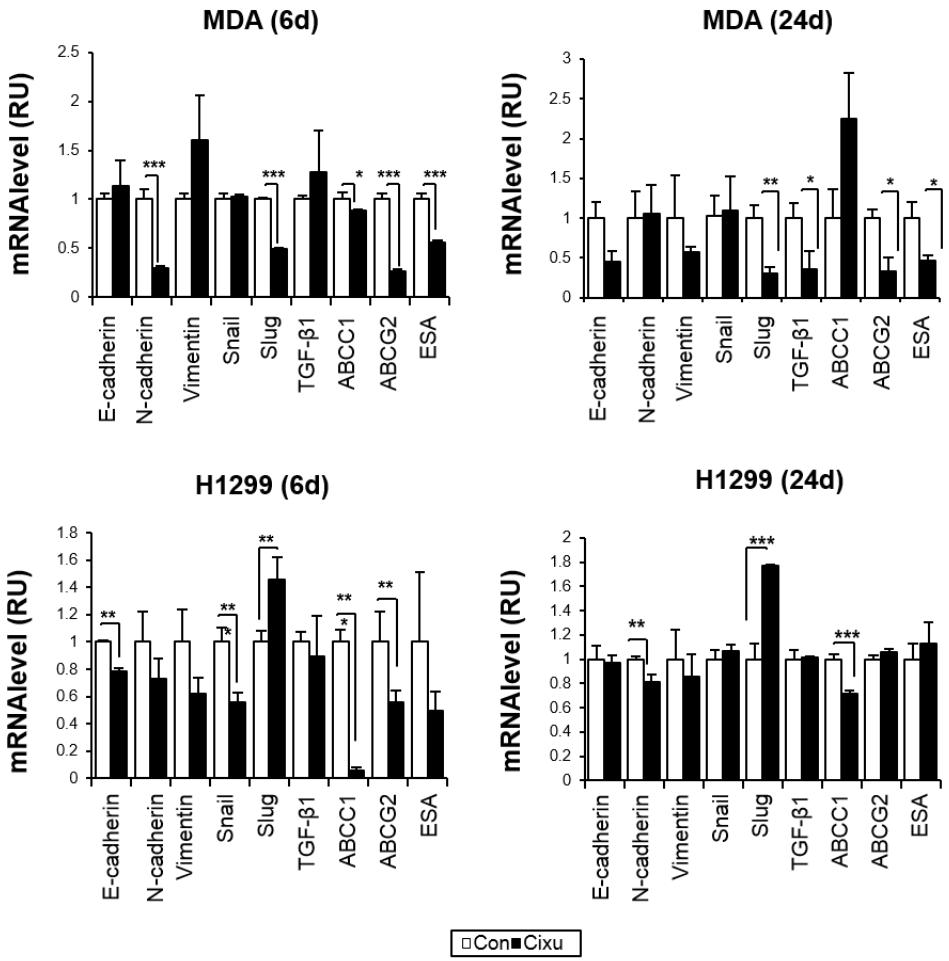

Figure 17. Cixutumumab-induced transcriptional changes of EMT and cancer stemnesss markers.

H1299 and MDA231 cells were treated with cixutumumab for 6 or 24 days, and the expression of each marker genes was determined by real-time PCR. Each bar represents the mean relative unit (RU) ± S.D of three identical wells of a single representative experiment. *P<0.05, **P<0.01, and ***P<0.001 by two-sided Student's t-test. Cixu, cixutumumab (25 μg/ml); Con, control.

2.2. The IGF-1R blockade alters infiltration of stromal cells into tumors.

For the failure of cixutumumab in inducing direct changes on cancer cells' phenotypes, it was hypothesized that IGF-1R blockade may alter the TME to tumor-promoting environment. Contribution of stromal cells, including TAM, CAF, endothelial cells, and other stromal cells to cancer progression has been reported by previous studies [63, 64, 86]. Therefore I analyzed the infiltration of each stromal cells by IHC for each representative marker with primary tumor tissue from each mouse model experiments. In the primary tumor tissue from mouse bearing orthotopically injected MDA231 cells, cixutumumab treatment revealed increased infiltration of VEGFR positive VE cells, CD45 positive leukocytes, F4/80 or Iba positive macrophages and fibroblast specific protein 1 (FSP-1) positive cancer-associated fibroblasts (Figure 18). Primary lung tumors from nude mice bearing orthotopically injected H1299 cells also showed increased infiltration of macrophages, VE cells, fibroblasts in drug treated group (Figure 19a), which means infiltration of stromal cells is not cell-specific events. Moreover, humanized mice which are closer to the patients' condition showed similar enhanced infiltration of each stromal cells by cixutumumab treatment (Figure 19b). These results implies that cixutumumab induces infiltration of stromal cells, facilitating cancer metastasis.

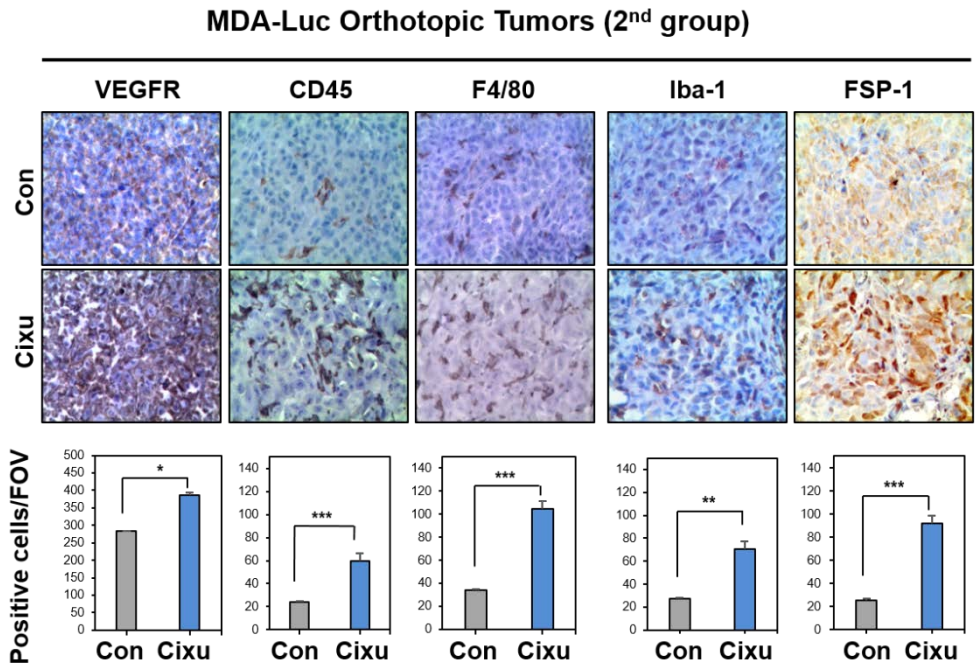

Figure 18. Effects of cixutumumab on stromal cell recruitment in MDA-Luc orthotopic tumors.

Excised primary injected tumors from MDA231-Luc orthotopic tumor models were immunostained with several antibodies to verify the recruitment of endothelial cells (anti-VEGFR), leukocytes (anti-CD45), macrophages (anti-F4/80, anti-Iba-1), and fibroblasts (anti-FSP-1) in mammary fat pad. Each bar on the graph below indicates the number of positive cells per field of view (FOV). *P < 0.05, **P < 0.01, and ***P < 0.001 by two-sided Student's t-test. Cixu, cixutumumab; Con, control.

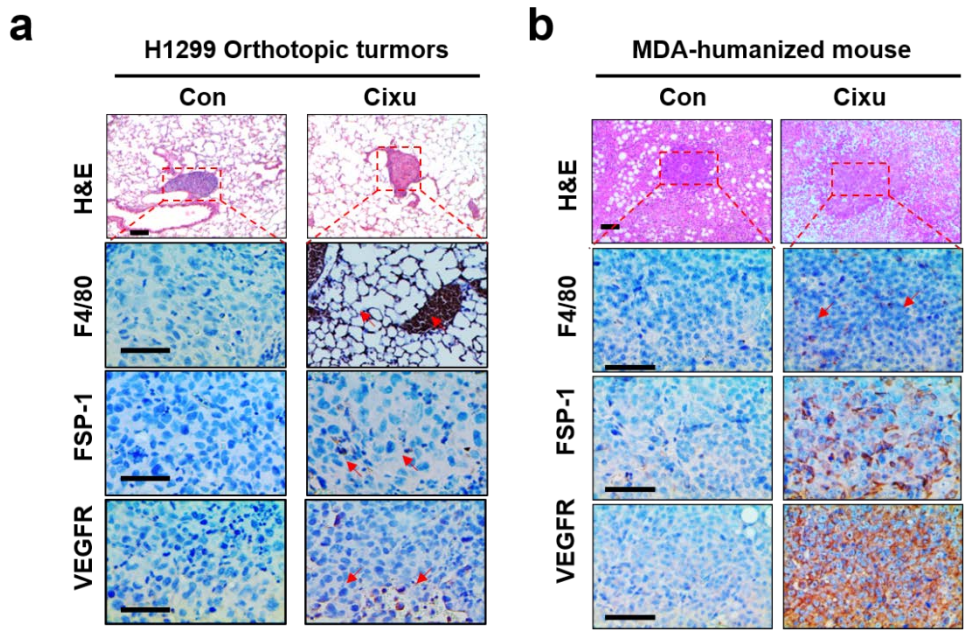

Figure 19. Effects of cixutumumab on stromal cell recruitment in H1299-Luc orthotopic tumors and MDA-humanized mouse tumors.

(a) Representative H&E staining and immunostaining images of excised primary lung tumors from H1299 orthotopic tumor models. (b) Representative H&E staining and immunostaining images of excised primary injected tumors from humanized mouse model. Red arrows indicate stained cells. Scale bar: 100 μm for H&E staining, 50 μm for immnunostaining, 400x magnification, Cixu: cixutumumab; Con: control.

3. IGF-1R blockade stimulates tumor angiogenesis through fibroblast and macrophages.

3.1. IGF-1R blockade fails to enhance angiogenic activity of VE cells.

As IGF-1R blockade induced tumor metastasis and increased infiltration of VE cells, I hypothesized that cixutumumab stimulates tumor angiogenesis and renders cancer metastasis. First, I evaluated the direct effect of cixutumumab by treatment drug with VE cell line, HUVECs. However, IGF-1R blockade did not stimulate the migration, tube formation and proliferation of HUVECs (Figure 20a, b). Various genes involved in the angiogenesis (VEGF, VEGFR-1, bFGF, PDGF-A and PDGF-B) of HUVECs remained unchanged after the drug treatment (Figure 20c). Because IGF-1R blockade showed no effects on angiogenic ability of VE cells, I next determined whether angiogenesis is stimulated by tumor secreted pro-angiogenic factors [87, 88].

Indirect effects mediated by drug-treated cancer cells were examined by co-culture system or treatment of conditioned media from cancer cells. However, co-culture with drug-pretreated H1299 cells or conditioned media from those cells did not affect migration ability of HUVECs (Figure 21a). Consistently, the gene expression of the aforementioned angiogenic factors was not significantly increased in the cixutumumab-treated cancer cells (Figure 21b). These results indicate that neither autocrine production of VE cells nor direct communication between VE and cancer cells appeared to cause the tumor angiogenesis.

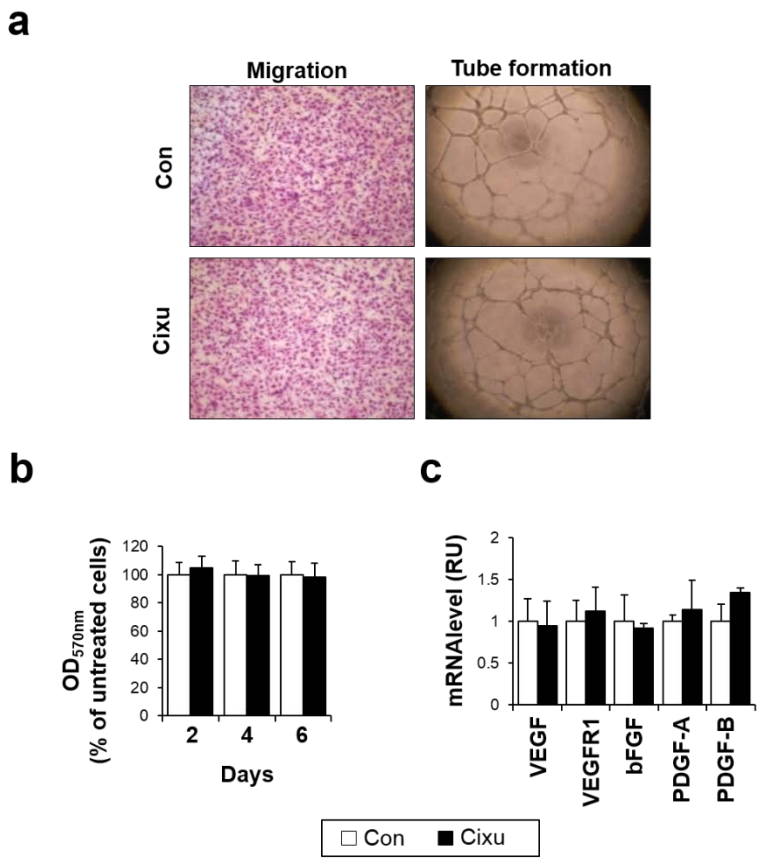

Figure 20. Direct effects of cixutumumab on HUVECs.

(a) Representative images of migration and tube formation assay of cixutumumab-treated HUVECs. (b) MTT assay for viability of HUVECs upon cixutumumab treatment. Each bar represents the mean ± S.D of five identical wells of a single representative experiment. (c) Real-time PCR analysis of angiogenic factors in HUVECs treated with cixutumumab for six days. Bars indicate the mean relative unit ± S.D of three replicates of a single representative experiment. Bars indicate the mean relative unit (RU) ± S.D of three replicates of a single representative experiment. Cixu: cixutumumab; Con: control.

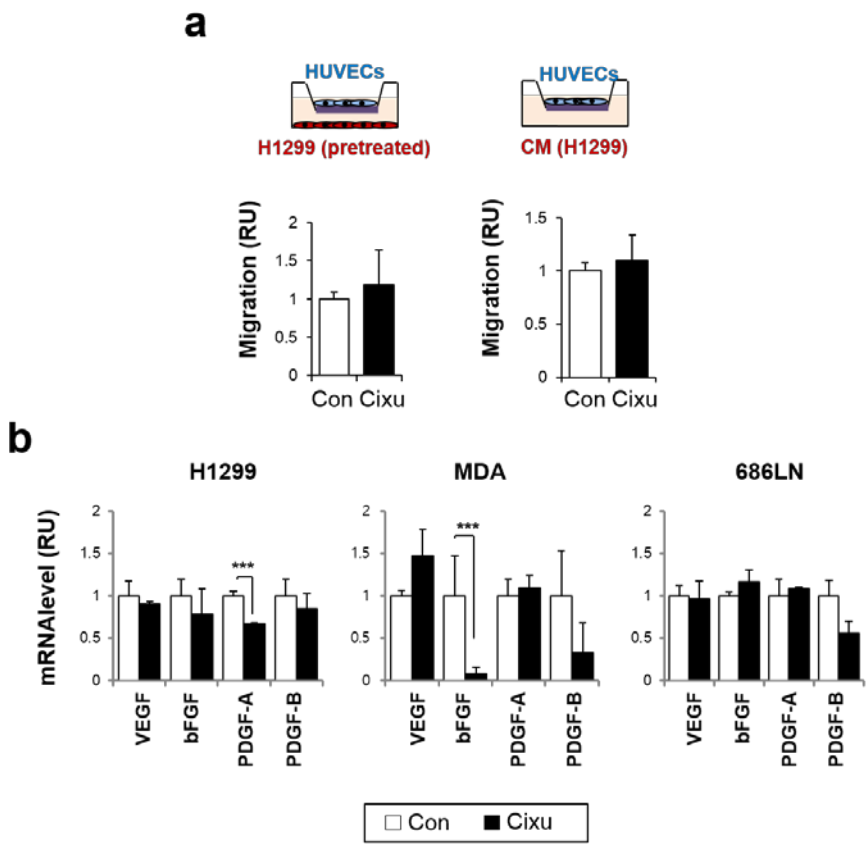

Figure 21. Effects of cixutumumab on angiogenesis-stimulating abilities of cancer cells.

(a) HUVECs were seeded in the top chamber of the transwell insert and allowed to migrate for 6 h. Left: cixutmumab-treated H1299 cells were seeded in the bottom chambers of the transwell. Right: CM from cixutumumab-treated H1299 cells were filled in the bottom chambers of the transwell. (b) Real-time PCR analysis of angiogenic factors in indicated cancer cells treated with cixutumumab for 6 days. Bars indicate the mean relative unit (RU) ± S.D of three replicates of a single representative experiment. Cixu: cixutumumab; Con: control.

3.2. IGF-1R blockade of cancer cells stimulates fibroblasts and macrophages.

Increased infiltration of fibroblasts and macrophages was observed in the primary tumor tissue treated with cixutumumab (Figure 18 and 19). As IGF-1R blockade showed no effects on VE cells, analysis was then carried out on the effects on these cells. First, I evaluated the direct effects of cixutumumab on proliferation and migration of fibroblast cell line (Wi38) and monocyte cell line (THP-1). MTT or MTS assay for each cell line revealed no significant effects on cell proliferation of Wi38 and THP-1 cells (Figure 22a). Cixutumumab-treated Wi38 and THP-1 cells' migration activities remained same in transwell migration assay (Figure 22b).

To analyze the indirect effects of cixutumumab mediated by cancer cells, I co-cultured H1299 cells and Wi38 or THP-1 cells in transwell. As a results, Wi38 and THP-1 cells migrate toward cixutumumab-pretreated H1299 cells, whereas the cixutumumab-pretreated stromal cells had a minimal impact on H1299 cell migration (Figure 23a). CM from cixutumumab-treated cancer cells, including H1299, MDA231 and 686LN cells also increased the migration of Wi38 and THP-1 cells compared with CM from untreated cancer cells (Figure 23b). To test whether this effect is limited to pharmacological ablation of IGF-1R by mAbs, I treated CM from H1299 cells with impaired expression of IGF-1R by shRNA and observed the similar effects of CM from drug-treated cancer cells (Figure 23c). Thus, ablation of IGF-1R in cancer cells affects migration of fibroblasts and monocytes.

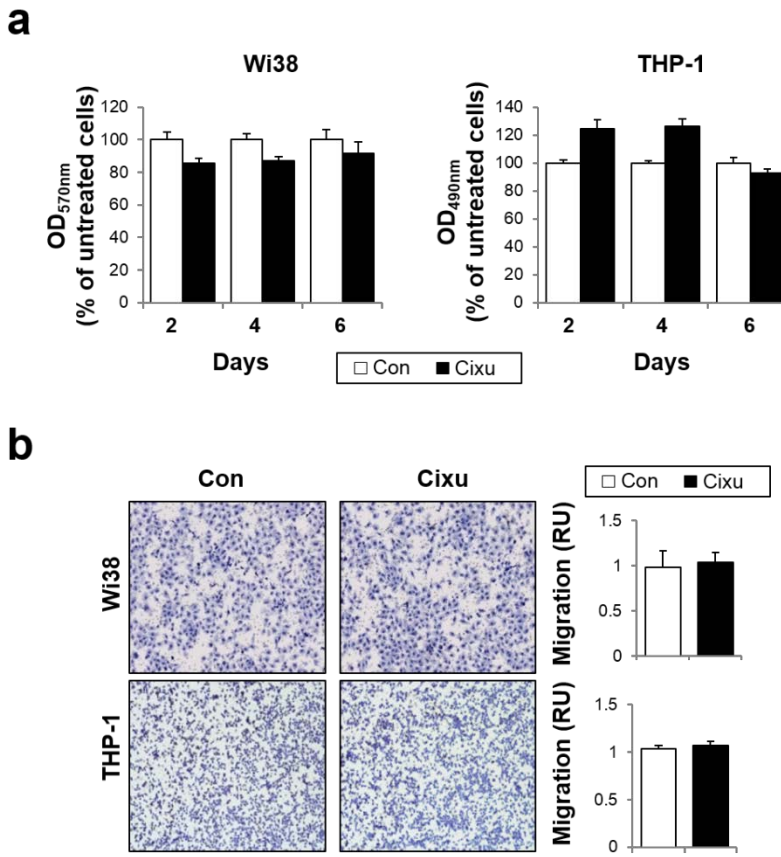

Figure 22. IGF-1R blockade in fibroblasts and monocytes does not affect proliferation and migration.

(a) MTT (Wi38) and MTS (THP-1) assays using cixutumumab-treated cells. Each bar represents the mean ± S.D of five identical wells of a single representative experiment. (b) Indicated cells were treated with cixutumumab for 6 days, and migration ability was determined by transwell migration assay. Left: Representative images of the migration assay for each cell type. Right: Each bar represents the mean relative unit (RU) ± S.D of three identical wells of a single representative experiment. Cixu: cixutumumab (25 μg/ml, six days for cell treatment); Con: control.

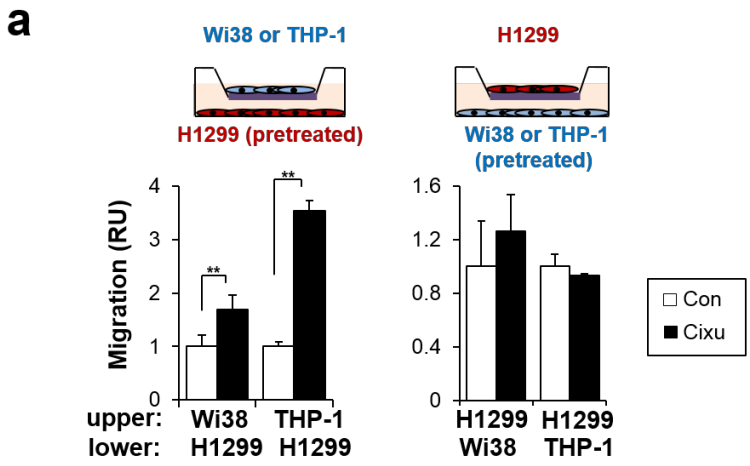
a
Wi38 or THP-1
H1299 (pretreated)
H1299
Wi38 or THP-1
(pretreated)
Migration (RU)
upper:
lower:
Wi38
H1299
THP-1
H1299
H1299
Wi38
H1299
THP-1
Con
Cixu

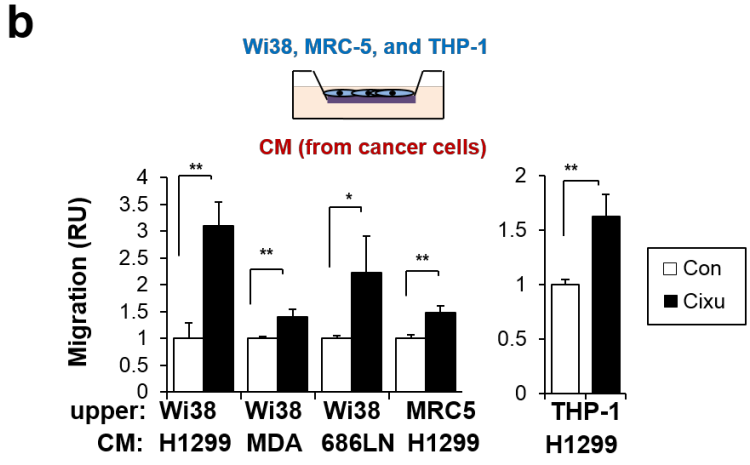
b
Wi38, MRC-5, and THP-1
CM (from cancer cells)
Migration (RU)
upper:
CM:
Wi38
H1299
Wi38
MDA
Wi38
686LN
MRC5
H1299
THP-1
H1299
Con
Cixu

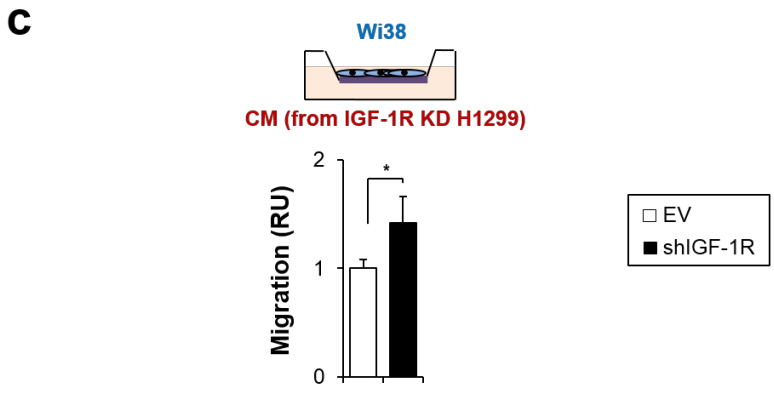
c
Wi38
CM (from IGF-1R KD H1299)
Migration (RU)
EV
shIGF-1R

Figure 23. IGF-1R impaired cancer cells enhance migration of fibroblasts and monocytes.

(a) Co-culture of cancer cells and stromal cells. Left: Wi38 or THP-1 cells were seeded in the top chamber of the transwell insert. Cixutumumab-treated H1299 cells were seeded in the bottom chambers of the transwell. Indicated stromal cells were allowed to migrate for 16-20 h. Right: H1299 cells were seeded in the top chamber of the transwell insert. Cixutumumab-treated Wi38 or THP-1 cells were seeded in the bottom chambers of the transwell. H1299 cells were allowed to migrate for 16 h. (b) Wi38, MRC-5 and THP-1 cells were seeded in the top-chamber of the transwell insert. The bottom chambers were filled with CM from cixutumumab-treated cancer cells. Cells of upper wells were allowed to migrate for 16-20 h. (c) The bottom chambers were filled with CM from H1299 cells with reduced IGF-1R expression. Wi38 cells were seeded in the top-chamber of the transwell insert and allowed to migrate for 16 h. Each bar represents the mean relative unit (RU) ±SD of three or four identical wells of a single representative experiment. *$P < 0.05$, and **$P < 0.01$ by two-sided Student's t-test. Cixu: cixutumumab (25 μg/ml, six days for cell treatment); Con: control.

3.3. Interaction between cixutumumab-treated cancer cells and stromal cells induced tumor angiogenesis.

From several co-culture assays, it was figured out that IGF-1R blocked cancer cells induce migration of fibroblast and macrophages not the VE cells, suggesting that the stromal cells recruited in the TME potentially could have influenced VE cells. Indeed, Wi38 cells exposed to cixutumumab-treated cancer cells significantly increased HUVECs' migration and tube formation when compared with vehicle-treated control cells (Figure 24).

I further confirmed this angiogenesis-stimulating effect of interaction between cancer cells and stromal cells using isolated primary cells. Ly6G negative/CD11b positive macrophages were isolated from tumors in nude mice bearing 686LN tumors. This population highly express macrophage surface marker, F4/80, compared to the Ly6G positive/CD11b positive populations (Figure 25). When co-cultured with cixutumumab-pretreated mouse breast cancer cell line (4T1-Luc) cells, migration of the primary macrophages increased (Figure 26a), and these cells also enhanced migration of mouse endothelial cells, SVECs (Figure 26b). To test the neutralizing effect of cixutumumab in mouse cells, I treated same dose of drug with 4T1 cells and SVECs, showed degradation of IGF-1R of these cells (Figure 26c).

Collectively, these findings suggest that IGF-1R blockade can promote communication between cancer and stromal cells, thereby promoting tumor angiogenesis. Therefore, increased metastasis upon cixutumumab treatment in mouse models can be explained by indirect stimulation of VE cells for angiogenesis through the interaction between IGF-1R blocked cancer cells and fibroblasts/macrophages.

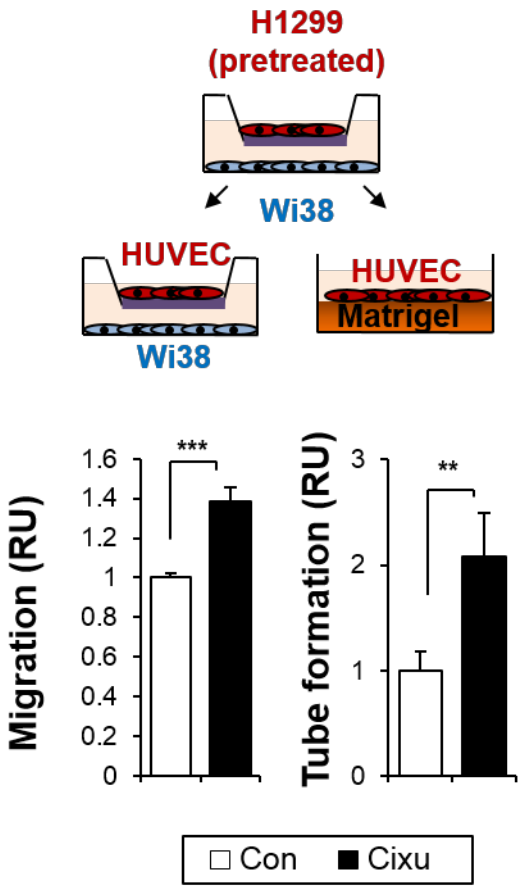

Figure 24. Cancer cells and fibroblasts communication stimulates VE cells.

Cixutumumab-treated H1299 cells were co-cultured with Wi38 cells in the transwell for 24 h. Left: HUVECs were seeded in the new top-chamber and allowed to migrate for 6 h. Right: HUVECs were seeded onto a Matrigel-coated 96 well plate, and incubated with CM from Wi38 cells for 10 h. Each bar represents the mean relative unit (RU) ±SD of three or four identical wells of a single representative experiment. **P < 0.01, and ***P < 0.001 by two-sided Student's t-test. Cixu: cixutumumab (25 μg/ml, six days for cell treatment); Con: control.

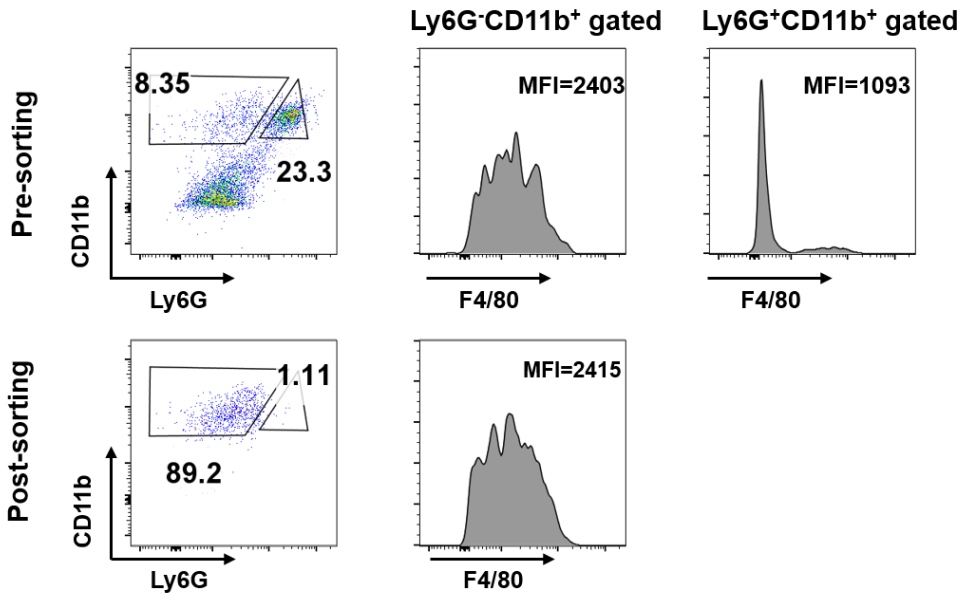

Figure 25. Isolation of primary macrophages from mouse tumor tissue.

Gating strategy of isolation of macrophages from 686LN tumor-bearing mice. Top: CD11b positive population after the MACS separation using microbeads were further sorted using flow cytometry for granulocyte marker (Ly6G) and macrophage marker (F4/80). Ly6G negative/CD11b positive cells showed increased macrophage population compared to the Ly6G positive/CD11b positive cells. Bottom: After sorting the Ly6G negative/CD11b positive cells, the purity was analyzed at the same condition and confirmed high purity consistent macrophage population. Numbers in the dot plot indicates percentage of the gated population. MFI: mean fluorescence intensity.

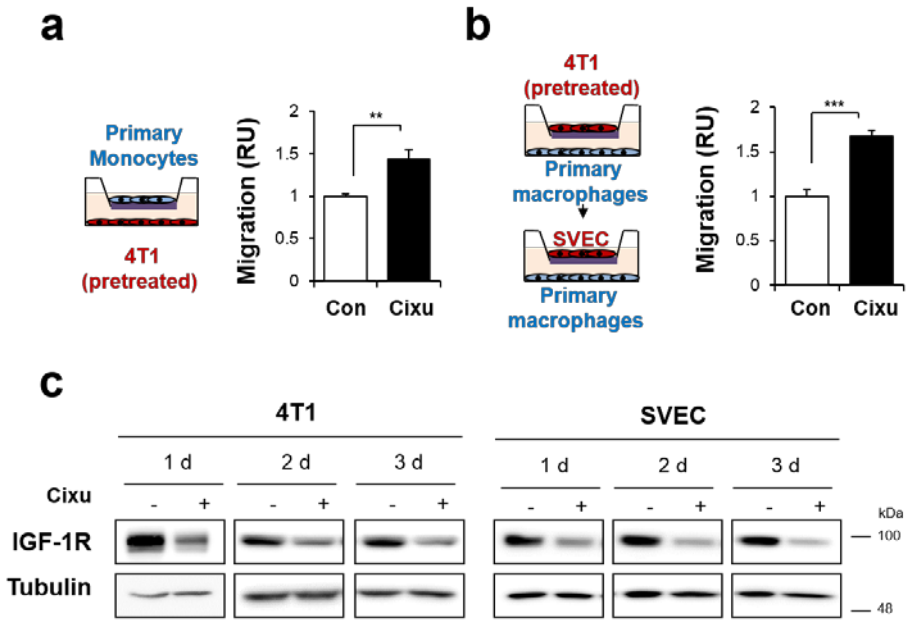

Figure 26. Increased angiogenesis by interaction between IGF-1R blocked cancer cells and isolated primary macrophages.

(a) Cixutumumab-treated 4T1-Luc cells were seeded in the bottom chambers of the transwell and primary macrophages were incubated in the top chamber of the transwell for 24 h. (b) Primary macrophages were co-cultured with cixutumumab-treated 4T1-Luc cells for 24 h. SVECs were seeded in the new top chamber and allowed to migrate for 6 h. (c) The 4T1 and SVEC cells were treated with cixutumumab for one, two and three days, and IGF-1R protein levels were determined by Western blotting. Each bar represents the mean relative unit (RU) ±SD of three or four identical wells of a single representative experiment. **P < 0.01, and ***P < 0.001 by two-sided Student's t-test. Cixu: cixutumumab (25 μg/ml, six days for cell treatment); Con: control.

4. Cancer interacts with stromal cells through IGF-2/IGF-2R pathway.

Next, I investigated the factors involved in cixutumumab-induced stromal cell recruitment. I hypothesized that the IGF axis could have contributed to the stromal cell recruitment, based on previous findings including: (1) signaling bypass through the IR in intrinsic/adaptive resistance to anti-IGF-1R therapies [46, 47], (2) counterbalance of the antiangiogenic effects of IGF-1R inhibitors via IGF-2 production [89] and (3) IGF-induced integrin-Src signalling module as a resistance mechanism against anti-IGF-1R monoclonal antibody-based anticancer therapies [49].

4.1. IGF-1R blockade activates transcription of IGF-2 in cancer cells.

To evaluate the relevance of IGF axis in resistance to anti-IGF-1R mAbs, I evaluated the mRNA expression of IGF-1, IGF-2, IGF-1R and IR under the cixutumumab treatment in cancer and stromal cell lines. Real-time PCR analysis revealed that increased IGF-2 transcription by cixutumumab treatment in cancer cells (Figure 27). Consistent protein levels of IGF-1, IR, and IGF-1R were also confirmed by western blotting in both cancer cells and stromal cell lines (Figure 28). As IGF-2 is a secreted growth factor, increased protein level of IGF-2 by cixutumumab was evaluated by western blotting of CM from cancer cells (Figure 29a). To visualize the increased production of IGF-2 upon IGF-1R blockade, cixutumumab treated cancer cells were immunofluorescence stained and confirmed increased expression of IGF-2 in cytosol area (Figure 29b). There are four promoter regions on IGF-2 gene and it has been reported that P3 and P4 driven IGF-2 mRNA level is increased in many human tumors [90, 91]. Luciferase assay also showed

greater levels of activity of IGF-2 promoters in the cixtumumab-treated cells than in vehicle-treated cells (Figure 30). Furthermore, IGF-1R shRNA-transfected H1299 cells also showed transcriptional increase in IGF-2 expression (Figure 31a). Further increase in IGF-2 secretion in cellular media was also confirmed by western blotting (Figure 31b). These data confirmed increased transcription of IGF-2 in cixutumumab-treated cancer cells, indicating that IGF-2 can be an important mediator of interaction with stromal cells.

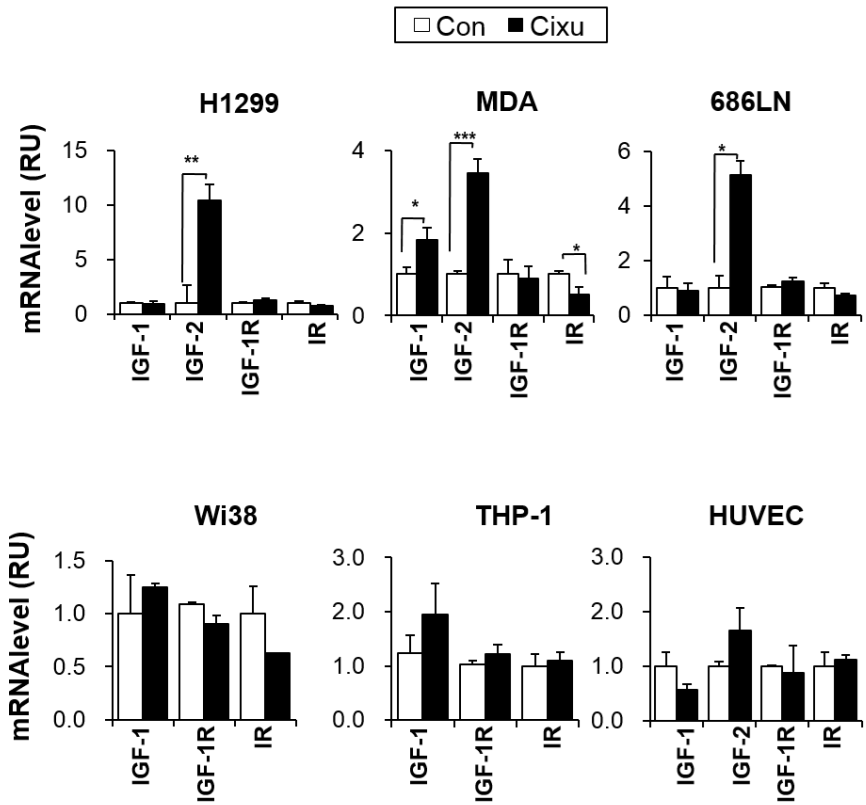

Figure 27. mRNA expression of ligand and receptor for IGF axis upon cixutumumab treatment.

Indicated cancer cells and stromal cells were treated with cixutumumab for six days (25 μg/ml) and expression of ligands and receptors of the IGF axis were determined by real-time PCR. Each bar represents the mean relative unit (RU) ±SD of three independent experiments. *P<0.05, **P < 0.01, and ***P < 0.001 by two-sided Student's t-test. Cixu: cixutumumab; Con: control.

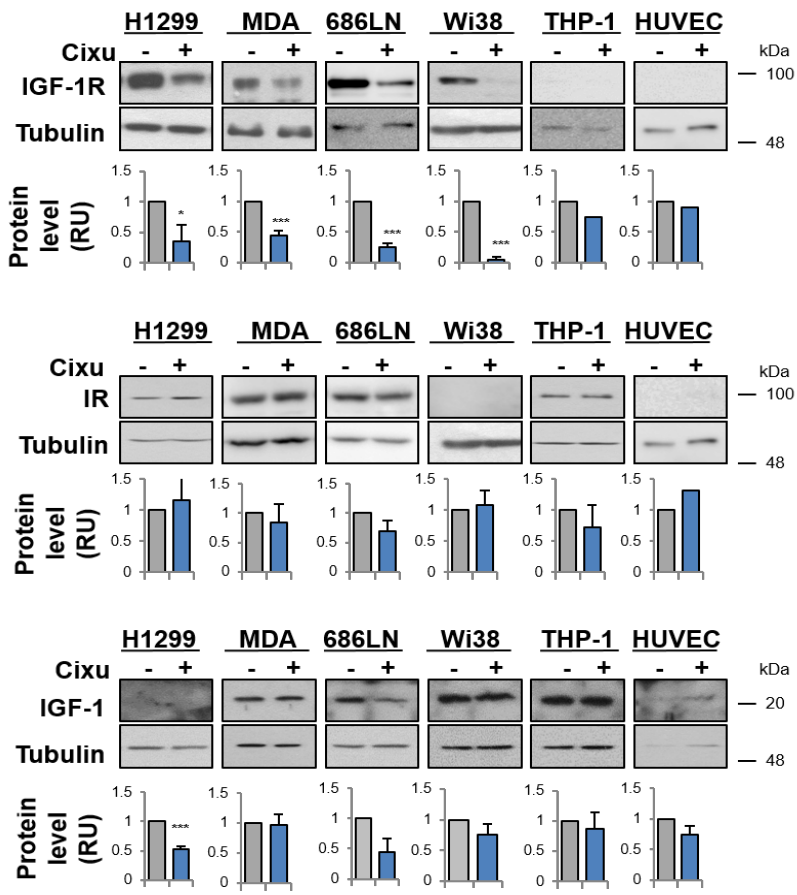

Figure 28. Protein expression of IGF-1R, IR and IGF-1 upon cixutumumab treatment.

Indicated cancer cells and stromal cells were treated with cixutumumab for six days (25 µg/ml) and western blotting for protein expression of IGF-1R, IR and IGF-1 was performed from cell lysates. Each graph below blots shows densitometric analysis quantifying the expression levels of the indicated proteins. Each bar represents the mean relative unit (RU) ±SD of three independent experiments. ***P < 0.001 by two-sided Student's t-test. Cixu: cixutumumab; Con: control.

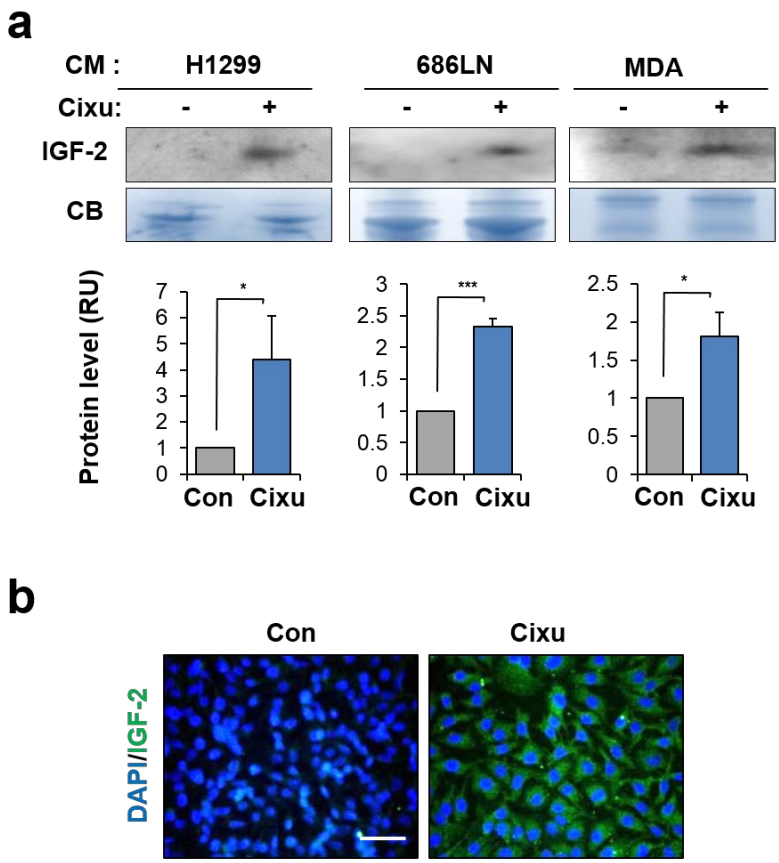

Figure 29. Increased IGF-2 production of cixutumumab-treated cancer cells.

(a) CM from cixutumumab-treated cancer cells were analyzed by Western blotting to confirm IGF-2 secretion during cixutumumab treatment. Lower blots present Coomassie Blue staining as a loading control. Graph below shows densitometric analysis of three independent Western blot assays. (b) IGF-2 immunofluorescence staining in cixutumumab-treated MDA231 cells (Scale bar: 10 μm 400x magnification). *P<0.05 and ***P < 0.001 by two-sided Student's t-test. Cixu: cixutumumab (25 μg/ml, six days); Con: control.

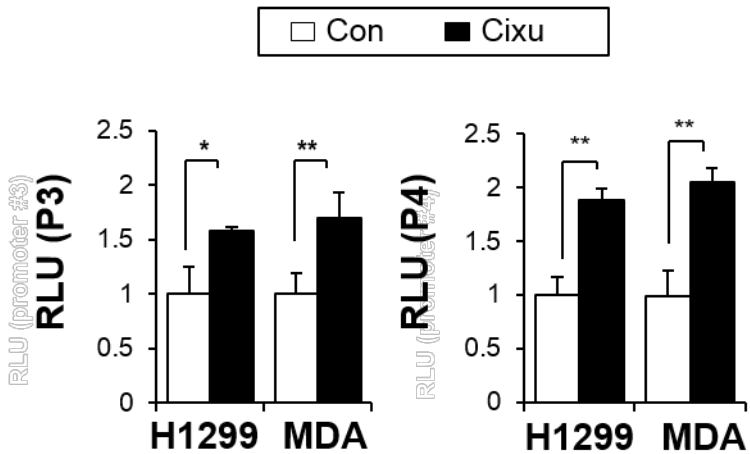

Figure 30. IGF-2 promoter activities of IGF-1R blocked cancer cells.

Indicated cells were treated with cixutumumab for six days (25 μg/ml), and each promoter activity was determined by luciferase assay. Left: P3 promoter, Right: P4 promoter. The values indicate the mean relative luciferase unit (RLU) ±SD. *P<0.05 and **P < 0.01 by two-sided Student's t-test. Cixu: cixutumumab; Con: control.

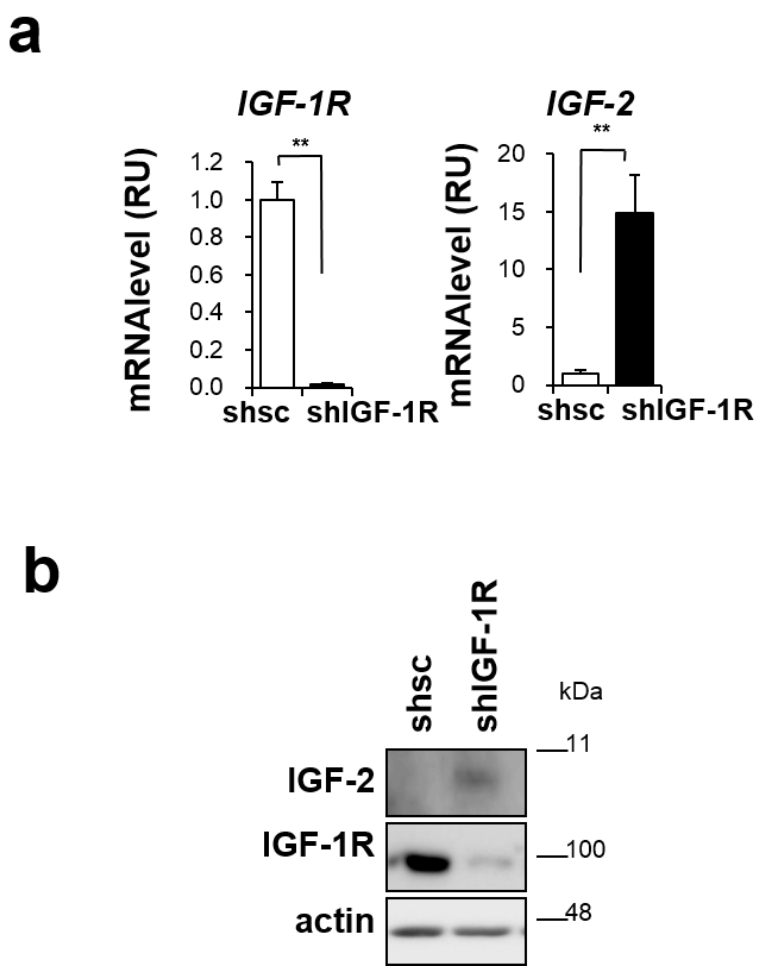

Figure 31. Expression of IGF-2 in shRNA-mediated IGF-1R knockdowned cancer cells.

(a) IGF-1R expression was stably reduced by shRNA in H1299 cells, and the expression of IGF-2 and IGF-1R was determined by real-time PCR (b) IGF-1R knockdowned cancer cell lysates were analyzed from IGF-1R expression and their CM was also analyzed for IGF-2 expression by western blotting. **P < 0.01 by two-sided Student's t-test. Sc: scramble.

4.2. IGF-2 delivers signal to stromal cells through IGF-2R.

While IGF-2 production from cixutumumab-treated cancer cells increased, HUVECs showed modest increase (Figure 27) and its mRNA level was not detectable in Wi38, MRC5 and THP-1 cells (Figure 32). Interestingly, stromal cells (Wi38, MRC5 and THP-1) that were directly recruited by drug treated cancer cells exhibited prominent IGF-2R expression when compared with HUVECs (Figure 32). Considering that cixutumumab-treated cancer cells failed to stimulate HUVECs (Figure 21), IGF-2R can be a receptor for signals from drug treated cancer cells.

I therefore assessed the role of IGF-2 and IGF-2R in cancer-stroma communication. I established IGF-2 stable knockdown H1299 cell lines using shRNA (Figure 33a) and analyzed the effect of IGF-1R blockade on their proliferation. Cell counting assay revealed that cixutumumab treatment induced a minimal change on the proliferation of IGF-2 knockdown H1299 cells (Figure 33b). In stable knockdown cells, IGF-2 transcription was not increased by cixutumumab as expectedly (Figure 34a). CM from the H1299 cells with IGF-2 knockdown was significantly less effective at inducing Wi38 and THP-1 migration than the CM from the vehicle-treated cells (Figure 34b). These results imply that increased IGF-2 upon IGF-1R blockade does not show autocrine effect of cancer cell proliferation, but affect recruitment of fibroblasts and monocytes.

Next, I established IGF-2R stable knockdown Wi38 and THP-1 cells to evaluate the role of IGF-2R in communication between cancer and stromal cells (Figure 35a). shRNA-induced knockdown of IGF-2R expression significantly suppressed the migration of Wi38 and THP-1 cells under treatment of CM from IGF-1R blocked cancer cells (Figure 35b). Therefore, these findings indicate that intercellular IGF-2/IGF-2R interactions mediate the recruitment of stromal cells by cancer cells during IGF-1R blockade.

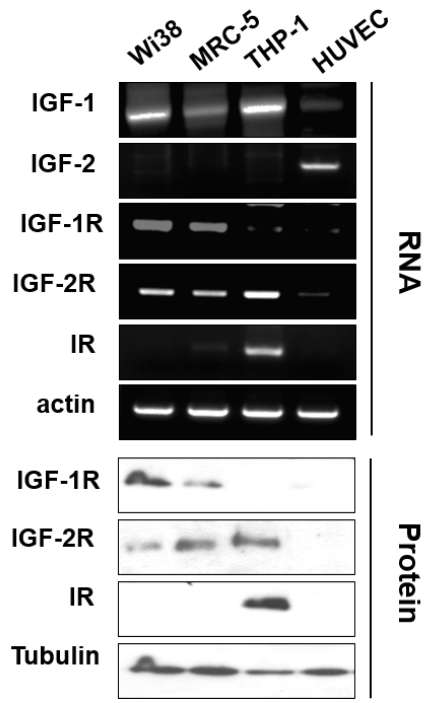

Figure 32. Expression of ligand and receptors in stromal cells.

IGF-1, IGF-2, IR, IGF-1R, and IGF-2R levels in indicated cell lines were compared by RT-PCR and western blotting.

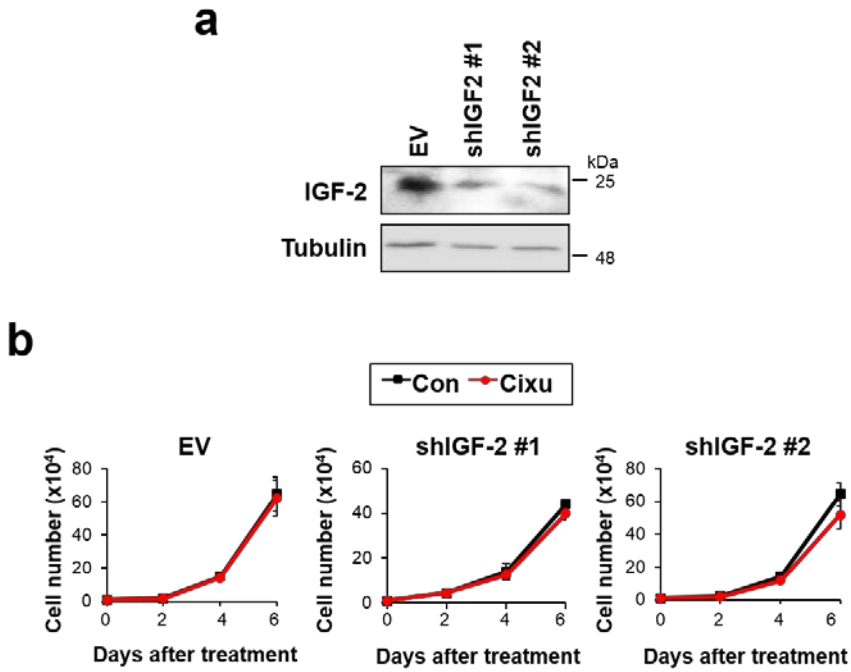

Figure 33. Proliferation of IGF-2 knockdown cells upon cixutumumab treatment.

(a) IGF-2 knock-down was confirmed by western blotting. (b) Cell proliferation assay in empty vector (EV) or shIGF-2-transfected H1299 cells treated with cixutumumab (25 μg/ml). EV: empty vector; Cixu: cixutumumab; Con: control.

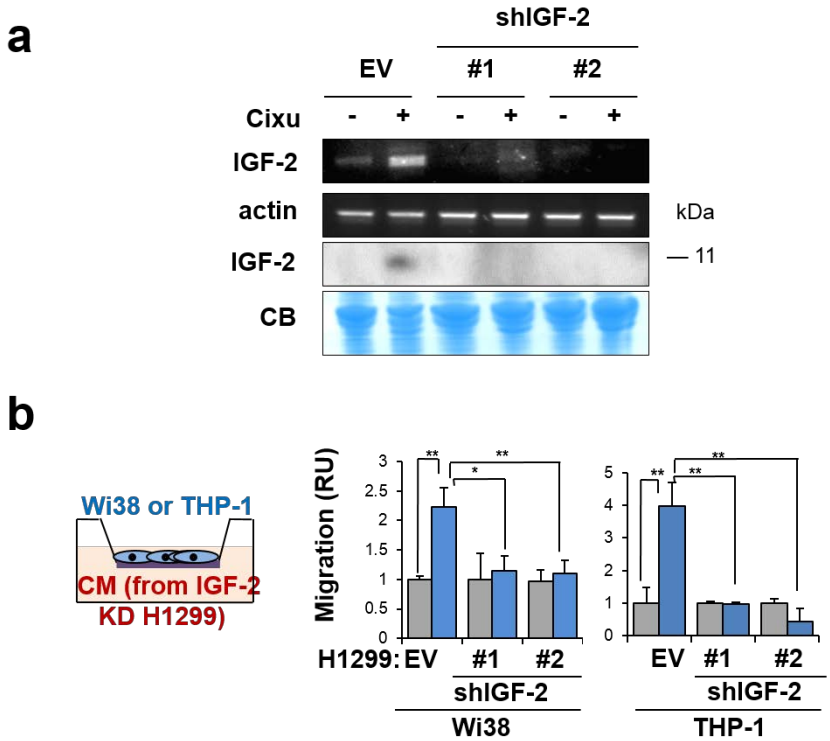

Figure 34. Role of IGF-2 in mediating communication between cancer cells and stromla cells.

(a) Empty vector (EV) or shIGF-2 transfected stable cells were treated with cixutumumab and expression of IGF-2 was determined by RT-PCR. (b) Wi38 or THP-1 cells were seeded in the top-chamber of the transwell insert. The bottom chambers were filled with CM from cixutumumab-treated H1299 cells transfected with empty vector or shIGF-2. Wi38 or THP-1 cells were allowed to migrate for 16-20 h. *P < 0.05 and **P < 0.01 by two-sided Student's t-test. RU: relative unit; EV: empty vector; Cixu: cixutumumab (25 μg/ml, six days for cell treatment); Con: control; CB: Coomassie blue staining.

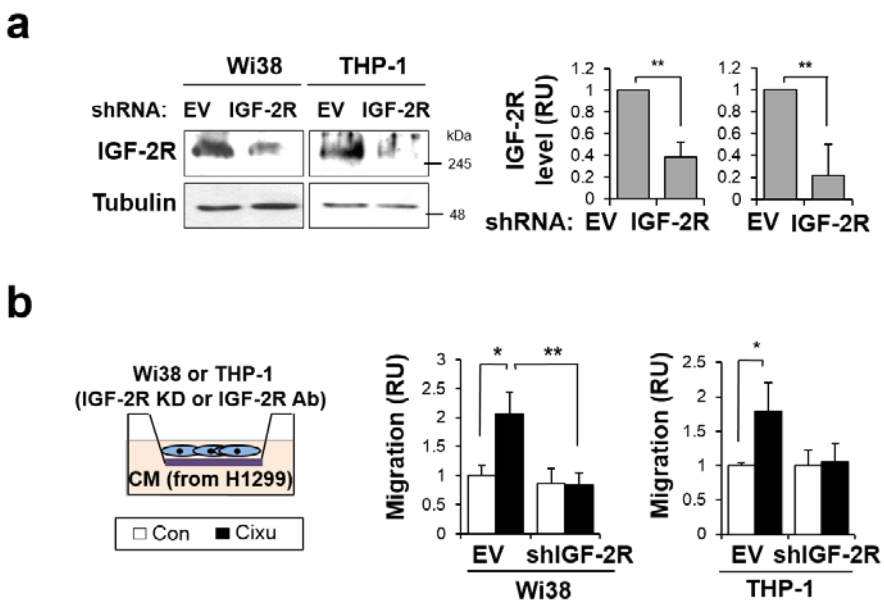

Figure 35. Role IGF-2R in mediating interaction between cancer and stromal cells.

(a) IGF-2R expression was stably reduced by shRNA in Wi38 and THP-1 cells as demonstrated by Western blotting (Left) and densitometric analysis (Right). (b) IGF-2R knockdown Wi38 or THP-1 cells were seeded in the top-chamber of the transwell insert. The bottom chambers were filled with CM from cixutumumab-treated H1299 cells. Wi38 or THP-1 cells were allowed to migrate for 16-20 h. *P < 0.05 and **P < 0.01 by two-sided Student's t-test. RU: relative unit; EV: empty vector; Cixu: cixutumumab (25 μg/ml, six days for cell treatment); Con: control.

5. Ablation of IGF-1R increases IGF-2 transcription via STAT3 activation.

5.1. IGF-1R blockade induces STAT3 phosphorylation in cancer cells.

I investigated the mechanisms that mediate the cixutumumab-induced IGF-2 transcription. By using a human phospho-receptor tyrosine kinases (RTKs) signaling array kit, it was shown that there was a markedly increased STAT3 phosphorylation at tyrosine 705 residue in cixutumumab-treated H1299 cells when compared with the control cells (Figure 36a). Increased phosphorylation of STAT3 upon cixutumumab treatment was also confirmed in MDA and 686LN cells by western blotting (Figure 36b). Consistently, shRNA-mediated IGF-1R knockdown in H1299 cells also induced increase in STAT3 phosphorylation at the same residue (Figure 37), thus indicating that IGF-1R blockade-induced STAT3 phosphorylation is not limited to anti-IGF-1R mAbs.

As STAT3 signaling pathway was reported to regulate IGF-2 gene transcription in myoblast [92], I determined the role of STAT3 in induction of IGF-2 by IGF-1R blockade by establishment of STAT3 stable knockdown cell lines (Figure 38a). In STAT3 stable knockdown cells, IGF-2 promoter activities were not increased upon cixutumumab treatment (Figure 38b). Moreover, western blot and RT-PCR analyses revealed that cixutumumab-induced IGF-2 expression were abrogated in H1299 cells in which STAT3 expression had been silenced by shRNA transfection (Figure 39). It has been reported that integrin/Src signaling is activated by cixutumumab [49], and Src activates STAT3 [93], therefore STAT3 activation during the cixutumumab treatment could have been mediated by integrin/Src signaling. Western blotting revealed that FAK was phosphorylated at tyrosine 397 in IGF-1R ablated cancer cells (Figure 40).

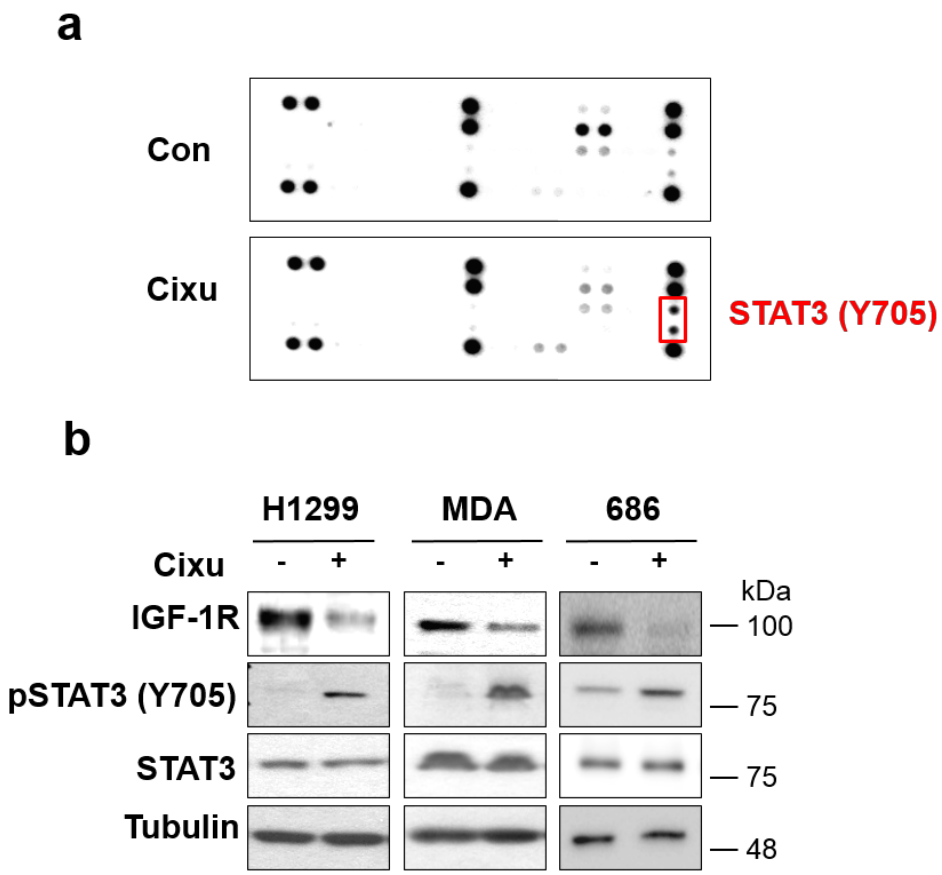

Figure 36. Cixutumumab-induced phosphorylation of STAT3 in cancer cells.

(a) Protein lysates from cixutumumab-treated H1299 cells were incubated with phospho-RTK arrays. Spots are in duplicate, with each pair corresponding to a specific phospho-RTK. The pair spots in the corners are positive controls. (b) STAT3 phosphorylation was analyzed by western blotting in cixutumumab-treated (25 μg/ml, six days) H1299, MDA231 and 686LN cell lines. Cixu: cixutumumab; Con: control.

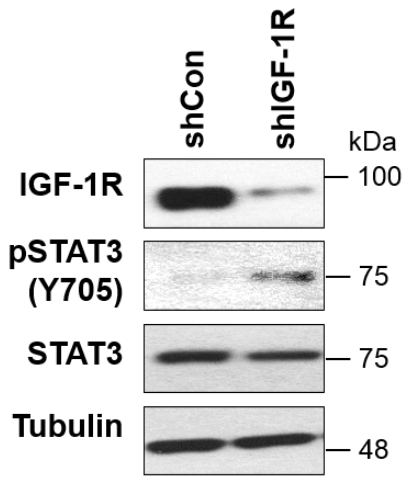

Figure 37. Loss of IGF-1R expression by shRNA increases phosphorylation of STAT3.

Expression of IGF-1R in H1299 cells were knocked down by shRNA, and phosphorylation of STAT3 was determined by western blotting. Con: control.

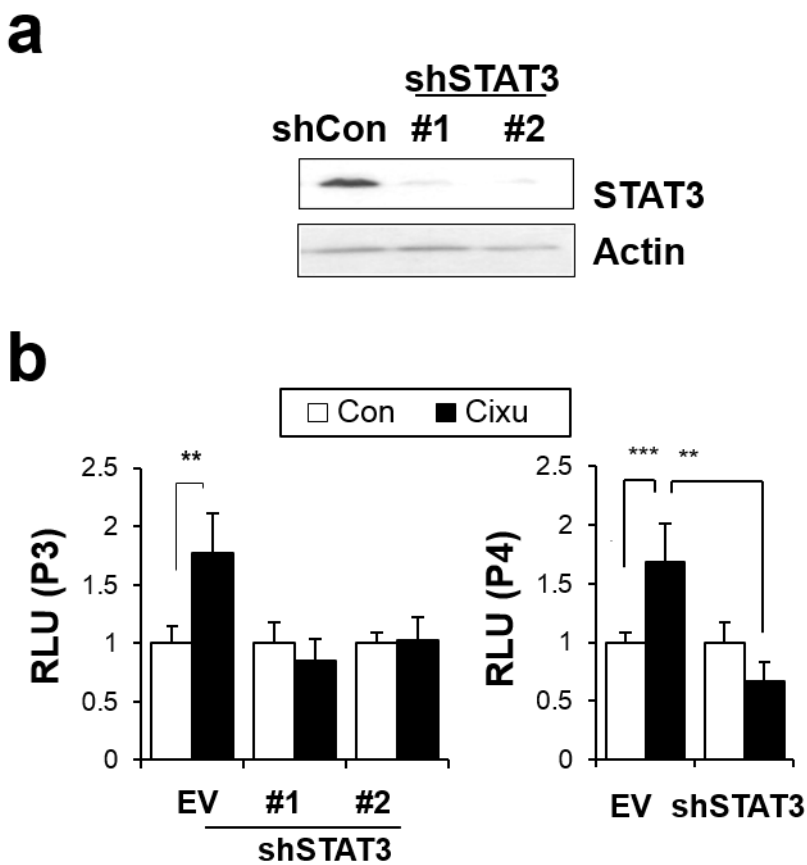

Figure 38. STAT3 regulates IGF-2 promoter activity in response to IGF-1R blockade.

(a) Knockdown of STAT3 in H1299 cells were confirmed by western blotting. (b) Luciferase assay for IGF-2 promoter activity. Left: P3 promoter. Right: P4 promoter. Each bar represents the mean relative luciferase unit (RLU) ±SD of four identical wells of a single representative experiment. **P < 0.01 and ***P < 0.001 by two-sided Student's t-test. Cixu: cixutumumab (25 μg/ml, six days); Con: control.

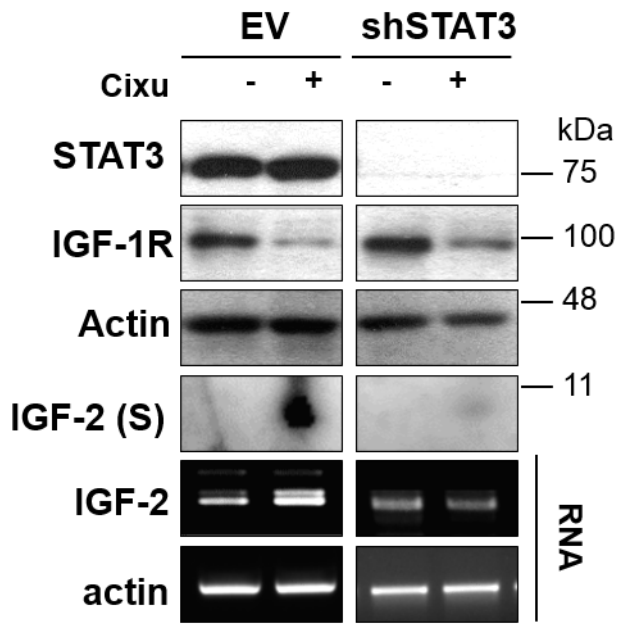

Figure 39. Transcriptional regulation of IGF-2 by STAT3 in response to IGF-1R blockade.

The effect of cixutumumab on IGF-2 expression in H1299 cells with reduced STAT3 expression was determined by RT-PCR and Western blotting. Cixu: cixutumumab (25 μg/ml, six days); Con: control.

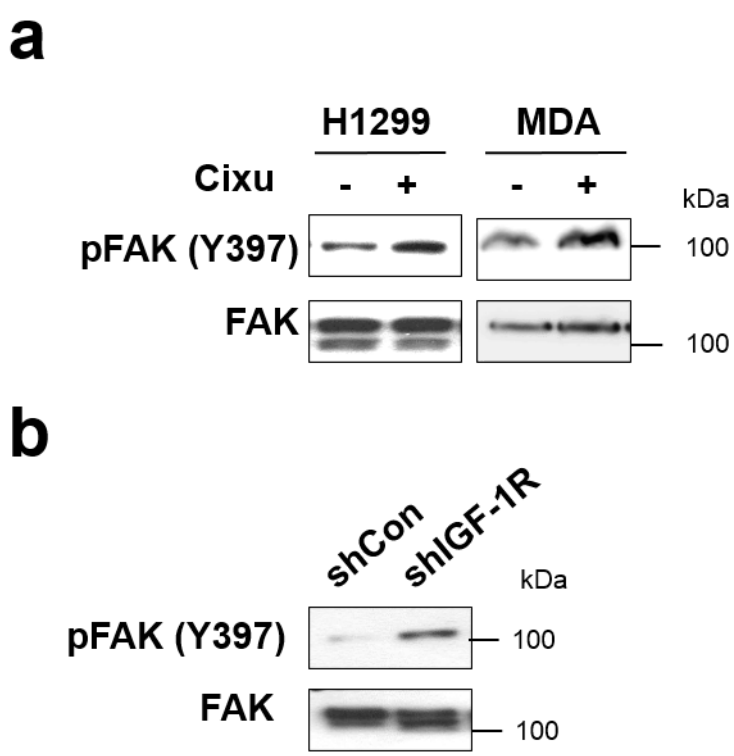

Figure 40. Phosphorylation of FAK by IGF-1R blockade.

(a) H1299 and MDA231 cells were treated with cixutumumab (25 μg/ml, six days) and phosphorylation of FAK was determined. (b) IGF-1R expression was decreased by shRNA transfection and increase in FAK phosphorylation was determined by western blotting. Cixu: cixutumumab (25 μg/ml, six days); Con: control.

5.2. STAT3 knockdown inhibits interaction between cancer and stromal cells.

To evaluate the knockdown of STAT3 on cellular behaviors, I performed several co-culture experiments and animal studies. H1299 cells with reduced STAT3 expression revealed a significantly decreased ability to recruit Wi38 cells (Figure 41a) and to mediate Wi38 cells' stimulation of HUVEC migration and tube formation (Figure 41b) on cixutumumab treatment.

I further established orthotopic breast cancer model with STAT3 knocked-down MDA231 cells. In cixutumumab-treated mice, STAT3 knockdown tumor showed decrease in mRNA and protein expression of IGF-2 (Figure 42), supporting STAT3-mediated IGF-2 transcription under IGF-1R blockade. To analyze the effect of STAT3 expression on recruitment of stromal cells, primary tumor tissues were immunofluorescence stained using anti-F4/80 antibodies for macrophages and anti-CD34 for endothelial cells. STAT3 knockdown in cancer cells showed significant decrease in infiltration of F4/80 positive macrophages and CD34 positive VE cells (Figure 43) when compared with control tumors. Collectively, STAT3 is a key player in cixutumumab-induced IGF-2 transcription, stromal cell infiltration and tumor angiogenesis.

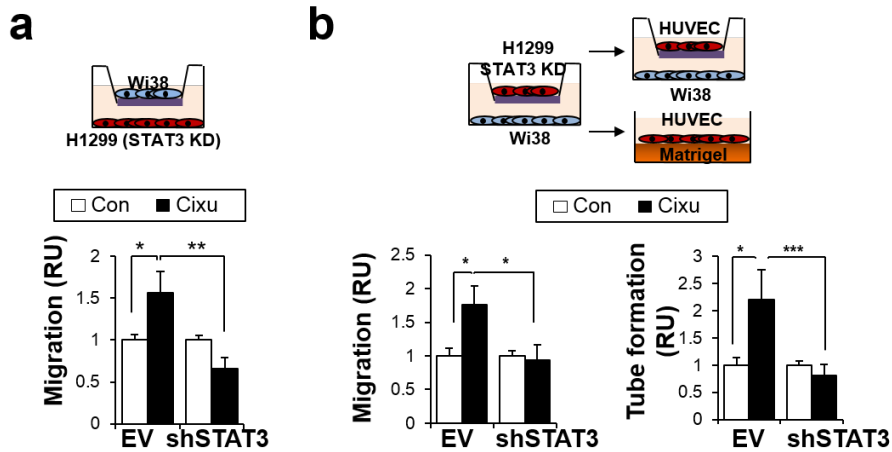

Figure 41. Effects of STAT3 knockdown in cancer cells on behaviors of stromal cells.

(a) Wi38 cells were seeded in the top-chamber of the transwell insert. Cixutumumab-treated H1299 cells transfected with empty vector or shSTAT3 expression were seeded in the bottom chambers of the transwell. Wi38 cells were allowed to migrate for 16 h. (b, Left) Empty vector- or shSTAT3-transfected H1299 cells were treated with cixutumumab and co-cultured with Wi38 cells in the transwell. After 24 h, HUVECs were seeded in the new top-chamber insert, and cell migration was analyzed after 6 h. (b, Right) HUVECs were seeded onto Matrigel, and incubated with media from Wi38 cells for 10 h.

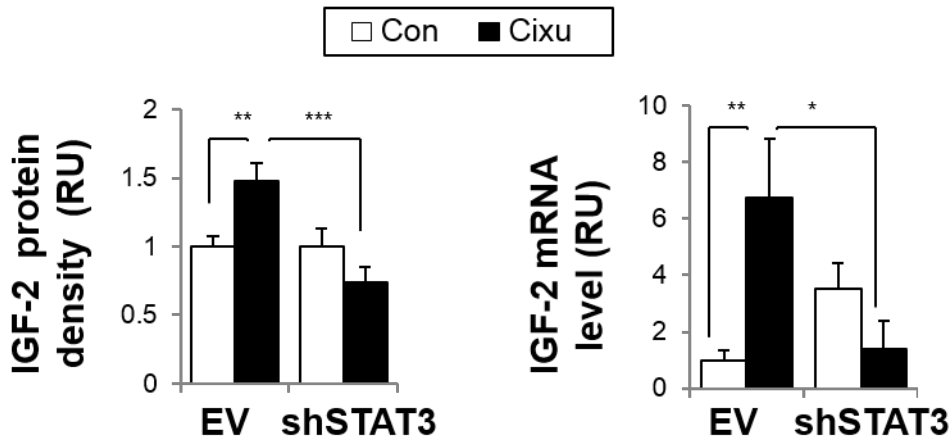

Figure 42. Expression of IGF-2 in STAT3 knockdown tumors upon cixutumumab treatment.

MDA231 cells stably transfected with either an empty vector or an expression carrying shSTAT3 were mixed with Wi38 cells (ratio 2:1), orthotopically injected into BALB/c-nude mice (n=3-5 per group), and treated with cixutumumab (10 mg/kg, intraperitoneally, once weekly) for five weeks. IGF-2 expression in the excised primary tumors was assessed by real-time PCR (Left) and densitometric quantification of western blotting (Right). Data are presented as mean densitometric quantification of western blotting or mRNA level ± S.D. *P < 0.05, ** P< 0.01, and ***P < 0.001 by two-sided Student's t-test. RU: relative unit; FOV: field of view; EV: empty vector; Cixu: cixutumumab; Con=control.

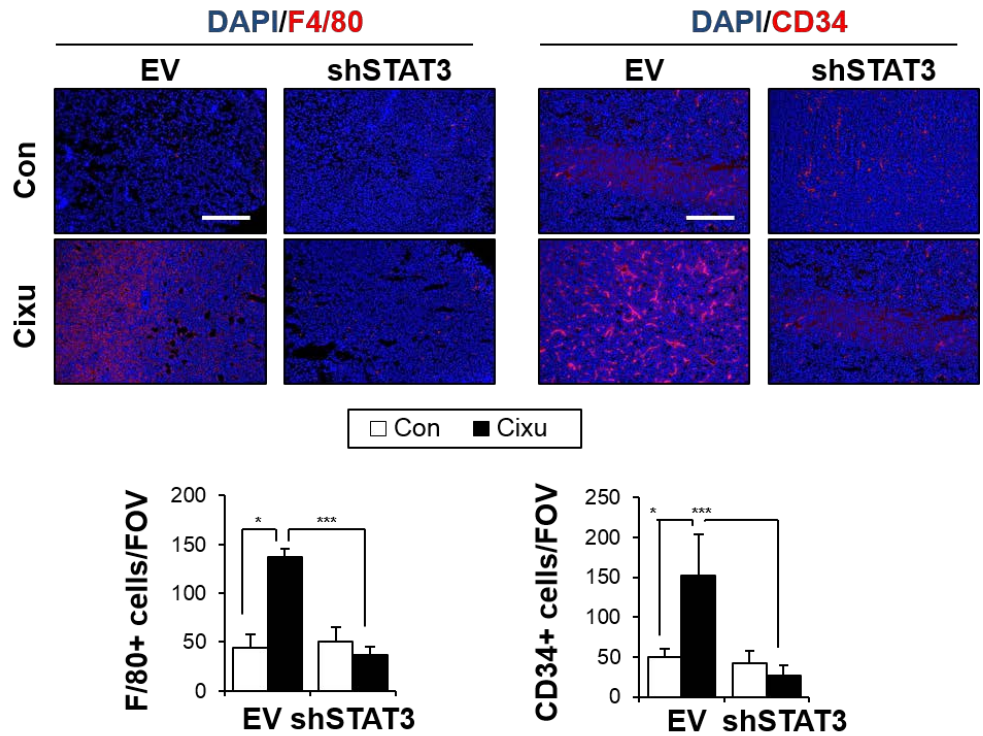

Figure 43. Response of STAT3 knockdown tumors to cixutumumab in mice.

The excised primary tumors were assessed by immunofluorescence staining using anti-F4/80 (Left) and -CD34 (Right) antibodies (Scale bar: 50 μm, 100x magnification). *P < 0.05 and ***P < 0.001 by two-sided Student's t-test. RU: relative unit; FOV: field of view; EV: empty vector; Cixu: cixutumumab; Con=control.

6. Stromal cell-derived CXCL8 stimulates tumor angiogenesis.

6.1. Increased production of CXCL8 from stromal cells upon interaction with cixutumumab-treated cancer cells.

Next step was to illuminate whether infiltrated stromal cells secrete soluble factors to recruit VE cells by analyzing Wi38 and THP-1 cells for the expression of key cytokines involved in pro-tumorigenic environment [94]. When incubated with CM from cixutumumab-treated cancer cells, Wi38 and THP-1 cells consistently increased CXCL8/IL8 transcription (Figure 44). Increase in CXCL8 transcripts was also observed in co-culture systems (Figure 45).

CXCL8 has been reported to be a small cytokine with potent chemoattractant and proangiogenic functions [95-98], and exhibit a wide range of actions on various types of cells including VE cells [64, 99, 100]. HUVECs express CXCR1 and CXCR2, and respond to CXCL8 [101, 102] and I also confirmed the HUVECs' responsiveness to CXCL8 by migration and tube formation assay (Figure 46). ELISA assay also confirmed the secretion of CXCL8 from Wi38 cells that were co-cultured with cixutumumab-treated MDA231 cells (Figure 47).

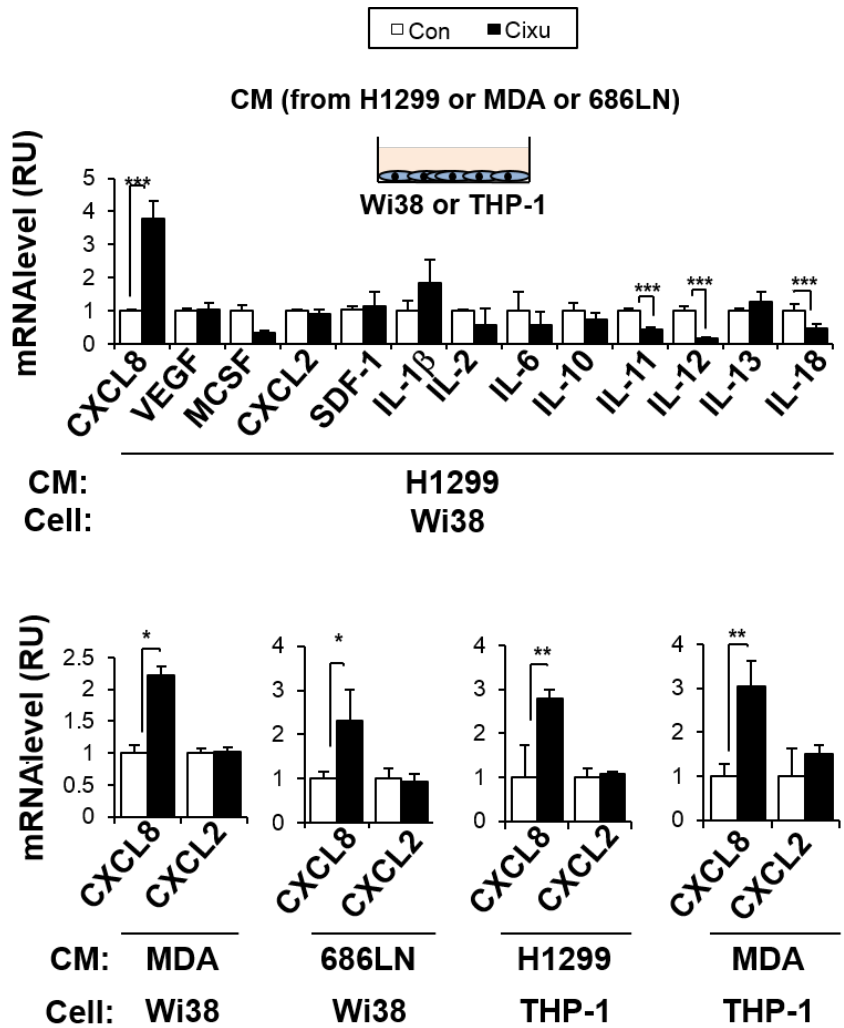

Figure 44. CM-induced CXCL8 in stromal cells.

Wi38 or THP-1 cells were serum starved for 24 h, and then stimulated with CM from cixutumumab-treated cancer cells (final concentration to 1 %). mRNA levels of several cytokines were analyzed by real-time PCR analysis. *P < 0.05, ** P< 0.01, and ***P < 0.001 by two-sided Student's t-test. RU: relative unit; Cixu: cixutumumab (25 μg/ml, six days for cell treatment); Con=control.

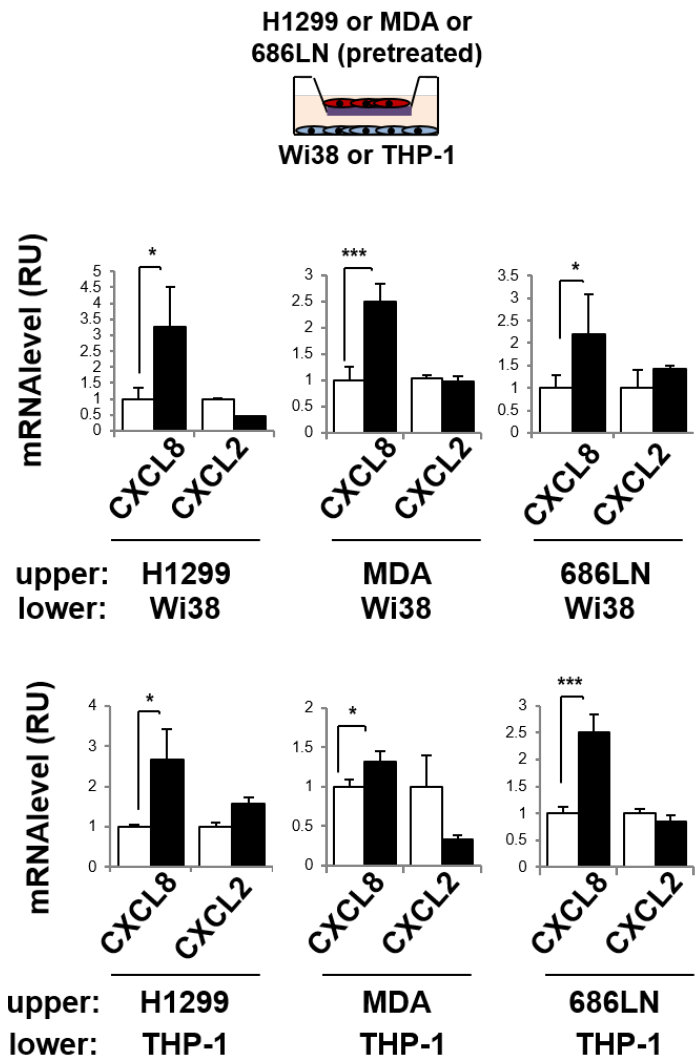

Figure 45. Coculture-induced CXCL8 in stromal cells.

Wi38 or THP-1 cells were co-cultured with cixutumumab-treated cancer cells in the traswell for 24 h, and the mRNA level of each target was determined by real-time PCR. *P < 0.05 and ***P < 0.001 by two-sided Student's t-test. RU: relative unit; Cixu: cixutumumab (25 μg/ml, six days for cell treatment); Con=control.

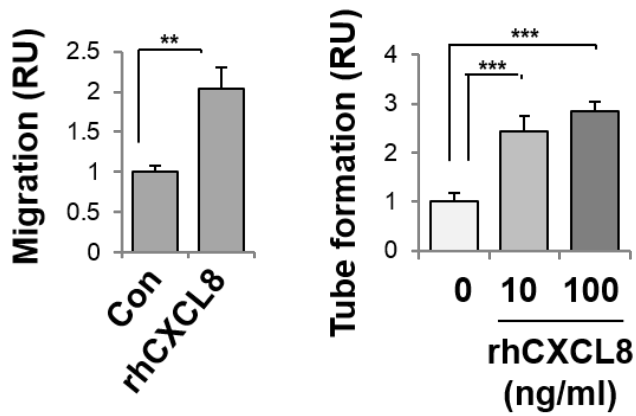

Figure 46. Response of HUVECs to CXCL8.

Left: Migration assay with rhCXCL8. HUVECs were seeded in basal media with or without rhCXCL8 (10 ng/ml) in the upper well and incubated for 6 h for migration. Right: HUVECs were seeded in basal media with or without rhCXCL8 onto a Matrigel-coated 96 well plate, and incubated for 10 h. Each bar represents the mean relative unit (RU) ±SD of three identical wells of a single representative experiment. ** P< 0.01 and ***P < 0.001 by two-sided Student's t-test. RU: relative unit;

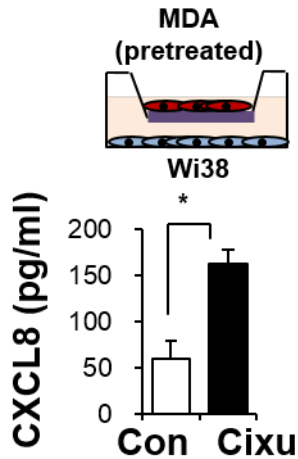

Figure 47. Secretion of CXCL8 upon coculture with cixutumumab-pretreated cancer cells.

Wi38 cells were co-cultured with cixutumumab-treated MDA231 cells, and CXCL8 secretion was determined by ELISA. Each bar represents the mean relative unit (RU) ±SD of three identical wells of a single representative experiment. *P < 0.05 by two-sided Student's t-test; Cixu: cixutumumab (25 μg/ml, six days for cell treatment); Con=control.

6.2. CXCL8 from stromal cells stimulates tumor angiogenesis.

Previous results suggest that intercellular IGF-2/IGF-2R interaction stimulates CXCL8 production form fibroblasts and monocytes. To evaluate whether CXCL8 production is mediated by IGF-2 from cancer cells, I stimulated Wi38 and THP-1 cells with rhIGF-2 and observed increase in CXCL8 transcripts (Figure 48). Next, I blocked IGF-2R expression by shRNA or neutralizing antibody in Wi38 cells to prove the role of IGF-2R mediated CXCL8 increase. When IGF-2R expression is ablated, CM from cixutumumab-trated cancer cells failed to increase CXCL8 transcripts (Figure 49). This was in line with that CM from H1299 cells with a reduced IGF-2 expression failed to stimulate CXCL8 transcription in Wi38 cells. When Wi38 cells were incubated with CM and IGF-2 neutralizing antibody, cixutumumab-treated cancer cells' CM could not induce CXCL8 transcription (Figure 50).

Therefore, I then assessed whether CXCL8 released from stromal cells plays a functional role in stimulating angiogenesis. Previously Wi38 cells incubated with cixutumumab-treated H1299 cells showed significantly increase in HUVECs' migration when compared with control cells (Figure 24). When CXCL8 expression in Wi38 cells was reduced by siRNA (Figure 51a), the ability of Wi38 cells to induce HUVEC migration was significantly decreased (Figure 51b). These findings suggested that macrophage- and fibroblast-induced CXCL8 secretion via communication between cancer and stromal cells may induce the recruitment of endothelial cells, leading to vascular formation.

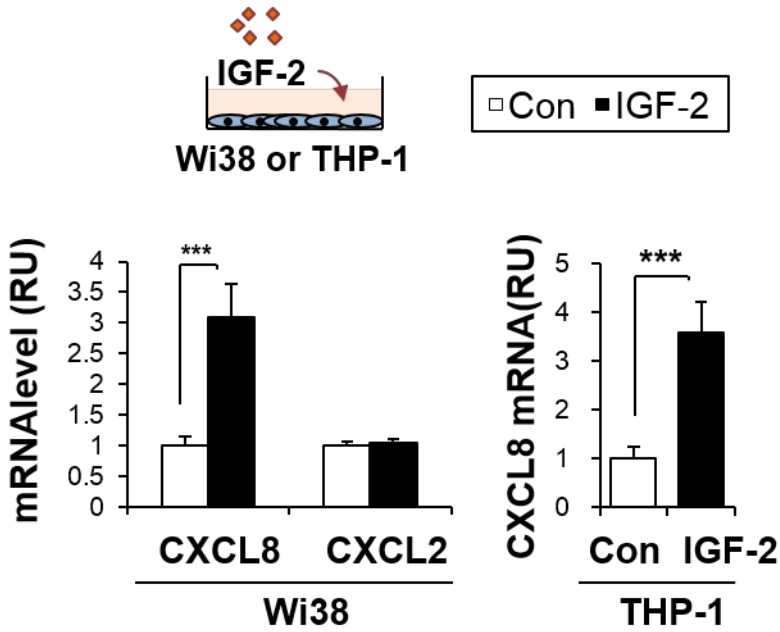

Figure 48. IGF-2-induced CXCL8 transcription in stromal cells.

Wi38 or THP-1 cells were treated with rhIGF-2 (100 ng/ml, 24 h), and CXCL8 mRNA levels were examined by real-time PCR. Each bar represents the mean relative unit (RU) ±SD of three identical wells of a single representative experiment. ***P<0.001 by two-sided student t test. RU: relative unit.

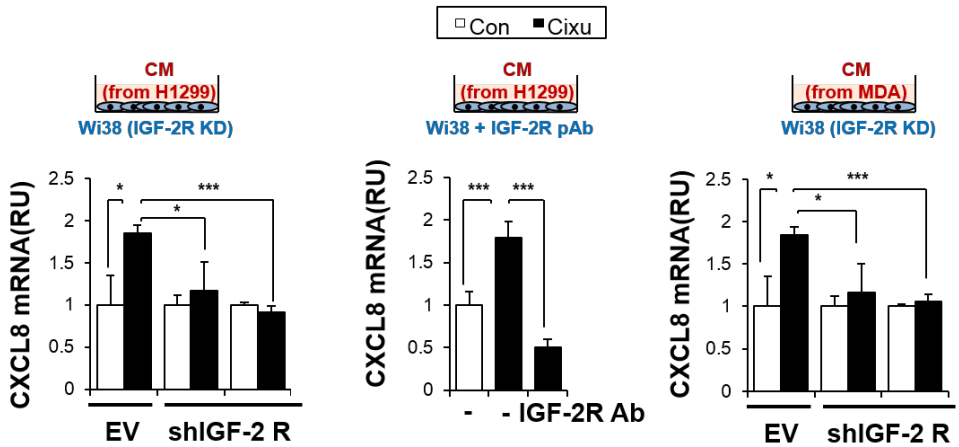

Figure 49. Effects of IGF-2R knockdown in stromal cells on CXCL8 transcription upon IGF-1R blockade.

IGF-2R expression was reduced by shRNA or neutralizing antibody (10 μg/ml) in Wi38 cells and followed by treatment with CM from cixutumumab-treated cancer cells for 24 h. CXCL8 mRNA levels were determined by real-time PCR. Each bar represents the mean relative unit (RU) ±SD of three identical wells of a single representative experiment. *P<0.05 and ***P<0.001 by two-sided student t test. RU: relative unit; EV: Empty vector; Cixu: cixutumumab (25 μg/ml, six days for cell treatment); Con: control.

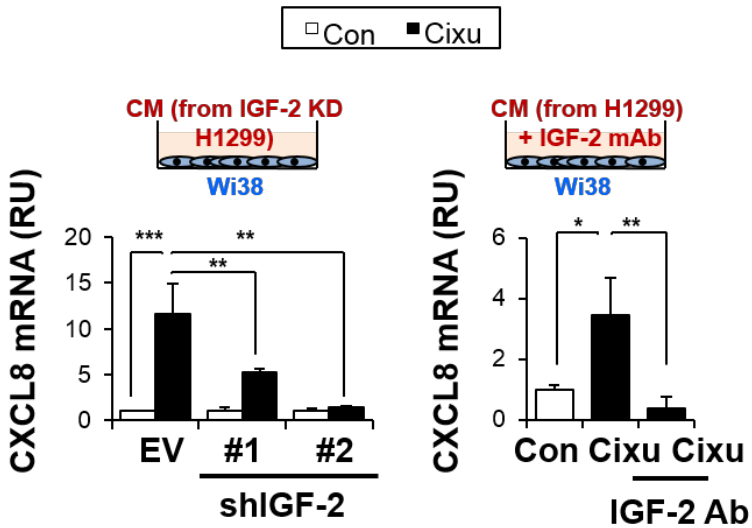

Figure 50. Effects of IGF-2 knockdown in cancer cells on CXCL8 transcription upon IGF-1R blockade.

Wi38 cells were incubated with CM from cixutumumab-treated H1299 transfected with empty vector or shIGF-2 (Left) or IGF-2 neutralizing antibody (5 μg/ml) and CM from cixutumumab-treated H1299 cells (Right). After 24 h, CXCL8 mRNA levels were examined by real-time PCR. Each bar represents the mean relative unit (RU) ±SD of three identical wells of a single representative experiment. *P<0.05, **P<0.01, and ***P<0.001 by two-sided student t test. RU: relative unit; EV: Empty vector; Cixu: cixutumumab (25 μg/ml, six days for cell treatment); Con: control.

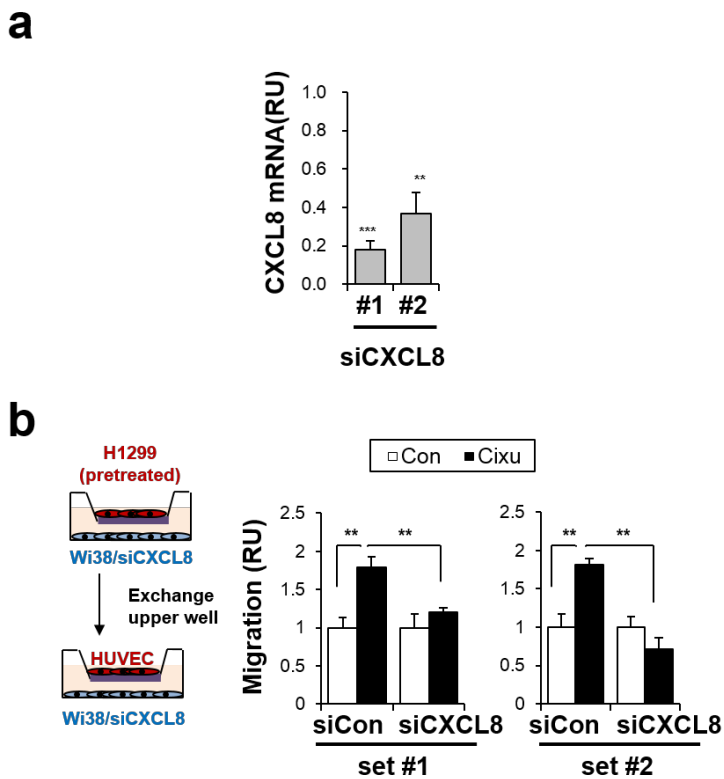

Figure 51. Stromal cells' stimulation of angiogenesis through CXCL8.

(a) Wi38 cells were transfected with negative control siRNA or siCXCL8, and knock-down of CXCL8 was confirmed by real-time PCR. (b) Transfected with each siRNA were seeded in the bottom chamber and co-cultured with cixutumumab-treated H1299 cells in the transwell. After 24 h, the top-chambers were removed, and HUVECs were seeded in the new top-chamber. HUVECs were allowed to migrate for 6 h. Each bar represents the mean relative unit (RU) ±SD of three identical wells of a single representative experiment. **P<0.01 and ***P<0.001 by two-sided student t test. RU: relative unit; Cixu: cixutumumab (25 μg/ml, six days for cell treatment); Con: control.

7. Increased infiltration of stromal cells under cixutumumab clinical trial

I investigated whether findings up to this point can be practically applied to understanding the mechanisms of cixutumumab resistance in human patients. To this end, I analyzed F4/80 positive macrophages, FSP-1 positive fibroblasts, and VEGFR positive VE cells along with the IGF-2 expression in HNSCC tissues resected from patients (n=6) undergoing a clinical trial with cixutumumab. Compared with HNSCC tissues from head and neck cancer tissue array (US Biomax Inc.), all six samples from cixutumumab-treated patients showed markedly increased numbers of macrophages, fibroblasts, and VE cells along with IGF-2 expression (Figure 52 and 53). Although additional studies utilizing a larger number of cases are required, these findings suggest that the cixutumumab-induced increases in tumor-associated macrophages and fibroblasts may play a role in IGF-2 expression and predict resistance to IGF-1R mAb-based therapies in cancer patients.

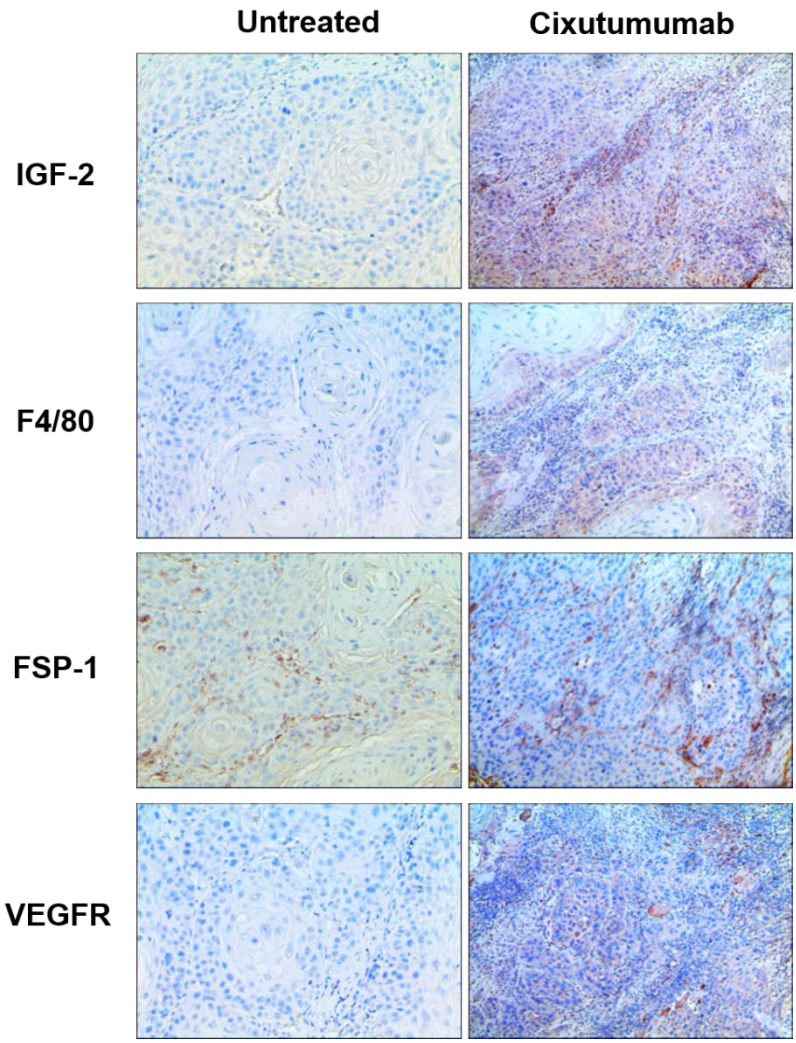

Figure 52. Clinical relevance of TME in HNSCC patients with cixutumumab treatment.

IHC analyses on IGF-2 expression, VEGFR+ vascular endothelial (VE) cells, F4/80+ macrophages, and FSP-1+ fibroblasts in the tissue samples from patients with HNSCC either naïve or treated with cixutumumab for three weeks. Representative images are shown.

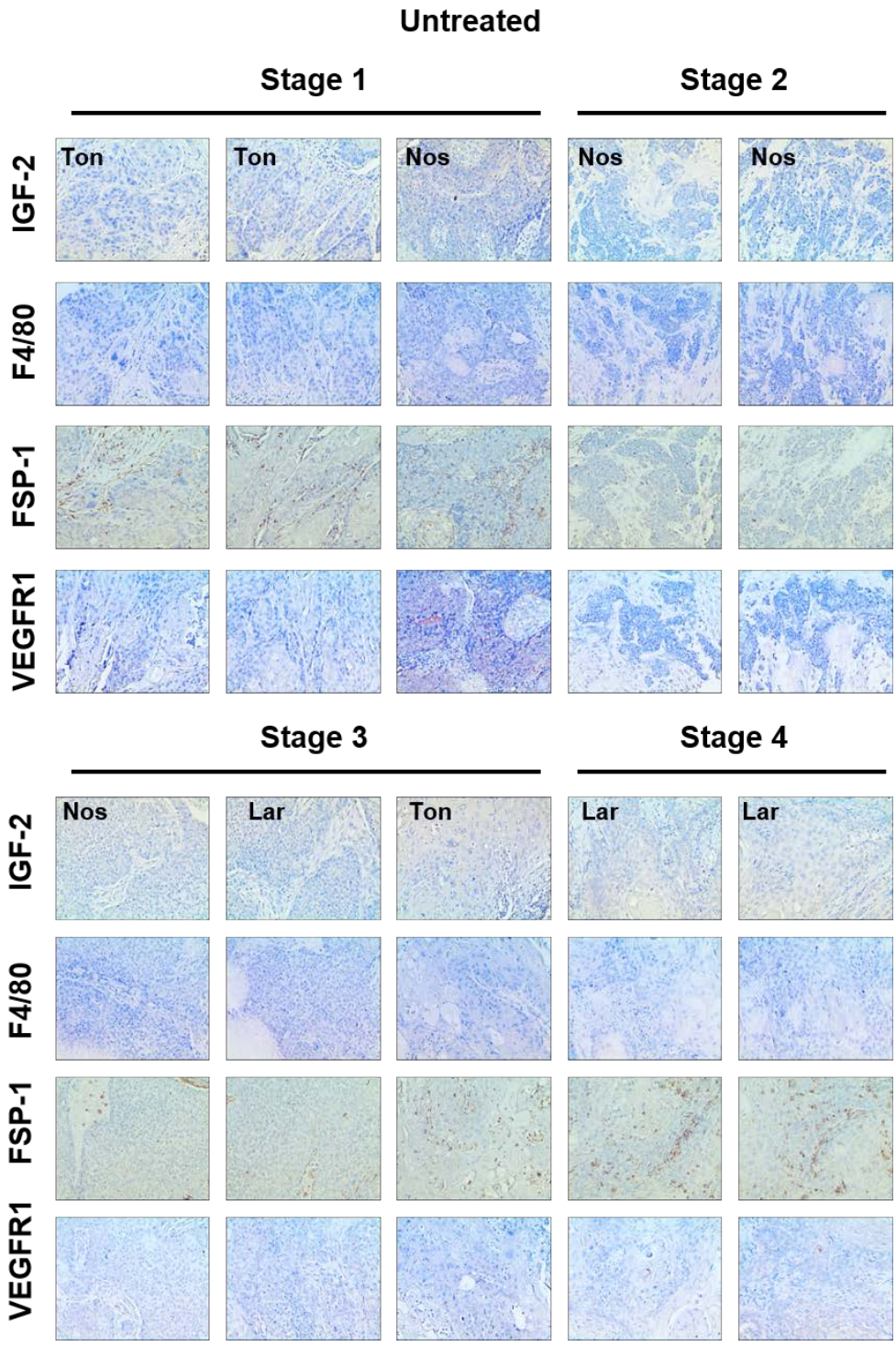
Untreated
Stage 1
Stage 2
IGF-2
F4/80
FSP-1
VEGFR1
Ton
Ton
Nos
Nos
Nos
Stage 3
Stage 4
Nos
Lar
Ton
Lar
Lar

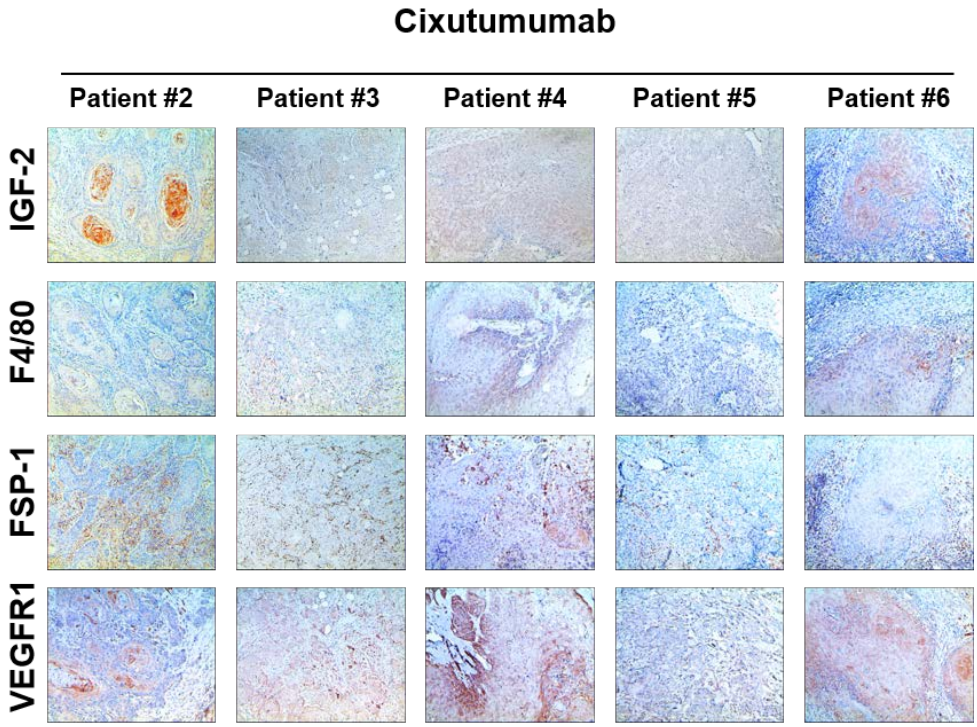

Figure 53. All images of immunostaining for IGF-2, VEGFR1, FSP-1, F4/80 in HNSCC patient tissue samples.

Inserted words indicate specific region of tumors. Lar: Larynx; Nos: Nose; Ton: Tongue.

V. DISCUSSION

Molecularly targeted therapies have come into the spotlight because of its potent therapeutic efficacies in some clinical cases with minimal side effects. However, most targeted drugs shorted of people's expectations in that exhibited only transitory efficacy, and resistance eventually develops. Genetic or epigenetic changes in tumor cells have been reported to contribute to cell-autonomous mechanisms of resistance to anticancer drugs. However, recent studies have enlightened the role of the TME in development of innate resistance to anticancer drugs [69-71, 103-106]. Most TME-mediated drug resistance occurs from interaction between cancer and stromal cells through secreted factors or cell adhesion molecules, providing cancer cells with stimulating signals for proliferation, survival and metastasis. As potent partnership between tumor and stroma receives attention, various therapeutic strategies targeting those tumor-promoting stromal cells have been suggested. This implies that studying progression and resistance of cancers in the view of TME is necessary to provide more effective therapies.

In this study, I suggest that IGF-1R-targed approaches induce a milieu that activates tumor angiogenesis, thus advancing cancer metastasis and promoting a tumor's adaptive-evasive response to the therapy. This study proves the following findings: 1) IGF-1R ablation by treatment with anti-IGF-1R mAb cixutumumab stimulates cancer cells to activate STAT3, leading to increase in IGF-2 transcription (Figure 54-1); 2) IGF-2 attracts monocytes and fibroblasts via utilization of IGF-2R on those cells (Figure 54-2); and 3) recruited monocytes and fibroblasts produce a wide variety of proangiogenic cytokines, most notably CXCL8 (Figure 54-3), which act as stimulators for VE cells (Figure 54-4), resulting in increased tumor angiogenesis and thus facilitating cancer metastasis (Figure 54-5). This provide mechanistic understanding of the interplay between tumors and their healthy counterparts within the TME in the emergence of adaptive-evasive abilities in the

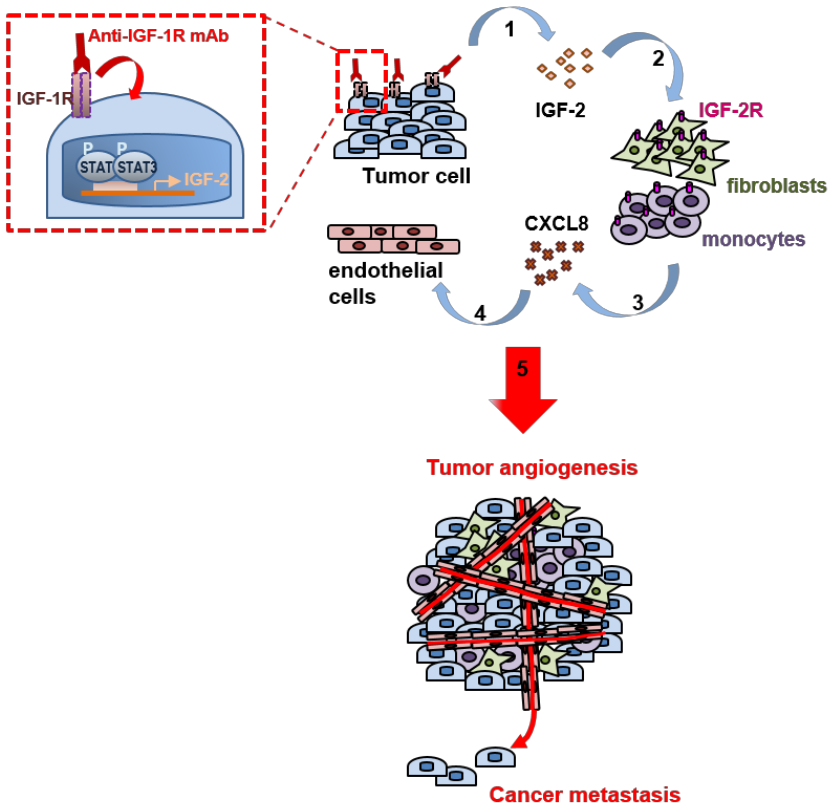

Figure 54. Schematic model of events noted in the TME on treatment with IGF-1R-targeted therapy.

IGF-1R blockade by mAbs in cancer cells leads to STAT3 activation, resulting in IGF-2 production (1). IGF-2 secreted from cixutumumab-treated cancer cells recruits monocytes and fibroblasts in the TME through IGF-2/IGF-2R interaction (2). Recruited stromal cells stimulated the production of the proangiogenic cytokine, CXCL8 (3). CXCL8 attracts endothelial cells (4). Increased tumor angiogenesis upon IGF-1R blockade promotes cancer metastasis (5).

face of an IGF-1R ablation.

Although IGF-1R signaling has been demonstrated as potent target of molecular targeted therapy by preclinical studies, final disease progression in the face of IGF-1R-targeted therapies has been reported in clinical trials. In this study, anti-IGF-1R mAb treatment in mice bearing orthotopic tumors of human cancer cells induced a period of stable disease followed by spontaneous metastasis and a reduced life span, which is debatably similar to the observations in clinical trials with figitumumab in combination with chemotherapy [44]. As IGF-1R degradation was confirmed after short-term or prolonged drug treatment in vitro and in vivo, this resistance is not a failure in the IGF-1R blockade. As mechanisms of resistance to anti-IGF-1R therapies, several studies have implicated cross talk via alternative epithelial RTKs, such as EGFR, IR, PDGF-β and HER2 [46-48, 107], or non-receptor transmembrane signalers, such as integrins [49], in cancer cells. However, studies for stromal cells' response to induce resistance to the anti-IGF-1R therapy has not been reported. In this study, anti-IGF-1R mAb induced infiltration of various stromal cells, including VE cells, macrophages and fibroblasts into primary tumors as proved by IHC analysis of mouse tumor tissues. These observations were in line with the well-established importance of communication among various cell types within the TME in mediating anticancer drug resistance [108]. Therefore, resistance to anti-IGF-1R therapy is not only likely due to activities in the tumor cells but also due to the complex interplay between tumor cells and their neighboring heterologous stromal cells within the TME.

The interaction between tumors and stromal cells in the TME is mediated through cell adhesion molecules and/or soluble factors [69]. For example, CCL2 secreted from both tumor and stromal cells was reported to mediate interaction between inflammatory monocytes and tumor cells [104]. These interaction between

cancer cells and their microenvironments sometimes inhibit the proliferation of cancer cells mostly in initial tumor formation process. However, as tumors progress, stromal cells also changes by several factors such as inflammation and hypoxia and elicits tumor-promoting condition such as maintenance of cancer stemness, and resistant to anticancer therapeutics. It has been reported that mesenchymal stem cells of the tumor-associated stroma is stimulated by tumor-derives IL-1 and secretes prostaglandin E2 (PGE2). Then PGE2 exerts autocrine stimulation to induce a group of cytokines by MSCs and paracrine stimulation to induce cancer stem cell formation [109]. In colorectal cancer metastasis, TGF-β-stimulated CAFs is known to trigger GP130/STAT3 signaling in tumor cells, thus facilitating survival of metastatic cells [110]. Those studies proved a complex interplay between cancer and stromal cells which affects various steps of cancer progression from cancer initiation to recurrence of cancer. IGF-2 levels have been implicated in drug-resistance in anti-IGF-1R inhibitors [46] and anti-EGFR monoclonal antibody [111], and this implies that IGF-2 can be a mediator of interaction between cancer and stromal cells. Indeed, transcriptional up-regulation of IGF2 in cancer cells after IGF-1R blockade by mAb was confirmed in this study. These results identify the importance of the intercellular IGF-2/IGF-2R system in cancer cell communication with the TME showing that: 1) macrophages and fibroblasts but not ECs migrate toward cixutumumab-treated cancer cells or CM obtained from the cancer cells; 2) IGF-2R expression is observed in macrophages and fibroblasts but not in HUVECs; and 3) the ability of cancer cells to chemoattract stromal cells is inhibited by silencing IGF-2 or IGF-2R expression in cancer cells or stromal cells, respectively. However, anti-IGF-1R mAb-treated cancer cells did not show any increased proliferation and migration (Figure 15 and 16), suggesting that secreted IGF-2 from cancer cells does not exert autocrine effects under the IGF-1R blockade. As IGF-2 has been reported to be overexpressed in many

cancers and exert the mitogenic effects [112-116], IGF-2 itself can contribute to tumorigenesis through its own signaling pathway. IGF-2 also can bind to IR-A to promote tumorigenesis and IR expression levels of cancer cells were not affected by cixutumumab (Figure 28). Consistent cellular proliferation under the cixutumumab may be explained by insufficient signaling effect to exert IGF-2's action in IGF-1R abolished status or the difference in ratio between IR-A and IR-B in individual cancer cells.

Subsequent experiments, including RTK arrays with cixutumumab-treated cancer cells' lysates and shRNA mediated knockdown, identified that up-regulated IGF-2 expression is primarily, if not solely, a result of cixutumumab-induced STAT3 activation. Transcription of IGF-2 is regulated by genomic imprinting: in its maternal allele, zinc finger protein CTCF binds to imprinting control region (ICR), suppressing IGF-2 transcription [117-119]. Diseases such as cancer and Beckwith-Wiedemann syndrome (BWS) showed dysregulated IGF-2 transcription arise from loss of imprinting [116, 120-123]. Transcription of IGF-2 is also dysregulated by several transcription factors, such as E2Ff3, ZFP57, and STAT3 [92, 124, 125]. Although sophisticated transcriptional mechanism of IGF-2 needs to be investigated, recent studies reported STAT3-mediated transcription of IGF-2 in induction of resistance to histone deacetylase inhibitors (HDIs). Treatment of HDIs induced direct binding of STAT3 to promoter of IGF-2, inducing IGF-2 transcription and activation of IGF-1R signaling cascade [126]. Moreover, acetylated STAT3 also increased the transcription of DNA methyltransferase 1 (DNMT1). DNMT1 then induced hypermethylation of ICR of IGF-2 and inhibited binding of the CTCF, resulting in loss of imprinting [127]. From those studies, it is possible that activated STAT3 upon cixutumumab may increase IGF-2 transcription by two ways: direct binding to promoter and loss of imprinting.

STAT3-mediated resistance development to anti-IGF-1R mAb is meaningful in that role of STAT3 in regulation of response to therapy has now been actively investigated [128, 129]. In metastatic breast cancer cells, STAT3-dependent overexpression of Bcl2 confer a survival advantage, resulting resistance to chemotherapy [130]. Cisplatin-resistant gastric cancer cells also showed activated status of STAT3 and inhibition of STAT3 increased sensitivity to chemotherapy [131]. Involvement of STAT3 in resistance to chemotherapy has also been reported in clinical study. When compared STAT3 activity in chemo-naïve tumors and chemo-resistant tumors from patients who treated with platinum- and taxane-based chemotherapy, recurrent tumors display higher levels of STAT3 phosphorylation [132]. STAT3-mediated development of drug resistance is not limited to chemotherapy: it is also involved in resistance to the molecular targeted anticancer drugs. In clinical study, patients' outcome to the cetuximab treatment, an anti-EGFR mAb, was different between positive phospho STAT3 and negative phospho STAT3-stained patients [133]. In lung cancer cells resistant to gefitinib, an anti EGFR TKI, STAT3-induced Akt activation was reported to be a novel resistance mechanism [134]. Similar findings linking STAT3 with resistance against the molecular targeted therapy have been reported in MEK inhibitors or B-RAF inhibitors [135, 136]. Moreover, it is reported that oncogene-addicted cancer cells showed positive feedback associated STAT3 activation, which finally induced resistance to various anticancer therapies [129, 137]. Considering previous reports for STAT3-mediated resistance and results from this study, STAT3 is a key player to develop the resistance to various anticancer therapies by activation of their target genes. However, it seems that STAT3-mediated drug resistance not involve always same target genes, as seen in no changes of VEGF transcription under the IGF-1R blockade in this study (Figure 21). This can be explained by the difference in pathways that lead STAT3 activation

upon each treatment.

We further demonstrated that the small cytokine CXCL8 which serves as a shared ligand of CXCR1 and CXCR2 [138], is significantly up-regulated in macrophages and fibroblasts in response to the IGF-2/IGF-2R interaction, subsequently inducing VE cell recruitment. Although IGF-2R is a scavenger receptor that regulates IGF-2 levels by endocytosis-mediated degradation [37], the action of IGF-2 through IGF-2R transmembrane signaling has also been demonstrated in previous studies [139-145]. CXCL8 is one of the major activators of the PI3K/Akt and ERK pathways and acts as a potent proangiogenic chemokine and chemoattractant for a wide range of cells, including endothelial cells [95-97, 146]. In addition, CXCL8 is involved in the initiation of tumor-associated inflammation, neovascularization, and tumor progression [98, 147]. Therefore, increased CXCL8 production in the TME potentially contributes to tumor angiogenesis and cancer progression. Thus, an attractive hypothesis is that increased epithelial IGF-2 production leads to macrophage and fibroblast chemotaxis, which subsequently stimulates CXCL8 expression in stromal cells through the IGF-2/IGF-2R axis, resulting in endothelial cell recruitment and cancer cell migration. In support of the supposition, our data using paraffin-embedded tissues from HNSCC patients in a cixutumumab clinical trial showed significant increases in tumor-associated macrophages, CAFs, vascular endothelial cells, and IGF-2 expression. Given that the downstream intracellular targets of CXCL8 include STAT3, increased CXCL8 in the tumor stroma promotes a positive intercellular feedback loop between CXCL8 and IGF-2 production. Previous studies have suggested that tumor-derived IGF-2 contributes to vasculogenesis by augmenting the recruitment of endothelial progenitor cells (EPCs) through its interaction with IGF-2R [139]. Therefore, IGF-2 secretion could have induced mobilization of EPCs and BM progenitor cells to the

TME, leading to an increased vasculature in cixutumumab-treated xenograft tumors. However, in this study, HUVECs did not show increased tube formation and migration activity under coculture with cixutumumab-pretreated cancer cells (Figure 21). This may be due to limited expression of IGF-1R, IR, and IGF-2R in HUVECs (Figure 32). Although in vitro experiments concluded that cixutumumab-treated cancer cells does not attract VE cells but it is possible that IGF-1R blocked cancer cells can activate the vasculogenesis through secretion of IGF-2. Further studies including various VE cells or primary cells may investigate the delicate mechanism of angiogenesis under the IGF-1R blockade.

To uncover the molecular mechanism between cancer cells and stromal cells, I used in vitro coculture system and incubation with CM, using representative cell lines. However, characteristics of each stromal cells can be different from cell lines. Although I confirmed consistent angiogenesis-stimulating effect in coculture between cancer cells and isolated macrophages, this study still has limitation to represent the real event occurs in tumor region. Further confirmation for interaction between cancer and stromal cells through IGF-2/IGF-2R in mouse model system is required. Moreover, tumor microenvironment in different anatomical site may be different from each other. This study showed similar involvement of same types of stromal cells in orthotopic mouse tumor models, indicating that different anatomical sites did not affect the communication. But, the molecular mechanism of communication can be dependent on site of each tumors. Collectively, this study investigate the molecular mechanism in which mostly in vitro systems, thus further study should focus on modeling of tumor microenvironment closer to real condition.

In conclusion, this study identifies anti-IGF-1R mAb-induced cancer-stromal cell communication via STAT3-dependent IGF-2 production in cancer cells and a positive IGF-2/CXCL8 feedback loop through the intercellular IGF-2/IGF-2R

system. Although additional validation studies using corroborated clinical samples from IGF-1R targeted therapies must be performed, current study reveals malignant progression of tumors in the face of an IGF-1R blockade through IGF-2 secretion in the TME. Given that several approaches to developing anti-IGF-2 mAb and STAT3 inhibitors for cancer treatment are ongoing in clinical trials [148], this study will have a clinical impact. Clinical trials are warranted to assess whether therapeutic strategies targeting STAT3 or IGF-2 would circumvent tumor angiogenesis and pro-invasive consequences, overcoming innate resistance to anti-IGF-1R mAb-based therapies.

VI. REFERENCES

1. Sawyers, C., *Targeted cancer therapy.* Nature, 2004. **432**(7015): p. 294-7.
2. Hait, W.N. and T.W. Hambley, *Targeted cancer therapeutics.* Cancer Res, 2009. **69**(4): p. 1263-7; discussion 1267.
3. Aggarwal, S., *Targeted cancer therapies.* Nat Rev Drug Discov, 2010. **9**(6): p. 427-8.
4. Felsher, D.W. and J.M. Bishop, *Reversible tumorigenesis by MYC in hematopoietic lineages.* Mol Cell, 1999. **4**(2): p. 199-207.
5. Felsher, D.W. and J.M. Bishop, *Transient excess of MYC activity can elicit genomic instability and tumorigenesis.* Proc Natl Acad Sci U S A, 1999. **96**(7): p. 3940-4.
6. Stegmeier, F., et al., *Targeted cancer therapies in the twenty-first century: lessons from imatinib.* Clin Pharmacol Ther, 2010. **87**(5): p. 543-52.
7. Fava, C. and G. Saglio, *Ponatinib for chronic myeloid leukaemia: future perspectives.* Lancet Oncol, 2016. **17**(5): p. 546-7.
8. Pinilla-Ibarz, J., et al., *Long-term BCR-ABL1 Tyrosine Kinase Inhibitor Therapy in Chronic Myeloid Leukemia.* Anticancer Res, 2015. **35**(12): p. 6355-64.
9. Cortes, J.E., et al., *Long-term bosutinib for chronic phase chronic myeloid leukemia after failure of imatinib plus dasatinib and/or nilotinib.* Am J Hematol, 2016. **91**(12): p. 1206-1214.
10. O'Hare, T., *A Decade of Nilotinib and Dasatinib: From In Vitro Studies to First-Line Tyrosine Kinase Inhibitors.* Cancer Res, 2016. **76**(20): p. 5911-5913.
11. Giordano, S.H., et al., *Systemic therapy for patients with advanced human epidermal growth factor receptor 2-positive breast cancer: American Society of Clinical Oncology clinical practice guideline.* J Clin Oncol, 2014.

32(19): p. 2078-99.

12. Gianni, L., et al., *5-year analysis of neoadjuvant pertuzumab and trastuzumab in patients with locally advanced, inflammatory, or early-stage HER2-positive breast cancer (NeoSphere): a multicentre, open-label, phase 2 randomised trial.* Lancet Oncol, 2016. **17**(6): p. 791-800.
13. Kim, Y., et al., *Differential Effects of Tyrosine Kinase Inhibitors on Normal and Oncogenic EGFR Signaling and Downstream Effectors.* Mol Cancer Res, 2015. **13**(4): p. 765-74.
14. Chan, B.A. and B.G. Hughes, *Targeted therapy for non-small cell lung cancer: current standards and the promise of the future.* Transl Lung Cancer Res, 2015. **4**(1): p. 36-54.
15. Price, T.J., et al., *Panitumumab versus cetuximab in patients with chemotherapy-refractory wild-type KRAS exon 2 metastatic colorectal cancer (ASPECCT): a randomised, multicentre, open-label, non-inferiority phase 3 study.* Lancet Oncol, 2014. **15**(6): p. 569-79.
16. Garassino, M.C. and V. Torri, *Afatinib for lung cancer: let there be light?* Lancet Oncol, 2014. **15**(2): p. 133-4.
17. Engle, J.A. and J.M. Kolesar, *Afatinib: A first-line treatment for selected patients with metastatic non-small-cell lung cancer.* Am J Health Syst Pharm, 2014. **71**(22): p. 1933-8.
18. Deeks, E.D., *Ceritinib: a Review in ALK-Positive Advanced NSCLC.* Target Oncol, 2016. **11**(5): p. 693-700.
19. Blackhall, F. and F. Cappuzzo, *Crizotinib: from discovery to accelerated development to front-line treatment.* Ann Oncol, 2016. **27 Suppl 3**: p. iii35-iii41.
20. Wu, J., J. Savooji, and D. Liu, *Second- and third-generation ALK inhibitors*

for non-small cell lung cancer. J Hematol Oncol, 2016. **9**: p. 19.

21. Holderfield, M., et al., *Targeting RAF kinases for cancer therapy: BRAF-mutated melanoma and beyond.* Nat Rev Cancer, 2014. **14**(7): p. 455-67.
22. Furman, R.R., et al., *Idelalisib and rituximab in relapsed chronic lymphocytic leukemia.* N Engl J Med, 2014. **370**(11): p. 997-1007.
23. Speranza, M.C., et al., *BKM-120 (Buparlisib): A Phosphatidyl-Inositol-3 Kinase Inhibitor with Anti-Invasive Properties in Glioblastoma*. Sci Rep, 2016. **6**: p. 20189.
24. Martin, M., et al., *A randomized adaptive phase II/III study of buparlisib, a pan-Class I PI3K inhibitor, combined with paclitaxel for the treatment of HER2- advanced breast cancer (BELLE-4).* Ann Oncol, 2016.
25. Robert, C., et al., *Improved overall survival in melanoma with combined dabrafenib and trametinib.* N Engl J Med, 2015. **372**(1): p. 30-9.
26. Chung, C. and S. Reilly, *Trametinib: a novel signal transduction inhibitor for the treatment of metastatic cutaneous melanoma.* Am J Health Syst Pharm, 2015. **72**(2): p. 101-10.
27. Ellis, L.M. and D.J. Hicklin, *VEGF-targeted therapy: mechanisms of anti-tumour activity.* Nat Rev Cancer, 2008. **8**(8): p. 579-91.
28. Takeda, K. and H. Daga, *Ramucirumab for the treatment of advanced or metastatic non-small cell lung cancer.* Expert Opin Biol Ther, 2016. **16**(12): p. 1541-1547.
29. Grabowski, J. and A. Glode, *Ramucirumab: A vascular endothelial growth factor receptor-2 inhibitor with activity in several malignancies.* Am J Health Syst Pharm, 2016. **73**(13): p. 957-68.
30. Gallagher, E.J. and D. LeRoith, *The proliferating role of insulin and insulin-like growth factors in cancer.* Trends Endocrinol Metab, 2010. **21**(10): p.

610-8.

31. Clayton, P.E., et al., *Growth hormone, the insulin-like growth factor axis, insulin and cancer risk.* Nat Rev Endocrinol, 2011. **7**(1): p. 11-24.
32. Pollak, M., *The insulin receptor/insulin-like growth factor receptor family as a therapeutic target in oncology.* Clin Cancer Res, 2012. **18**(1): p. 40-50.
33. Maki, R.G., *Small is beautiful: insulin-like growth factors and their role in growth, development, and cancer.* J Clin Oncol, 2010. **28**(33): p. 4985-95.
34. Firth, S.M. and R.C. Baxter, *Cellular actions of the insulin-like growth factor binding proteins.* Endocr Rev, 2002. **23**(6): p. 824-54.
35. Pollak, M., *The insulin and insulin-like growth factor receptor family in neoplasia: an update.* Nat Rev Cancer, 2012. **12**(3): p. 159-69.
36. Gombos, A., et al., *Clinical development of insulin-like growth factor receptor--1 (IGF-1R) inhibitors: at the crossroad?* Invest New Drugs, 2012. **30**(6): p. 2433-42.
37. Gao, J., et al., *Targeting the insulin-like growth factor axis for the development of novel therapeutics in oncology.* Cancer Res, 2012. **72**(1): p. 3-12.
38. Gualberto, A. and M. Pollak, *Emerging role of insulin-like growth factor receptor inhibitors in oncology: early clinical trial results and future directions.* Oncogene, 2009. **28**(34): p. 3009-21.
39. Yee, D., *Insulin-like growth factor receptor inhibitors: baby or the bathwater?* J Natl Cancer Inst, 2012. **104**(13): p. 975-81.
40. Juergens, H., et al., *Preliminary Efficacy of the Anti-Insulin–Like Growth Factor Type 1 Receptor Antibody Figitumumab in Patients With Refractory Ewing Sarcoma.* Journal of Clinical Oncology, 2011. **29**(34): p. 4534-4540.
41. Malempati, S., et al., *Phase I/II Trial and Pharmacokinetic Study of*

Cixutumumab in Pediatric Patients With Refractory Solid Tumors and Ewing Sarcoma: A Report From the Children's Oncology Group. Journal of Clinical Oncology, 2012. **30**(3): p. 256-262.

42. Ramalingam, S.S., et al., *Randomized Phase II Study of Erlotinib in Combination With Placebo or R1507, a Monoclonal Antibody to Insulin-Like Growth Factor-1 Receptor, for Advanced-Stage Non–Small-Cell Lung Cancer.* Journal of Clinical Oncology, 2011. **29**(34): p. 4574-4580.
43. S. Patel, A.P., J. Crowley, et al., , *A SARC global collaborative phase II trial of R1507, a recombinant human monoclonal antibody to the insulin-like growth factor-1 receptor (IGF1R) in patients with recurrent or refractory sarcomas.* J Clin Oncol, 2009. **27:15s, 2009 (suppl; abstr 10503)**.
44. Langer, C.J., et al., *Randomized, phase III trial of first-line figitumumab in combination with paclitaxel and carboplatin versus paclitaxel and carboplatin alone in patients with advanced non-small-cell lung cancer.* J Clin Oncol, 2014. **32**(19): p. 2059-66.
45. Scagliotti, G.V., et al., *Randomized, phase III trial of figitumumab in combination with erlotinib versus erlotinib alone in patients with nonadenocarcinoma nonsmall-cell lung cancer.* Ann Oncol, 2015. **26**(3): p. 497-504.
46. Garofalo, C., et al., *Efficacy of and resistance to anti-IGF-1R therapies in Ewing's sarcoma is dependent on insulin receptor signaling.* Oncogene, 2011. **30**(24): p. 2730-40.
47. Ulanet, D.B., et al., *Insulin receptor functionally enhances multistage tumor progression and conveys intrinsic resistance to IGF-1R targeted therapy.* Proc Natl Acad Sci U S A, 2010. **107**(24): p. 10791-8.
48. Huang, F., et al., *Differential mechanisms of acquired resistance to insulin-*

like growth factor-i receptor antibody therapy or to a small-molecule inhibitor, BMS-754807, in a human rhabdomyosarcoma model. Cancer Res, 2010. **70**(18): p. 7221-31.

49. Shin, D.H., et al., *Combating resistance to anti-IGFR antibody by targeting the integrin beta3-Src pathway.* J Natl Cancer Inst, 2013. **105**(20): p. 1558-70.

50. Bissell, M.J. and W.C. Hines, *Why don't we get more cancer? A proposed role of the microenvironment in restraining cancer progression.* Nat Med, 2011. **17**(3): p. 320-9.

51. Quail, D.F. and J.A. Joyce, *Microenvironmental regulation of tumor progression and metastasis.* Nat Med, 2013. **19**(11): p. 1423-37.

52. Hanahan, D. and L.M. Coussens, *Accessories to the crime: functions of cells recruited to the tumor microenvironment.* Cancer Cell, 2012. **21**(3): p. 309-22.

53. Hanahan, D. and R.A. Weinberg, *Hallmarks of cancer: the next generation.* Cell, 2011. **144**(5): p. 646-74.

54. Egeblad, M., E.S. Nakasone, and Z. Werb, *Tumors as organs: complex tissues that interface with the entire organism.* Dev Cell, 2010. **18**(6): p. 884-901.

55. Wynn, T.A., A. Chawla, and J.W. Pollard, *Macrophage biology in development, homeostasis and disease.* Nature, 2013. **496**(7446): p. 445-55.

56. Ruffell, B., N.I. Affara, and L.M. Coussens, *Differential macrophage programming in the tumor microenvironment.* Trends Immunol, 2012. **33**(3): p. 119-26.

57. Qian, B.Z. and J.W. Pollard, *Macrophage diversity enhances tumor progression and metastasis.* Cell, 2010. **141**(1): p. 39-51.

58. Lewis, C.E. and J.W. Pollard, *Distinct role of macrophages in different tumor microenvironments.* Cancer Res, 2006. **66**(2): p. 605-12.

59. Gabrilovich, D.I., S. Ostrand-Rosenberg, and V. Bronte, *Coordinated regulation of myeloid cells by tumours.* Nat Rev Immunol, 2012. **12**(4): p. 253-68.

60. Gabrilovich, D.I. and S. Nagaraj, *Myeloid-derived suppressor cells as regulators of the immune system.* Nat Rev Immunol, 2009. **9**(3): p. 162-74.

61. Kalluri, R. and M. Zeisberg, *Fibroblasts in cancer.* Nat Rev Cancer, 2006. **6**(5): p. 392-401.

62. Cirri, P. and P. Chiarugi, *Cancer associated fibroblasts: the dark side of the coin.* Am J Cancer Res, 2011. **1**(4): p. 482-97.

63. Bremnes, R.M., et al., *The role of tumor stroma in cancer progression and prognosis: emphasis on carcinoma-associated fibroblasts and non-small cell lung cancer.* J Thorac Oncol, 2011. **6**(1): p. 209-17.

64. Cirri, P. and P. Chiarugi, *Cancer-associated-fibroblasts and tumour cells: a diabolic liaison driving cancer progression.* Cancer Metastasis Rev, 2012. **31**(1-2): p. 195-208.

65. Ferrara, N. and R.S. Kerbel, *Angiogenesis as a therapeutic target.* Nature, 2005. **438**(7070): p. 967-74.

66. Meads, M.B., R.A. Gatenby, and W.S. Dalton, *Environment-mediated drug resistance: a major contributor to minimal residual disease.* Nat Rev Cancer, 2009. **9**(9): p. 665-74.

67. Tredan, O., et al., *Drug resistance and the solid tumor microenvironment.* J Natl Cancer Inst, 2007. **99**(19): p. 1441-54.

68. Junttila, M.R. and F.J. de Sauvage, *Influence of tumour micro-environment heterogeneity on therapeutic response.* Nature, 2013. **501**(7467): p. 346-54.

69. Hazlehurst, L.A., T.H. Landowski, and W.S. Dalton, *Role of the tumor microenvironment in mediating de novo resistance to drugs and physiological mediators of cell death.* Oncogene, 2003. **22**(47): p. 7396-402.

70. Straussman, R., et al., *Tumour micro-environment elicits innate resistance to RAF inhibitors through HGF secretion.* Nature, 2012. **487**(7408): p. 500-4.

71. Shree, T., et al., *Macrophages and cathepsin proteases blunt chemotherapeutic response in breast cancer.* Genes Dev, 2011. **25**(23): p. 2465-79.

72. Crawford, Y., et al., *PDGF-C mediates the angiogenic and tumorigenic properties of fibroblasts associated with tumors refractory to anti-VEGF treatment.* Cancer Cell, 2009. **15**(1): p. 21-34.

73. Chen, Q., X.H. Zhang, and J. Massague, *Macrophage binding to receptor VCAM-1 transmits survival signals in breast cancer cells that invade the lungs.* Cancer Cell, 2011. **20**(4): p. 538-49.

74. Franks, S.E., et al., *Transgenic IGF-IR overexpression induces mammary tumors with basal-like characteristics, whereas IGF-IR-independent mammary tumors express a claudin-low gene signature.* Oncogene, 2012. **31**(27): p. 3298-309.

75. Jones, R.A., et al., *Reversibility and recurrence of IGF-IR-induced mammary tumors.* Oncogene, 2009. **28**(21): p. 2152-62.

76. DiGiovanni, J., et al., *Deregulated expression of insulin-like growth factor 1 in prostate epithelium leads to neoplasia in transgenic mice.* Proc Natl Acad Sci U S A, 2000. **97**(7): p. 3455-60.

77. Okada, S., et al., *Early development of human hematopoietic and acquired immune systems in new born NOD/Scid/Jak3null mice intrahepatic*

engrafted with cord blood-derived CD34 + cells. Int J Hematol, 2008. **88**(5): p. 476-82.

78. D. D. Karp, L.G.P.-A., S. Novello, P. Haluska, L. Garland, F. Cardenal, L. J. Blakely, P. D. Eisenberg, A. Gualberto and C. J. Langer, *High activity of the anti-IGF-IR antibody CP-751,871 in combination with paclitaxel and carboplatin in squamous NSCLC.* J Clin Oncol (Meeting Abstracts) 2008. **26**(15S): p. 8015.

79. Schmitz, S., et al., *Phase II study of figitumumab in patients with recurrent and/or metastatic squamous cell carcinoma of the head and neck: clinical activity and molecular response (GORTEC 2008-02).* Ann Oncol, 2012. **23**(8): p. 2153-61.

80. Ma, C.X., et al., *A phase I trial of the IGF-1R antibody Cixutumumab in combination with temsirolimus in patients with metastatic breast cancer.* Breast Cancer Res Treat, 2013. **139**(1): p. 145-53.

81. Singh, A. and J. Settleman, *EMT, cancer stem cells and drug resistance: an emerging axis of evil in the war on cancer.* Oncogene, 2010. **29**(34): p. 4741-51.

82. Voulgari, A. and A. Pintzas, *Epithelial-mesenchymal transition in cancer metastasis: mechanisms, markers and strategies to overcome drug resistance in the clinic.* Biochim Biophys Acta, 2009. **1796**(2): p. 75-90.

83. Polyak, K. and R.A. Weinberg, *Transitions between epithelial and mesenchymal states: acquisition of malignant and stem cell traits.* Nat Rev Cancer, 2009. **9**(4): p. 265-73.

84. Mani, S.A., et al., *The epithelial-mesenchymal transition generates cells with properties of stem cells.* Cell, 2008. **133**(4): p. 704-15.

85. Paranjape, A.N., et al., *Introduction of SV40ER and hTERT into*

mammospheres generates breast cancer cells with stem cell properties. Oncogene, 2012. **31**(15): p. 1896-909.

86. Qian, B.Z., et al., *FLT1 signaling in metastasis-associated macrophages activates an inflammatory signature that promotes breast cancer metastasis.* J Exp Med, 2015. **212**(9): p. 1433-48.

87. Kerbel, R.S., *Tumor angiogenesis: past, present and the near future.* Carcinogenesis, 2000. **21**(3): p. 505-15.

88. Wang, Y.H., et al., *Vascular endothelial cells facilitated HCC invasion and metastasis through the Akt and NF-kappaB pathways induced by paracrine cytokines.* J Exp Clin Cancer Res, 2013. **32**(1): p. 51.

89. Bid, H.K., et al., *Potent inhibition of angiogenesis by the IGF-1 receptor-targeting antibody SCH717454 is reversed by IGF-2.* Mol Cancer Ther, 2012. **11**(3): p. 649-59.

90. Singh, P., et al., *Differential activation of IGF-II promoters P3 and P4 in Caco-2 cells during growth and differentiation.* Gastroenterology, 1998. **114**(6): p. 1221-9.

91. von Horn, H., et al., *GH is a regulator of IGF2 promoter-specific transcription in human liver.* J Endocrinol, 2002. **172**(3): p. 457-65.

92. Wang, K., et al., *JAK2/STAT2/STAT3 are required for myogenic differentiation.* J Biol Chem, 2008. **283**(49): p. 34029-36.

93. Garcia, R., et al., *Constitutive activation of Stat3 by the Src and JAK tyrosine kinases participates in growth regulation of human breast carcinoma cells.* Oncogene, 2001. **20**(20): p. 2499-513.

94. Lazennec, G. and A. Richmond, *Chemokines and chemokine receptors: new insights into cancer-related inflammation.* Trends Mol Med, 2010. **16**(3): p. 133-44.

95. Heidemann, J., et al., *Angiogenic effects of interleukin 8 (CXCL8) in human intestinal microvascular endothelial cells are mediated by CXCR2.* J Biol Chem, 2003. **278**(10): p. 8508-15.

96. Hill, K.S., et al., *Met receptor tyrosine kinase signaling induces secretion of the angiogenic chemokine interleukin-8/CXCL8 in pancreatic cancer.* PLoS One, 2012. **7**(7): p. e40420.

97. Matsuo, Y., et al., *CXCL8/IL-8 and CXCL12/SDF-1alpha co-operatively promote invasiveness and angiogenesis in pancreatic cancer.* Int J Cancer, 2009. **124**(4): p. 853-61.

98. Wislez, M., et al., *High expression of ligands for chemokine receptor CXCR2 in alveolar epithelial neoplasia induced by oncogenic kras.* Cancer Res, 2006. **66**(8): p. 4198-207.

99. Maxwell, P.J., et al., *Tumor-derived CXCL8 signaling augments stroma-derived CCL2-promoted proliferation and CXCL12-mediated invasion of PTEN-deficient prostate cancer cells.* Oncotarget, 2014. **5**(13): p. 4895-908.

100. Gales, D., et al., *The Chemokine CXCL8 in Carcinogenesis and Drug Response.* ISRN Oncol, 2013. **2013**: p. 859154.

101. Agarwal, A., et al., *Identification of a metalloprotease-chemokine signaling system in the ovarian cancer microenvironment: implications for antiangiogenic therapy.* Cancer Res, 2010. **70**(14): p. 5880-90.

102. Li, A., et al., *IL-8 directly enhanced endothelial cell survival, proliferation, and matrix metalloproteinases production and regulated angiogenesis.* J Immunol, 2003. **170**(6): p. 3369-76.

103. Wilson, T.R., et al., *Widespread potential for growth-factor-driven resistance to anticancer kinase inhibitors.* Nature, 2012. **487**(7408): p. 505-9.

104. Qian, B.Z., et al., *CCL2 recruits inflammatory monocytes to facilitate breast-tumour metastasis.* Nature, 2011. **475**(7355): p. 222-5.

105. Sun, Y., et al., *Treatment-induced damage to the tumor microenvironment promotes prostate cancer therapy resistance through WNT16B.* Nat Med, 2012. **18**(9): p. 1359-68.

106. Chung, A.S., et al., *An interleukin-17-mediated paracrine network promotes tumor resistance to anti-angiogenic therapy.* Nat Med, 2013. **19**(9): p. 1114-23.

107. Abraham, J., et al., *Evasion mechanisms to Igf1r inhibition in rhabdomyosarcoma.* Mol Cancer Ther, 2011. **10**(4): p. 697-707.

108. Blouin, S., M.F. Basle, and D. Chappard, *Interactions between microenvironment and cancer cells in two animal models of bone metastasis.* Br J Cancer, 2008. **98**(4): p. 809-15.

109. Li, H.J., et al., *Cancer-stimulated mesenchymal stem cells create a carcinoma stem cell niche via prostaglandin E2 signaling.* Cancer Discov, 2012. **2**(9): p. 840-55.

110. Calon, A., et al., *Dependency of colorectal cancer on a TGF-beta-driven program in stromal cells for metastasis initiation.* Cancer Cell, 2012. **22**(5): p. 571-84.

111. Zanella, E.R., et al., *IGF2 is an actionable target that identifies a distinct subpopulation of colorectal cancer patients with marginal response to anti-EGFR therapies.* Sci Transl Med, 2015. **7**(272): p. 272ra12.

112. Livingstone, C., *IGF2 and cancer.* Endocr Relat Cancer, 2013. **20**(6): p. R321-39.

113. Hartmann, L.C., et al., *Benign breast disease and the risk of breast cancer.* N Engl J Med, 2005. **353**(3): p. 229-37.

114. Murphy, S.K., et al., *Frequent IGF2/H19 domain epigenetic alterations and elevated IGF2 expression in epithelial ovarian cancer.* Mol Cancer Res, 2006. **4**(4): p. 283-92.

115. Zhao, R., et al., *Loss of imprinting of the insulin-like growth factor II (IGF2) gene in esophageal normal and adenocarcinoma tissues.* Carcinogenesis, 2009. **30**(12): p. 2117-22.

116. Kohda, M., et al., *Frequent loss of imprinting of IGF2 and MEST in lung adenocarcinoma.* Mol Carcinog, 2001. **31**(4): p. 184-91.

117. Bell, A.C. and G. Felsenfeld, *Methylation of a CTCF-dependent boundary controls imprinted expression of the Igf2 gene.* Nature, 2000. **405**(6785): p. 482-5.

118. Hark, A.T., et al., *CTCF mediates methylation-sensitive enhancer-blocking activity at the H19/Igf2 locus.* Nature, 2000. **405**(6785): p. 486-9.

119. Phillips, J.E. and V.G. Corces, *CTCF: master weaver of the genome.* Cell, 2009. **137**(7): p. 1194-211.

120. Sakatani, T., et al., *Loss of imprinting of Igf2 alters intestinal maturation and tumorigenesis in mice.* Science, 2005. **307**(5717): p. 1976-8.

121. Suzuki, H., et al., *Altered imprinting in lung cancer.* Nat Genet, 1994. **6**(4): p. 332-3.

122. Joyce, J.A., et al., *Imprinting of IGF2 and H19: lack of reciprocity in sporadic Beckwith-Wiedemann syndrome.* Hum Mol Genet, 1997. **6**(9): p. 1543-8.

123. Ravenel, J.D., et al., *Loss of imprinting of insulin-like growth factor-II (IGF2) gene in distinguishing specific biologic subtypes of Wilms tumor.* J Natl Cancer Inst, 2001. **93**(22): p. 1698-703.

124. Lui, J.C. and J. Baron, *Evidence that Igf2 down-regulation in postnatal*

tissues and up-regulation in malignancies is driven by transcription factor E2f3. Proc Natl Acad Sci U S A, 2013. **110**(15): p. 6181-6.

125. Tada, Y., et al., *The stem cell transcription factor ZFP57 induces IGF2 expression to promote anchorage-independent growth in cancer cells.* Oncogene, 2015. **34**(6): p. 752-60.

126. Lee, S.C., et al., *Essential role of insulin-like growth factor 2 in resistance to histone deacetylase inhibitors.* Oncogene, 2016. **35**(42): p. 5515-5526.

127. Min, H.Y., et al., *Essential role of DNA methyltransferase 1-mediated transcription of insulin-like Growth Factor 2 in Resistance to Histone Deacetylase Inhibitors.* Clin Cancer Res, 2016.

128. Tan, F.H., et al., *The role of STAT3 signaling in mediating tumor resistance to cancer therapy.* Curr Drug Targets, 2014. **15**(14): p. 1341-53.

129. Zhao, C., et al., *Feedback Activation of STAT3 as a Cancer Drug-Resistance Mechanism.* Trends Pharmacol Sci, 2016. **37**(1): p. 47-61.

130. Real, P.J., et al., *Resistance to chemotherapy via Stat3-dependent overexpression of Bcl-2 in metastatic breast cancer cells.* Oncogene, 2002. **21**(50): p. 7611-8.

131. Huang, S., et al., *Inhibition of activated Stat3 reverses drug resistance to chemotherapeutic agents in gastric cancer cells.* Cancer Lett, 2012. **315**(2): p. 198-205.

132. Duan, Z., et al., *Signal transducers and activators of transcription 3 pathway activation in drug-resistant ovarian cancer.* Clin Cancer Res, 2006. **12**(17): p. 5055-63.

133. Dobi, E., et al., *Impact of STAT3 phosphorylation on the clinical effectiveness of anti-EGFR-based therapy in patients with metastatic colorectal cancer.* Clin Colorectal Cancer, 2013. **12**(1): p. 28-36.

134. Wu, K., et al., *Gefitinib resistance resulted from STAT3-mediated Akt activation in lung cancer cells.* Oncotarget, 2013. **4**(12): p. 2430-8.

135. Liu, F., et al., *Stat3-targeted therapies overcome the acquired resistance to vemurafenib in melanomas.* J Invest Dermatol, 2013. **133**(8): p. 2041-9.

136. Girotti, M.R., et al., *Inhibiting EGF receptor or SRC family kinase signaling overcomes BRAF inhibitor resistance in melanoma.* Cancer Discov, 2013. **3**(2): p. 158-67.

137. Lee, H.J., et al., *Drug resistance via feedback activation of Stat3 in oncogene-addicted cancer cells.* Cancer Cell, 2014. **26**(2): p. 207-21.

138. Miller, M.D. and M.S. Krangel, *Biology and biochemistry of the chemokines: a family of chemotactic and inflammatory cytokines.* Crit Rev Immunol, 1992. **12**(1-2): p. 17-46.

139. Maeng, Y.S., et al., *Endothelial progenitor cell homing: prominent role of the IGF2-IGF2R-PLCbeta2 axis.* Blood, 2009. **113**(1): p. 233-43.

140. Groskopf, J.C., et al., *Proliferin induces endothelial cell chemotaxis through a G protein-coupled, mitogen-activated protein kinase-dependent pathway.* Endocrinology, 1997. **138**(7): p. 2835-40.

141. Hawkes, C., et al., *Heterotrimeric G proteins and the single-transmembrane domain IGF-II/M6P receptor: functional interaction and relevance to cell signaling.* Mol Neurobiol, 2007. **35**(3): p. 329-45.

142. Matsunaga, H., et al., *Activation of a calcium-permeable cation channel by insulin-like growth factor II in BALB/c 3T3 cells.* Am J Physiol, 1988. **255**(4 Pt 1): p. C442-6.

143. Zhang, Q., et al., *Insulin-like growth factor II signaling through the insulin-like growth factor II/mannose-6-phosphate receptor promotes exocytosis in insulin-secreting cells.* Proc Natl Acad Sci U S A, 1997. **94**(12): p. 6232-7.

144. Minniti, C.P., et al., *The insulin-like growth factor II (IGF-II)/mannose 6-phosphate receptor mediates IGF-II-induced motility in human rhabdomyosarcoma cells.* J Biol Chem, 1992. **267**(13): p. 9000-4.

145. El-Shewy, H.M., et al., *Phospholipase C and protein kinase C-beta 2 mediate insulin-like growth factor II-dependent sphingosine kinase 1 activation.* Mol Endocrinol, 2011. **25**(12): p. 2144-56.

146. Douglas, I.S. and M.R. Nicolls, *Chemokine-mediated angiogenesis: an essential link in the evolution of airway fibrosis?* J Clin Invest, 2005. **115**(5): p. 1133-6.

147. Sparmann, A. and D. Bar-Sagi, *Ras-induced interleukin-8 expression plays a critical role in tumor growth and angiogenesis.* Cancer Cell, 2004. **6**(5): p. 447-58.

148. Wang, X., et al., *STAT3 inhibition, a novel approach to enhancing targeted therapy in human cancers (review).* Int J Oncol, 2012. **41**(4): p. 1181-91.

VII. 국문 초록

다양한 약물 개발과 함께 임상에 적용 가능한 항암치료의 폭이 넓어졌음에도 불구하고 오늘날 암의 치료에 있어 가장 큰 장애물은 여전히 치료에 대한 내성 때문에 결국에는 발생하는 암의 재발이다. 따라서 이상적인 항암치료의 계획은 시행하고자 하는 치료와 관련된 내성을 극복하는 방안을 꼭 고려하여 세워야 한다. 현재까지 개발된 표적 항암 치료제의 표적들 중 한가지로서 알려진, 인슐린 유사 성장인자 신호전달체계는 리간드, 해당 수용체, 결합 단백질간의 매우 복잡한 상호작용에 의하여 조절된다. 이 신호전달체계는 항암치료에 있어 매우 유망한 표적으로서 연구되어 왔으며, 주로 단일클론항체 약물을 필두로 한 인슐린유사성장인자수용체-1 (IGF-1R)을 표적으로 하는 다양한 약제들이 암세포의 IGF 신호전달체계를 억제하고자 개발되어 왔다. 하지만, 현재까지 이러한 약물들의 임상적인 효능은 그리 좋지 않으며, 이러한 점이 IGF 신호전달체계를 표적으로 하는 약물의 개발을 어렵게 하였다. 따라서, 많은 연구자들이 IGF-1R을 표적으로 하는 단일클론항체약물의 내성 발생에 대하여 주로 암세포 자체에서 치료에 의하여 지속적인 유전자 결함이 쌓이면서 약효가 상쇄된다는 관점의 연구를 보고하였다. 하지만, 암의 특성상, 다양한 종류의 성질을 가진 암세포들이 모여있을 뿐만 아니라 암세포가 아닌 면역세포, 섬유아세포, 혈관내피세포 등 다양한 세포들이 모인 하나의 기관과 같은 입장에서 내성을 연구하고자 하는 시도도 최근 들어 나타나고 있다. 이러한 다양한 세포집단과 암세포를 통틀어서 미세종양환경 (tumor microenvironment, TME)이라고 부르며, 암세포와 미세환경의 다양한 세포들간의 상호작용은 암의 진행, 약물에 대한 내성의 발

생에 큰 역할을 하는 것이 밝혀졌다. 본 연구는 일련의 실험을 통하여 IGF-1R을 표적으로 하는 치료에 대한 내성의 발생기전을 종양미세환경적 관점에서 연구하고자 하였다. IGF-1R 억제제의 임상실험의 해당 암종인 유방암, 폐암, 두경부암에 대한 마우스 모델을 통하여 IGF-1R 억제제에 의한 암전이의 촉진 및 마우스의 생존율 감소를 관찰하였으며, IGF-1R을 억제하는 항암치료에 대한 내성이 발생하는 과정 중에서 미세종양환경과 암세포간의 상호작용이 미치는 영향에 대하여 다음과 같은 몇 가지 분자적 기전을 밝혔다: (1) IGF-1R을 단일클론항체 약물을 이용하여 발현을 억제하였을 때, 암세포의 STAT3를 활성화하여 IGF-2의 전사를 증가시킨다; (2) IGF-2는 단핵구와 섬유아세포가 가지고 있는 IGF-2R를 통하여 이러한 세포의 암조직으로의 유입을 증가시키며; (3) 유입된 주변세포들은 혈관신생을 증가시키는 사이토카인, 특히 CXCL8의 발현을 촉진시키며, 혈관내피세포를 끌어들여 암조직에 혈관신생을 촉진시키며, 결과적으로 암의 전이를 돕는다. 따라서 본 연구는 IGF-1R을 표적으로 하는 임상 치료법에 대한 내성 발생에서 암세포와 미세종양환경을 구성하고 있는 세포간의 상호작용이 매개하는 반응을 분자적인 수준에서 규명하여, 이러한 임상치료계획에 있어서 내성의 발생을 회피할 수 있는 대안을 제시한다.

***Keywords*: tumor microenvironment / drug resistance / insulin like growth factor receptor 1 (IGF-1R / insulin like growth factor-2 (IGF-2) / STAT3**

Student number: 2011-31107